2009-07-01

Hydrogen Bonding and Cucurbituril Complexation as Self-Assembly Mechanisms

Lu Cui
University of Miami, complex_nk@hotmail.com

UNIVERSITY OF MIAMI

HYDROGEN BONDING AND CUCURBITURIL COMPLEXATION AS SELF-ASSEMBLY MECHANISMS

By

Lu Cui

A DISSERTATION

Submitted to the Faculty
of the University of Miami
in partial fulfillment of the requirements for
the degree of Doctor of Philosophy

Coral Gables, Florida

June 2009

UNIVERSITY OF MIAMI

A dissertation submitted in partial fulfillment of
the requirements for the degree of
Doctor of Philosophy

HYDROGEN BONDING AND CUCURBITURIL COMPLEXATION AS SELF-ASSEMBLY MECHANISMs

Lu Cui

Approved:

_____ Angel E. Kaifer, Ph.D. Professor of Chemistry	_____ Terri A. Scandura, Ph.D. Dean of the Graduate School
_____ Vaidyanathan Ramamurthy, Ph.D. Professor of Chemistry	_____ Francisco M. Raymo, Ph.D. Professor of Chemistry
_____ Hongtan Liu, Ph.D. Professor of Mechanical and Aerospace Engineering	

CUI, LU (Ph.D., Chemistry)

Hydrogen Bonding And Cucurbituril Complexation As Self-Assembly Mechanisms (June 2009)

Abstract of a dissertation at the University of Miami.

Dissertation supervised by Professor Angel E. Kaifer.
No. of pages in text. (162)

The supramolecular interactions of small organic molecules with different host molecules are investigated in this dissertation. Additionally, the author also describes the self-assembly mechanisms in hydrogen bonding motif. These studies were carried out by many techniques including, NMR, cyclic voltammetry, steady state voltammetry, mass spectroscopy, UV-visible spectroscopy and fluorescence spectroscopy.

Chapter 1 introduces the science of supramolecular chemistry and the background of cucurbiturils, one of the most important host molecules studied in this research work. It describes the structures and binding behaviors of each host molecule. Additionally, the selectivity and binding properties in the host-guest interactions involved cucurbiturils are discussed.

Chapter 2 compares the electrochemical properties of cationic and neutral ferrocene derivatives upon addition of cucurbiturils. It is observed that the cationic ferrocene compounds bind to cucurbit[7]uril much stronger compared to the neutral ferrocene compounds. The positive charged side chains favor to interact with cucurbit[7]uril portals and thus stabilize the complexes. Besides, the author describes a simple analytical method to determine the binding constants by a competitive binding with a standard reference compound, cobaltocenium, which is reported to bind strongly to cucurbit[7]uril.

Chapter 3 described the research of the pH-dependent binding affinity between cucurbit[7]uril and ferrocene guests. The electrochemical behavior of ferrocene moiety in aqueous solution was investigated by cyclic voltammetry in the presence of cucurbit[7]uril in acidic and basic environment respectively. The protonation and deprotonation processes affect the binding behaviors of the ferrocene residues with cucurbit[7]uril.

Chapter 4 describes the synthesis and characterization of a new series of 4-phenyl-pyridinium derivatives. These compounds contain a phenyl-pyridinium residue which is favorable to be bound by cucurbit[8]uril. The 1:1 and 1:2 host-guest binding stoichiometries are both observed by UV-visible spectroscopy. These new compounds can be dimerized encapsulated inside the cucurbit[8]uril portals without being electrochemical reduced.

Chapter 5 is a brief introduction into the science of hydrogen bonding. This chapter investigates the application of multiple hydrogen-bonding in supramolecular chemistry extensively. Multiple hydrogen bonds with their directionality and reversibility are of great interest and importance in the design and investigations of well-defined supramolecular assemblies. The potential of hydrogen bonding is limitless and is still developing.

Chapter 6 describes the synthesis and photochemical behaviors of a series of ureido-pyrimidione derivatives. All of the DDAA derivatives form stable, non-covalent dimers in non-polar solvents. The dimeric molecular assemblies of these hydrogen bonding motifs in their DDAA pyrimidinedione units are investigated by NMR, X-ray crystallography, fluorescence spectroscopy and computations. Additionally, their hetero-

dimerization is well studied by fluorescence spectroscopy. The observation and comparison of fluorescence quenching on the photochemical fluorophore for each compound by ferrocene-DDAA and isopropyl-DDAA reveal the electron transfer process through the quadruple hydrogen bonding motifs.

ACKNOWLEDGEMENT

First of all, I would like to extend my sincerest appreciation to my supervisor, Professor Angel E. Kaifer, who provided me with the opportunity of joining this dynamic group and enabled me to continue pursuing my dream of obtaining a Ph.D. in Chemistry. His profound knowledge, keen vision, rigorous attitude toward science, down-to-earth style, and especially his discipline have made an indelible impression upon me. I believe the experience I acquired under his mentorship will help me throughout my life and career.

I am also deeply appreciative of the help and advice I received from Professor V. Ramamurthy, Professor Françisco M. Raymo and Professor Hongtan Liu. Their guidance and support throughout my doctoral program, their invaluable advice about the research, and their helpful suggestions about my dissertation writing made all of this possible.

I would like to give special thanks to Professor Burjor Captain, and Professor Joel T. Mague for solving the X-ray crystal structures. Special thanks are also extended to Professor Rajeev Prabhakar for his help with the computing calculations.

I would also like to thank my lab mates and friends for their help and collaboration, especially Dr. Suresh Gadde, for his time，patience and great advice in the computational calculating part of this project in Chapter 2.

I owe my deepest thanks to my parents and my husband for their love, understanding, and support. They have never wavered in their belief in me and my research, and have given me the love and support essential to complete this dissertation.

I am very grateful that I had the opportunity to study and work in the Department of Chemistry at University of Miami, which is a wonderful community. I would like to thank all the staff for their kindness, care and help, without which my life here as an international student would have been significantly more difficult. I would also like to thank all the faculty members and my colleagues, who informed and inspired me. I will always cherish the memory of my stay at the University of Miami.

TABLE OF CONTENTS

LIST OF FIGURES

Chapter 1

Chapter 2

Figure 6.20

LIST OF TABLES

Chapter 2

Chapter 3

Chapter 4

Chapter 6

LIST OF SCHEMES

Chapter 2

Chapter 3

Chapter 4

Chapter 5

Chapter 6

Chapter 1

INTRODUCTION TO SUPRAMOLECULAR CHEMISTRY AND CUCURBITURILS

1.1 Introduction to supramolecular chemistry

Supramolecular chemistry refers to the study of chemistry concerning host-guest interactions through weak non-covalent bonds. The creation of nanoscale molecular or supramolecular architectures that have specific structures, properties, and functions has been of great interest in the last decade.[1]

1.2 Common host molecules in supramolecular chemistry

In the family of macrocyles of common host molecules, various hosts such as cyclodextrins, calixarenes, cucurbiturils and octaacids are the main host molecules and molecular assemblys which can encapsulate or interact with the reactant guest molecules.

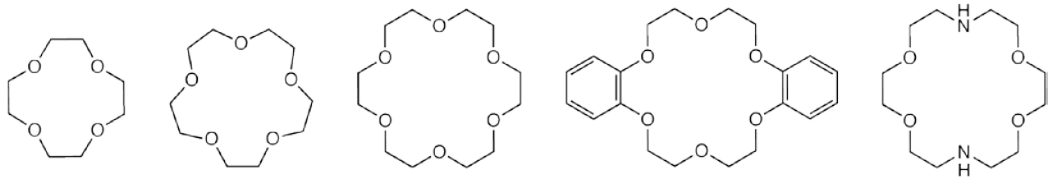

Figure 1.1 structures of common crown ethers: 12-crown-4, 15-crown-5, 18-crown-6, dibenzo-18-crown-6 and diaza-18-crown-6.

Crown ether was first synthesized using a simple method in 1967 by Charles Pedersen, who shared the 1987 Nobel Prize in Chemistry.[2] Crown ethers consist of a ring containing several ether groups and they can bind certain cations at the interior of the ring and form

complexes. Among them, 15-crown-5 and 18-crown-6 are very famous for their high affinity to bind sodium cation or potassium cation. The binding affinity is well studied with metal ions.

Cyclodextrins (CDs) are natural products which are made from starch by cyclodextrinase. With repeating chiral glucolpyranose subunits, they are good molecular receptors for many small molecules in aqueous solution. They have attracted much interest because of its functionalized derivatives' great solubility in water. However, the two sides of CD are different and such structure leads to many interest properties. Smaller cavity opening is lined by primary hydroxyl groups, while the larger cavity opening is lined by secondary hydroxyl groups. Cyclodextrins are able to include hydrophobic molecules and form complexes like many other supramolecular hosts, so they are widely used as supramolecular carriers.

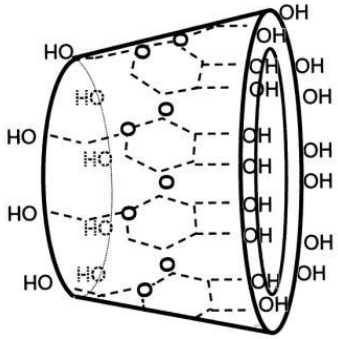

Figure 1.2 γ-CD toroid structure showing spatial arrangement.

Calixarene is a macrocycle prepared from phenols and aldehydes with a basket shape. These host molecules contain aromatic building blocks and they can bind to guest molecules in their hydrophobic cavities like the cyclodextrins. Calixarenes exhibit great selectivity towards cations. Resorcinarene is a type of calixarene when resorcinol is coupled with aldehyde and its

structure is more rigid compared to a flexible calixarene. With hydrogen bonds to hold the structure together, six resorcinarene units form hexamer nanoscale molecular assembly.[3]

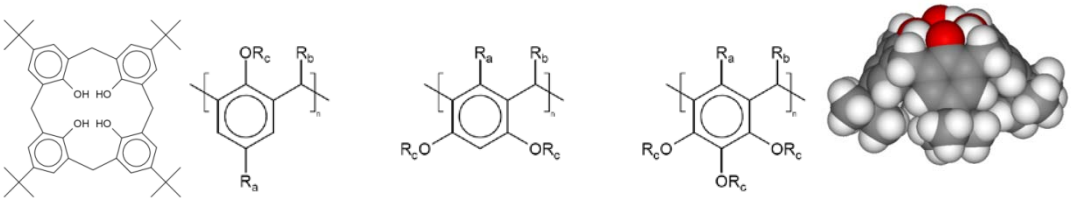

Figure 1.3 From left to right: calixarene; three functionalized calixarenes; and space filling model of resorcinarene.

Octa acid is another important type of host molecule studied in supramolecular chemistry. It was first reported in 2004 by Gibb's group.[4] This molecule contains eight carboxylic acid units, four of them in the top and four at the bottom of the molecular cavity. The deep hydrophobic internal cavity leads to the strong binding of octa acid to guests with solvophobic interactions in basic aqueous solutions.

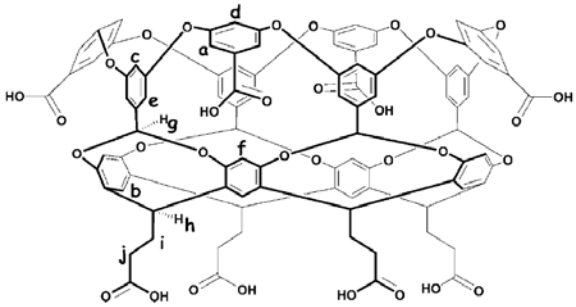

Figure 1.4 Chemical structure of host octa acid

Cucurbiturils are a series of macrocyclic methylene-bridged molecules that contain glycoluril repeating units.[5,6] This family of compounds possesses a cage-like structure resembling a pumkin and their names are derived from the Latin word for pumpkin

Cucurbitaceae. They are capable to bind small guest molecules in their internal hydrophobic cavities, which are very similar to cyclodextrins and calixarenes. The emerging family of cucurbit[n]urils (CBn, n=5,6,7,…) now has become one of the preeminent class of synthetic receptors, along with other macrocycles, which are mentioned above. With a range of sizable cavities, they display a marked preference toward hosting positively charged guest species, and the related supramolecular chemistry has been extensively studied.[7]

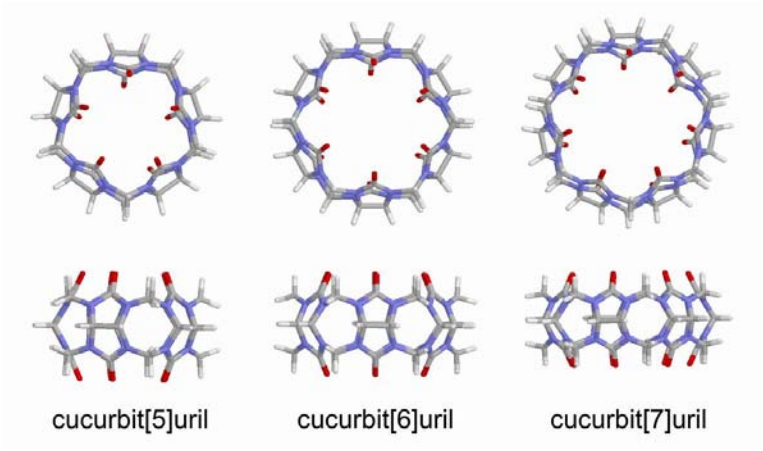

Figure 1.5 Computer models of cucurbiturils (top view and side view).

1.3 Synthesis and structures of cucurbiturils

Mock first reported in 1981 that the condensation of glycoluril and formaldehyde delivers the cyclic hexameric macrocycle cucurbit[6]uril (CB6), the most common and well studied member of the cucurbituril family. Its synthesis first appeared in the literature 100 years ago, but it was not fully characterized due to the lack of analytical techniques. The structure and its chemical behavior were not reported until 1981 by Mock and co-workers. X-ray crystallography showed a macrocyclic cavitand structure containing six dimethanoglycouril units.

However, the synthesis of other macrocyclic of CB6 homologues composed of different number of glycouril units were not detected until almost 20 years later. Kim and Day reported the reactions to form cucurbiturils containing 5-8 repeating glycouril units under mild controllable conditions.[8,9]

1.4 Complexation of guests with cucurbiturils in supramolecular chemistry

Cucurbiturils are symmetric cyclic glycoluril oligomers molecular containers with large internal cavities in which small molecules can be encapsulated. The family of cucurbiturils is receiving considerable attention because of the potential applications in many fields. These molecular container receptors can reach high binding affinities with suitable guests in aqueous solution. All cucurbituril homologues share some similar properties. They all have rigid structures with an equatorial plane of symmetry. Guest molecules can be encapsulated in the hydrophobic cavity via two portals lined by polar carbonyl groups. They also show high electron density at both of the carbonyl portals and inner cavity walls which enhance the selectivity in binding.

Although different cucurbituril homologues have a common depth (the distance between the carbonyl groups from two sides) value, which is about 9.1 Å, however, their cavity sizes and portal dimensions vary corresponding to the numbers of glycouril units. According to their cavity sizes, each type of cucurbituril exhibits remarkable selectively binding properties to guests through two portals, around the portal rim or in the cavity. The interactions of

cucurbiturils with guests, solvent, and other solutes play a part in the applications of recognition and binding properties.

Cucurbiturils are efficient host molecules in molecular recognition. They are well known to have a particularly high affinity for positively charged or cationic compounds. The high association constants of cucurbiturils with positively charged molecules are attributed to the carbonyl groups on each side of the cavity. These electron-rich oxygen atoms are favorable to interact with cations with a high affinity.

CB6 is a novel molecular container assembly with a hollow core of about 5.5Å diameter which was first reported by Kim's group. In aqueous solution containing sodium ions, two sodium (Na^+) ions and their coordinated water molecules can interact with the carbonyl groups on both sides of CB6. Such Na^+-bound CB6 exhibit excellent binding with small organic molecules in aqueous solution. Interestingly, the encapsulation and release process of guest molecules can be controlled by complexation and decomplexation of the sodium ions at the portals. Meanwhile, CB6 is a weak base and it can be protonated in acidic media. Competition binding between metal-binding and CB6 protonation is represented in **Figure 1.6**.

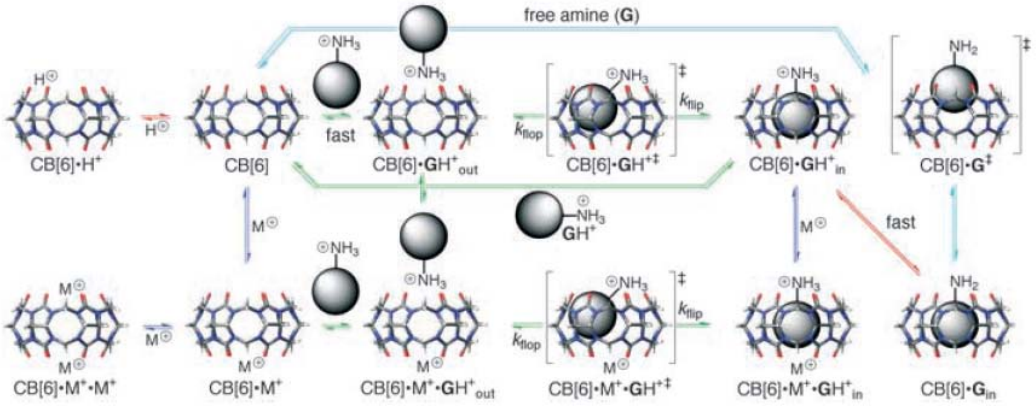

Figure 1.6 Scheme for molecular binding recognition by CB6.

Host-guest interactions also influence the solubility behavior of cucurbiturils. For example, the solubility of CB6 in pure water is very poor; however, it is greatly improved in a solution of potassium hydroxide or in an acidic solution. The host forms a positively charged complex with a potassium ion or a hydronium ion respectively which have much greater solubility than the uncomplexed neutral CB6.

Supramolecular recognition behavior of CB6 was well studied during the 1980s toward small ions and molecules with extremely high binding affinity (K_a up to 10^8 M^{-1}).[6,10] Mock and co-workers reported that alkyl amines and alkane diamines exhibit selectivity for CB6. Kim and co-workers have demonstrated numerous supramolecular architectures using CB6, including polyrotaxanes, rotaxane dendrimers, and rotaxane based molecular switches.[11-13] Inspired by their outstanding recognition properties, many groups have extended their work on CB6's homologues, cucurbit[7]uril (CB7), cucurbit[8]uril (CB8) and other cucurbituril hosts since these new molecules were created. The synthesis, isolation and full characterization of CB7 and CB8 have led to a wide range of new areas in the study of larger guests or even multiple guests encapsulated inside the cucurbituril homologue cavities. Kim and co-workers reported their expanded relevant work from CB6 to CB7 and CB8.[9] These studies are widely used in chemical sensors, catalysts and other supramolecular assemblies.[10]

CB7 is a good receptor to bind with many positively charged organic molecules such as adamantanes, bicyclooctanes, naphthalene, stilbene, viologen, *o*-carborane, ferrocene, and colbatocene and derivatives.[14] Among these guest molecules, ferrocene, cobaltocenium and viologen and their derivatives have been studied extensively due to their facile modification

and electronic or optical properties. The binding affinity of CB7 on these small organic molecules can be very high.[11] For instance, the association equilibrium constant of CB7 with the positively charged 1-aminoadamantane hydrochloride is experimentally determined at 4.23×10^{12} M^{-1}.

The formation of inclusion complexes between ferrocene and CB7 was first reported by our group in 2003.[15] CB7 forms a very stable complex ($K \sim 3 \times 10^{9}$ M^{-1}) with hydroxymethylferrocene. In collaboration with other groups, we reported that a cationic ferrocene derivative is bound by CB7 with high equilibrium association constant (*K*). The positive charge on the guest, positioned to interact with one of the host's rings of carbonyl oxygens, leads to a sizable increase in the corresponding *K* value, which reaches 3×10^{12} M^{-1}. This led to the investigation of the inclusion complex formed between a series of ferrocene derivatives and CB7, which was shown to exhibit high to modest *K* values. For example, CB7 forms an inclusion complex with the dicationic ferrocene derivative bis(trimethylammoniomethyl) ferrocene in aqueous solution with an ultrahigh stability similar to that of the avidin-biotin complex. The new high-affinity, host–guest pair reported here could serve as an extremely strong but redox-active reversible fastener in self-assembling chemical and biological supramolecular systems.[16]

Our previous work on these complexes has focused on the determination of their structures and thermodynamic stabilities. We have also described the voltammetric behavior of some water-soluble ferrocene derivatives in the presence of the CB7 host. As we know, ferrocene undergoes a one-electron oxidation process, and ferrocene residue is hindered by

encapsulation inside the CB7 cavity. It also means that the equilibrium association constant of the CB7 complex decreases by 1-2 orders of magnitude upon oxidation of the ferrocene residue. Voltammetric experiments were performed with the neutral ferrocene derivative, hydroxymethylferrocene, which revealed that the half-wave potential ($E_{1/2}$) value only experiences a modest anodic shift. The contrast between the CB7-induced, half-wave potential shifts in these two cases is striking and lead the conclusion that the binding behavior of CB7 with neutral and cationic ferrocene derivatives are really different.

Kim's previous investigation on inclusion behavior coupled with the redox chemistry of methyl viologen (MV^{2+}) in CB7 revealed that CB7 prefers the charged species, MV^{2+} and cation radical $MV^{+}\cdot$, to the fully reduced neutral MV^{0} species as guests.[17] CB7 binds MV^{2+} strongly ($K_{2+} = \sim 2\times10^{5}\ M^{-1}$) while it binds $MV^{+}\cdot$ with a slightly lower binding affinity. However, further reduction of the guest to MV^{0} substantially decreases its binding by CB7, which is proved by the electrochemical data. Besides, the cation radical $MV^{+}\cdot$ has an equilibrium of dimers and monomers.

Furthermore, dimerization of $MV^{+}\cdot$ is effectively suppressed by forming a stable complex with CB7 in aqueous solution and the redox process(MV^{2+}/ $MV^{+}\cdot$) of the CB7·MV^{2+} complex occurs predominantly via a direct electron transfer pathway. Kim et al. also extended their study to the larger host, CB8.[18] They have taken advantage of these binding interactions to design and prepare various switchable molecular systems. Our group has utilized CB8 for the redox control of self-assembly and size selection with dendronized viologens and aromatic electron donors.

Compared to CB6 and CB7, which are well studied for the binding with small organic molecules, CB8 can bind multiple guests in its larger cavity simultaneously. This interesting discovery led people to extend their study to CB8's multiple binding behaviors to other small molecules. This feature allows for a particularly interesting dimension of control in the design of supramolecular architecture.

Our group previously reported the unusual redox-coupled inclusion behavior of methyl viologen in CB8 demonstrating that the binding stoichiometry of a host-guest complex can be effectively controlled by the redox chemistry of the guest.[19] Our group also studied the binding interactions and the comparison between the large cucurbituril hosts, CB7 or CB8.[20] Their binding affinity to many small organic molecules were studied in details, such as cationic anthraquinone derivatives, diquat (DQ^{2+}) and paraquat (PQ^{2+}).[20,21]

First, it was found that the presence of metal cations significantly influences the extent of complexation in the study of cationic anthraquinone derivatives with CB7.[21] Besides, inclusion complexation was observed to slow down the electrochemical processes associated with reduction of the anthraquinone residues. It is concluded that anthraquinone residues can serve as reasonable substrates for inclusion by CB7 with modest resulting binding affinities.

In our previous work the binding properties of CB7 with guests diquat (DQ^{2+}) and paraquat (PQ^{2+}) were studied.[20] CB7 and CB8 have been the subject of particular attention within the CB family. Kim's group and our group reported in 2002 that paraquat forms a highly stable inclusion complex with CB7.[22,23] Kim and co-workers reported the formation

of a 1:1 inclusion complex between paraquat and CB8.[22] CB8 was found to enhance the formation of the radical cation dimer upon one-electron reduction of paraquat. CB8 can encapsulate PQ^{2+} to form a highly stable ternary complex with a suitable aromatic electron donor included in the cavity.

The binding interactions between the hosts CB7 and CB8 with the guest molecules, diquat and paraquat, span a relatively wide range of binding affinities. These interactions involve the formation from very stable to very weak complexes. It is concluded that binding of a guest to CB7 or CB8 is affected by the guest's hydrophobic core. The core which fits well inside the host cavity could help to improve the binding stabilities. On the other hand, the positive charges on the guest also distribute to the ion-dipole interactions between the guest and the carbonyl oxygens at cucurbituril portals.[20]

CB8, the cucurbituril homologue with a larger cavity, has attracted a lot of interest since it is capable of hosting two suitable aromatic guests and form stable ternary inclusion complexes. As mentioned before, Kim et al. reported the formation of stable CB8 complexes which contain a charge transfer process.[22] They also reported that CB8 can effectively bind two viologen or tetrathiafulvalene cation radicals, providing additional stabilization to the dimers formed by these species.[18, 24, 25] The CB8 encapsulated complexes can be stabilized by π donor-acceptor charge transfer or homo-dimerization of viologen radicals. Our group also studied this unique ability of CB8 on the redox control of dendrimer self-assembly.[19, 26]

A number of different guest molecules encapsulation by CB6, CB7 and CB8 has been studied. But only a few of them has demonstrated the position of linear guest molecules

interacting with CB hosts in details. Previously our group has studied how to control the positioning of CB7 with respect to the viologen core based on the length and polarity of the alkyl chain attached to the pyridinium nitrogens.[27] Specifically, CB7 localizes over the viologen core with a pseudorotaxane structure when the alkyl chain is shorter than three carbons or derivatised with polar groups such as amines or alcohols. CB7 was found to exhibit considerable binding selectivity to form pseudo-rotaxane complexes with host occupying the central residue. This binding selectivity on different binding sites of a guest molecule is of great interest.

Cucurbit[10]uril (CB10) was first reported by the group of Day as its complex with cucurbit[5]uril (CB5) in the cavity.[28] The structure of the complex was established by X-ray crystallography. Chemical exchange between free and bound CB5 inside CB10 was observed through the use of ^{13}C-labeled CB5. The smallest homologue of cucurbituril, CB5, is limited by its small portal and the volume of its cavity. It can encapsulate very small molecules such as N_2 inside. CB5 also binds cations such as NH_4^+, Pb^{2+} at the rim or binds two NH_4^+ ions at both openings.

1.5 Applications based on CB interactions

In summary, cucurbituril, as a member in the supramolecular host family, it has been extensively explored in the host-guest interactions. Cucurbituril has an internal hydrophobic cavity which is accessible through two symmetrical ureido-carbonyl lined portals. The internal cavity of cucuribituril is able to partially or fully encapsulate a range of small molecules. The

binding behavior is stabilized through hydrophobic effects within the cavity and ion-dipole or dipole-dipole interactions between the guest and the portals.

The formation of a complex between two or more chemical units is one of the most basic and important processes in supramolecular chemistry. Molecular recognition, reversible encapsulation, photochemical and electrochemical controlling, self assembly and molecular aggregation formation using cucurbiturils have created many challenging fields in host-guest chemistry. The host-guest interactions of cucurbiturils may give rise to a range of applications including waste remediation, molecular switches, column chromatography, catalyzing charge-transfer reactions, drug delivery, nanomachine components, and self-sorting systems.

Chapter 2

INVESTIGATION OF THE BINDING BEHAVIOR BETWEEN FERROCENE DERIVATIVES AND THE HOSTS CUCURBIT[6]URIL AND CUCURBIT[7]URIL

2.1 Cucurbit[6]uril and cucurbit[7]uril comparison

Cucurbiturils are interesting macrocyclic molecules consisting of glycoluril repeat units. These molecular containers are capable of binding other molecules within their cavity. Cucurbiturils were first synthesized in 1905 by Behrend but their structure was not characterized until the work of Mock and co-workers, who published the first structural determination of CB6 in 1981.[29]

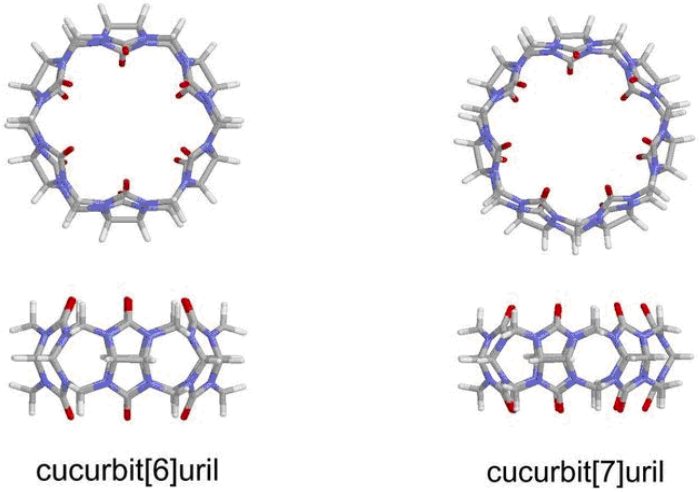

Figure 2.1 Structure of cucurbit[6]uril (CB6) and cucurbit[7]uril (CB7).

In this chapter, our interest is focused on the selective encapsulation of three guest molecules with hosts CB6 and CB7. The purposes of this work are :

1. To study the size, shape and charge effects of electroactive guests in their encapsulation with CB6 and CB7.

2. To determine the degree of encapsulation by using ^{1}H NMR spectroscopy and electrochemical measurements.

3. To compare diffusion coefficients determined from ^{1}H NMR spectroscopic and electrochemical experiments in aqueous solution.

4. To study the electrochemical behavior of encapsulated guests.

As we intend to investigate the specific encapsulation by CB6 and CB7, which are known to have proper size cavity for many small molecules, we designed a series of alkylammonium cations containing an electroactive ferrocenyl-methyl group, two methyl groups and a fourth aliphatic group of variable length.

The synthesis and structure of these molecules are shown below.

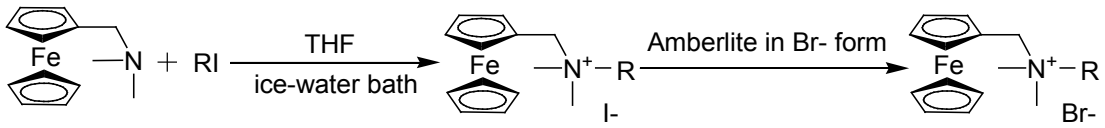

Guest	R
Fc-m	CH_3
Fc-b	$(CH_2)_3CH_3$
Fc-h	$(CH_2)_6CH_3$

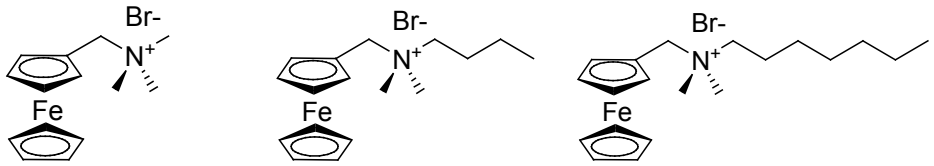

Fc-m Fc-b Fc-h

Figure 2.2 Synthesis and structures of Fc-m, Fc-b and Fc-h. [30]

2.2 Binding properties monitored by ^{1}H NMR spectroscopic analysis

2.2.1 Binding of CB6 with Fc-m, Fc-b and Fc-h

The binding interactions between Fc-m and CB6 were initially investigated by ^{1}H NMR spectroscopy in 0.1 M NaCl/D_2O solution as shown above in **Figure 2.3**. ^{1}H NMR spectra obtained showed that the signals at 3.1 ppm (a) corresponding to the methyl proton peak and the ferrocene proton peaks (1, 1' and b) are not broadened or shifted by the presence of CB6. This indicates that there may be extremely weak interactions between Fc-m and host CB6. However, the spectra recorded with Fc-b showed the representative broadening of the protons (a, b, c and d) in the presence of the host CB6 as shown below in **Figure 2.4**, which indicates the formation of the inclusion complex between CB6 and the butyl substituent chain. We can conclude that the shallow interaction is due to the short length of the butyl chain.

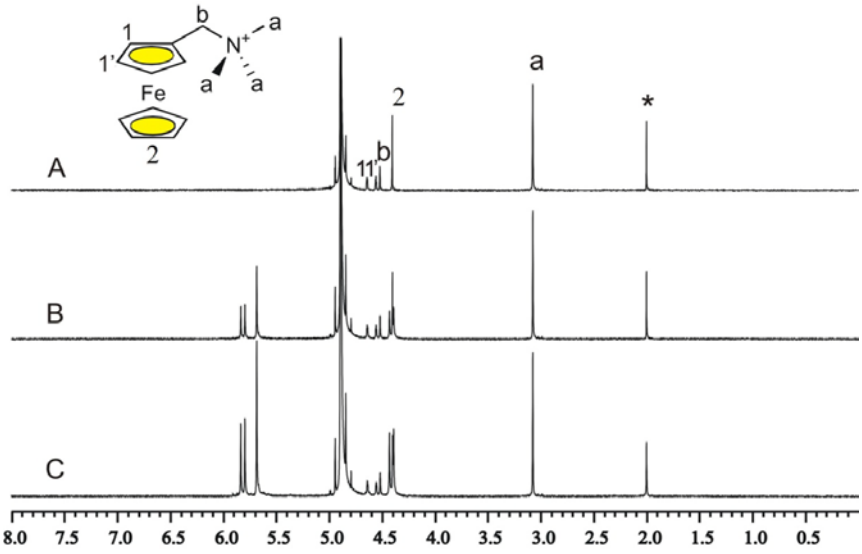

Figure 2.3 ^{1}H NMR spectra (400 MHz, 0.1 M NaCl/D_2O) of 1.0 mM Fc-m (A) in the absence and in the presence of (B) 0.5 equiv, (C) 1.0 equiv CB6. [* Sodium acetate (at 2 ppm) was used as a standard reference for concentrations.]

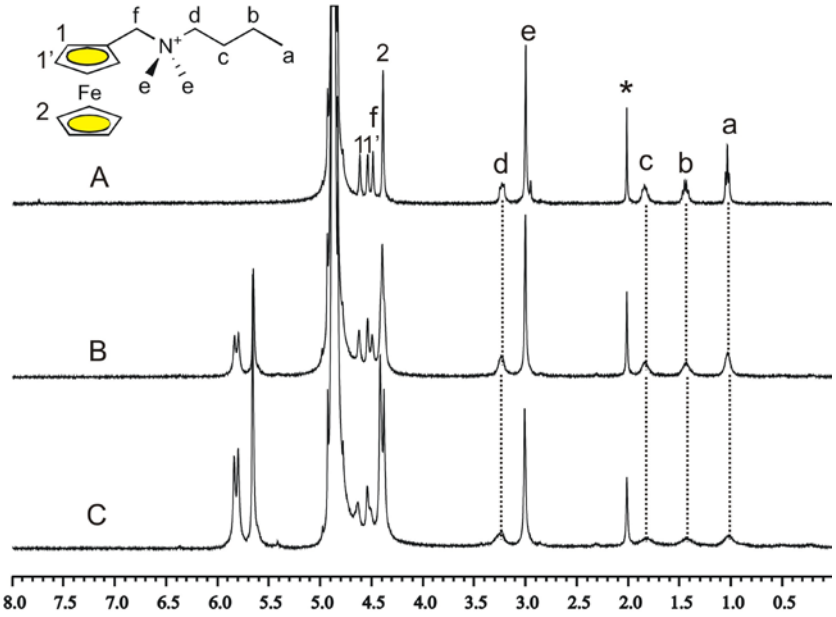

Figure 2.4 ^{1}H NMR spectra (400 MHz, 0.1 M NaCl/D_2O) of 1.0 mM Fc-b (A) in the absence, and in the presence of (B) 0.5 equiv and (C) 1.0 equiv CB6. [* Sodium acetate (at 2 ppm) was used as a standard reference for concentrations.]

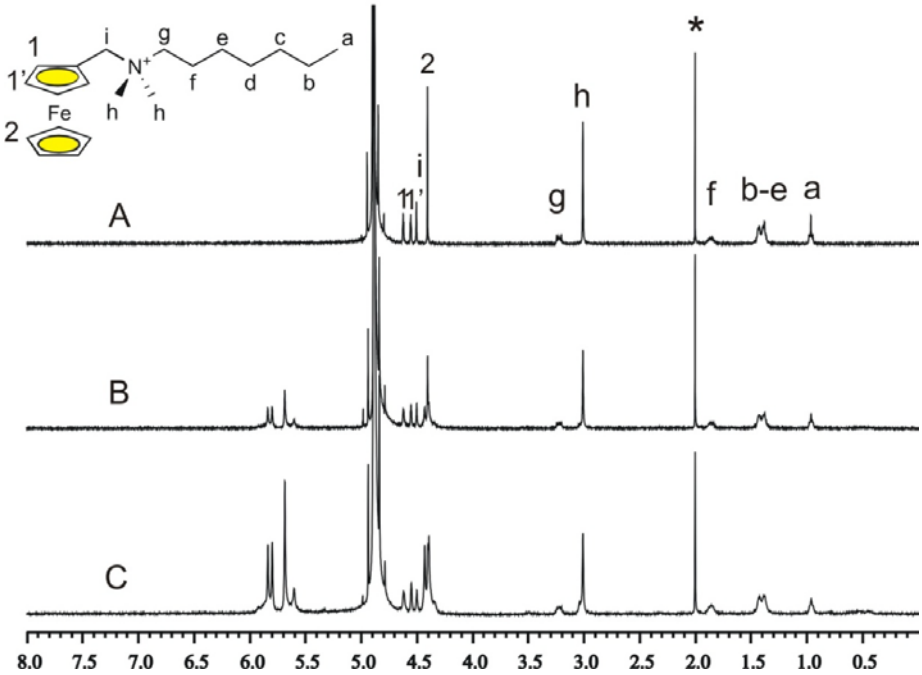

Figure 2.5 ^{1}H NMR spectra (400 MHz, 0.1 M NaCl/D_2O) of 1.0 mM Fc-h (A) in the absence and in the presence of (B) 0.5 equiv and (C) 1.0 equiv CB6. [* Sodium acetate (at 2 ppm) was used as a standard reference for concentrations.]

However, we may also observe the presence of some small resonances signals in the range between ca. 0 ppm and ca. 1 ppm upon addition of CB6 (**Figure 2.4**). We assume that the new peaks are from 1:1 CB6·Fc-b complex and that both and free peaks are very broadened by exchange processes. Similar phenomenon was also observed in **Figure 2.5**, which shows the ^{1}H NMR spectra corresponding to the interactions between Fc-h and CB6. The spectroscopic data indicate that the interaction of Fc-h with CB6 is quite similar to that of Fc-b. Since the solubility of CB6 is not very good, the inclusion complex of Fc-b/Fc-h with 1.0 equiv CB6 start to precipitate out of solution.

2.2.2 Binding of CB7 with Fc-m, Fc-b and Fc-h

On the other hand, a series of titration experiments for a fixed concentration of Fc-m and increasing concentrations of CB7 revealed that at a 1:1 ratio of host to guest, shown in **Figure 2.6** (C), only the signals of the guest appeared upfield shifted. In other words, there are no signals characteristic of the unbound guest, which indicates the strong binding between guest and host ($K>10^{5}M^{-1}$).

However, when an excess amount of guest is present, as shown in the ^{1}H NMR spectrum in **Figure 2.6** (B), the ferrocene proton resonances shifted upfield in the presence of the host with signals for both bound and free guest visible when the concentration of host CB7 is lower than that of guest Fc-m. This suggests a slow exchange on the NMR timescale between free Fc-m and bound Fc-m.[31] Furthermore, the lack of shift for the methyl protons (a) obviously demonstrates that the preferred mode of binding is on the ferrocene residue, not on

the alphatic chain. In the case of Fc-m, the presence of 1.0 equiv. of CB7 results in upfield shifts of ca 0.9 ppm for the proton resonances of the ferrocene. Both of the two series of doublet peaks corresponding to the CB7's methyl protons at the portals in the ^{1}H NMR spectrum of CB7 split into two sets centered at δ = 5.9 ppm, 4.4 ppm, illustrating the differences between the two portals created by the interaction of the Fc-m with CB7.

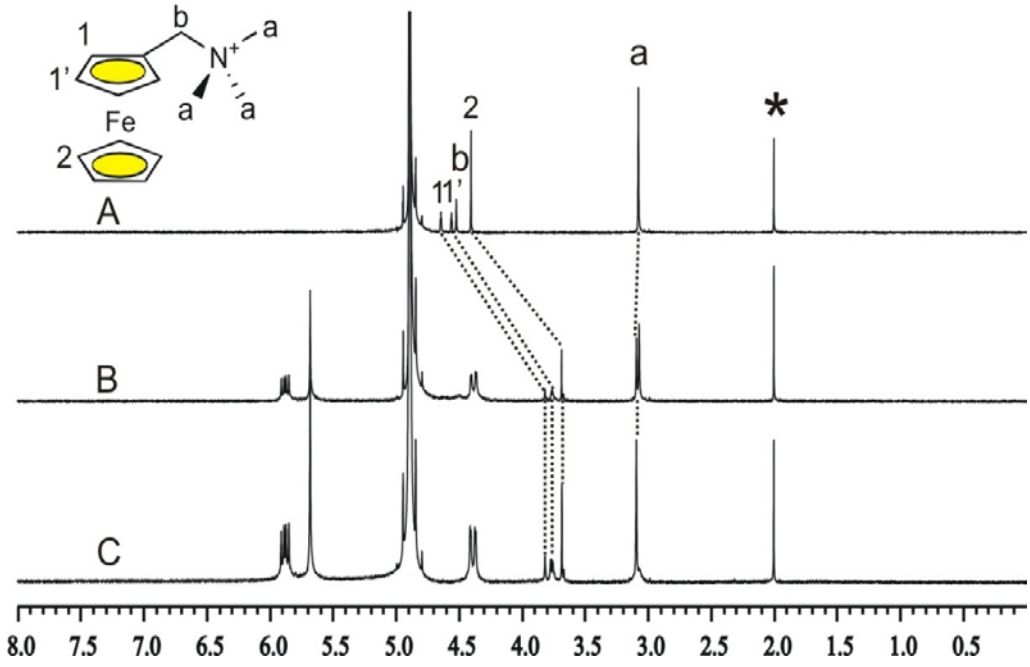

Figure 2.6 ^{1}H NMR spectra (400 MHz, 0.1 M NaCl/D_2O) of 1.0 mM Fc-m (A) in the absence and in the presence of (B) 0.5 equiv and (C) 1.0 equiv of CB7. [* Sodium acetate (at 2 ppm) was used as a standard reference for concentrations.]

The resulting inclusion complex is highly stable (K = 4 x 10^{12} M^{-1} in pure water) and CB7 is believed to include the ferrocenyl unit in its cavity, while the positively charged nitrogen is located close to the center of one of the cavity portals, generating favorable ion-dipole interactions with the carbonyl groups at the cavity opening.

We investigated the binding interactions of the other two cationic ferrocene derivatives (Fc-b and Fc-h) with CB7 and found very similar results. For instance, **Figure 2.7** shows ^{1}H NMR spectroscopic data on the interaction of CB7 and butyl ferrocene derivative Fc-b.

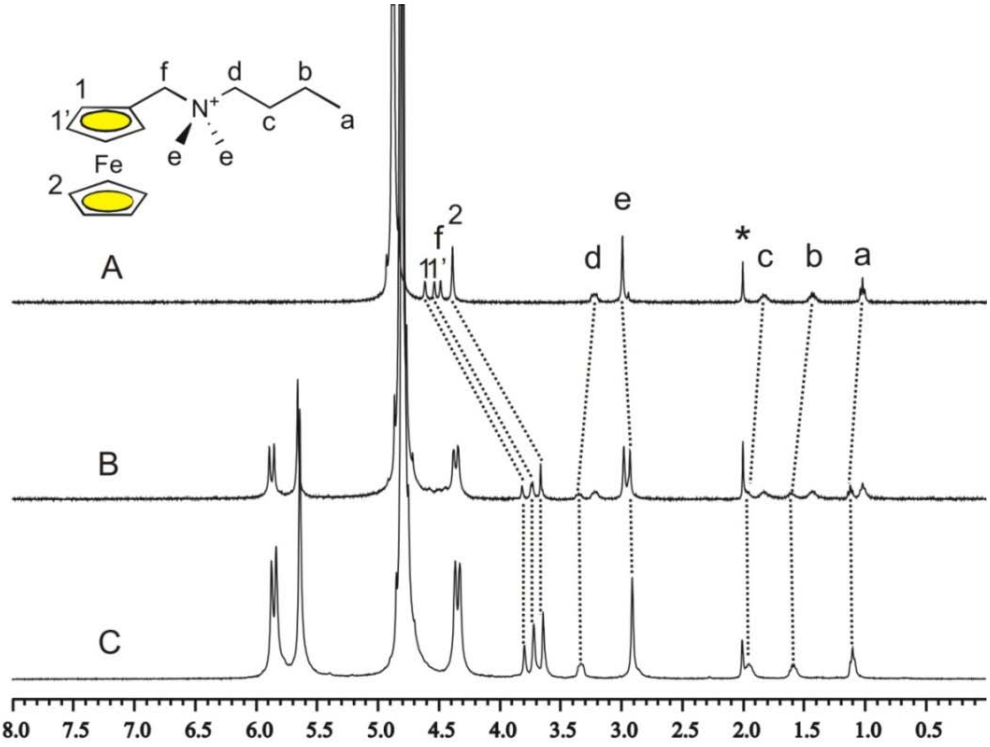

Figure 2.7 ^{1}H NMR spectra (400 MHz, 0.1 M NaCl/D_2O) of 1.0 mM Fc-b (A) in the absence and in the presence of (B) 0.5 equiv and (C) 1.0 equiv of CB7. [* Sodium acetate (at 2 ppm) was used as a standard reference for concentrations.]

The presence of the host leads to a pronounced upfield shift of the ferrocene protons (1, 1' and 2), while the signals corresponding to the protons on the butyl chain (a-d) shift slightly downfield. This pattern of complexation-induced shifts reveals that the ferrocenyl unit is included by CB7, while the butyl chain remains outside the cavity. The *N*-methyl protons (e) shift slightly to higher field, which indicates that they may be closer to the cavity than the a-d protons. The methylene protons (f) that bridge the ferrocenyl unit to the nitrogen shift upfield

along with the ferrocenyl protons, providing clear evidence that they are all fully included by CB7. The simultaneous observation of proton signals for the free and CB7-bound guest (**Figure 2.7** B) indicates that the chemical exchange between both species is slow in the NMR time scale, in excellent agreement with previous observations made with guest Fc-m. In fact, the NMR data set shown in **Figure 2.7** suggests that the binding interactions between the butyl derivative Fc-b and CB7 are essentially identical to those previously observed between Fc-m and CB7.

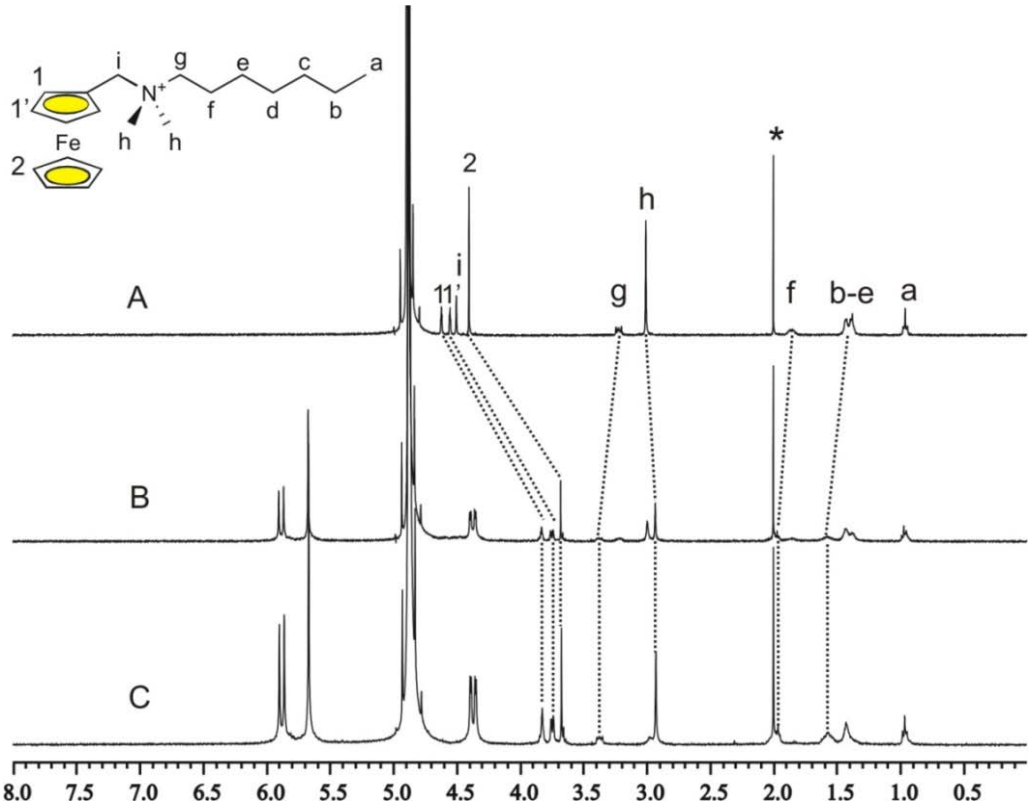

Figure 2.8 ^{1}H NMR spectra (400 MHz, 0.1 M NaCl/D_2O) of 1.0 mM Fc-h (A) in the absence and in the presence of (B) 0.5 equiv and (C) 1.0 equiv of CB7. [* Sodium acetate (at 2 ppm) was used as a standard reference for concentrations.]

Quite similar results were obtained from the ^{1}H NMR titration experiments on guest Fc-h, as shown in **Figure 2.8**. Further lengthening of the aliphatic substituent has no effect on the NMR spectroscopic data. These experiments confirm that CB7 prefers to bind on the ferrocene residue rather than on the aliphatic chain.

The ^{1}H NMR spectroscopic data indicate that the CB7 host forms highly stable and tight inclusion complexes with Fc-h in aqueous solution. We conclude that the binding interactions of all three cationic derivatives with host CB7 are essentially identical, giving rise to highly stable complexes in which the ferrocenylmethyl unit is engulfed inside the CB7 cavity.

The extremely high association equilibrium constant of the complex formed between guest Fc-m and CB7 in pure water and the strong similarities of the NMR spectroscopic data obtained in binding studies between the host and all the ferrocene-containing cationic guests clearly imply that the *K* values in 0.1 M NaCl for guests Fc-m, Fc-b and Fc-h are more than high enough to guarantee quantitative complexation of the guest upon mixing with 1.0 equiv of CB7 at millimolar concentration levels.

2.3 Study of binding behavior from cyclic voltammetry (CV) and steady-state voltammetry

Figure 2.9 shows the contrast between the CV for Fc-b in the absence and in the presence of 1.1 equiv. of CB6 and CB7 respectively. In the absence of host (black), Fc-b was clearly observed to undergo a fast, reversible, one-electron oxidation process in aqueous solution. The presence of 1.1 equiv. CB6 leads to decreased current levels for the redox wave

(red line). Meanwhile the CV response shifts to slightly less positive potentials. Since the nitrogen atom with one positive charge is expected to interact with the carbonyl oxygen portal on CB6, the electron density redistribution at the ferrocene residue leads to such electrochemical behavior.

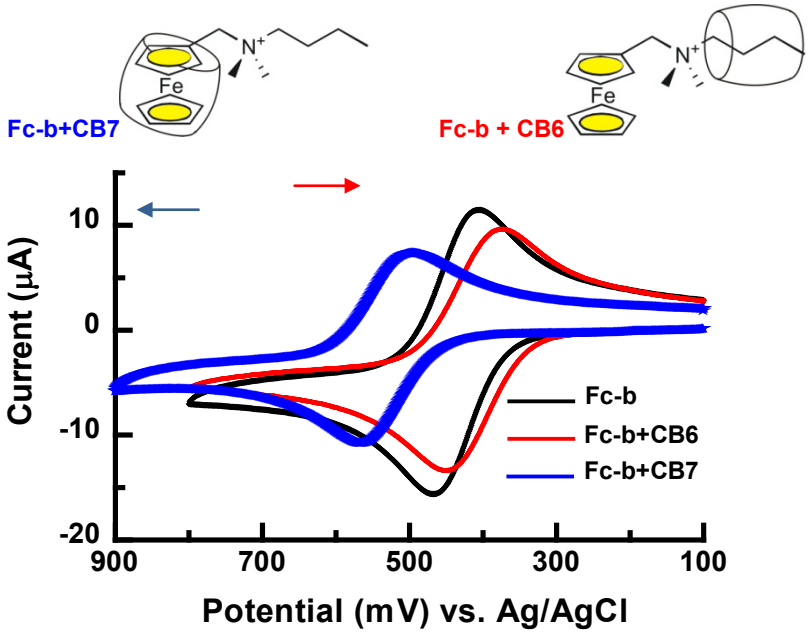

Figure 2.9 CV response on glassy carbon (0.071cm^2) of 1.0 mM Fc-b in the absence (black) and in the presence of 1.1 equiv. CB6 (red) and in the presence of 1.1 equiv. CB7 (blue). The aqueous solution also contains 0.1 M NaCl. Scan rate=0.1V·s^{-1}

On the other hand, the cyclic voltammetric (CV) behavior of guest Fc-b is dominated by the one-electron oxidation of the ferrocene residue as anticipated. As expected this electrochemical process is extremely fast, leading to reversible behavior in the CV experiments (**Figure 2.9**). Addition of 1.1 equiv of CB7 to the Fc-b solution fully converts the guest into its CB7 inclusion complex, which exhibits a more positive half-wave potential ($E_{1/2}$) for ferrocene oxidation and decreased current levels. This potential shift reveals that the guest

molecule interacts with CB7 on the ferrocene residue, which is in agreement with the ^{1}H NMR spectroscopic data. This behavior is identical to our reported observations with guest Fc-m in the presence of CB7. The CB7 complex is obviously bulkier than the free guest, and its diffusion to the electrode surface is slower, thus yielding smaller currents. The anodic shift in the $E_{1/2}$ value reflects the differential stabilization by CB7 of the reduced (ferrocene) form of the guest as compared to its oxidized (ferrocenium) form. It also means that the stability of the inclusion complex is decreased by oxidation of the ferrocene residue.

Similar voltammetric results were recorded with Fc-h as shown in **Figure 2.10**. The presence of CB7 leads to the $E_{1/2}$ shift to much more positive potentials. However, the reason of $E_{1/2}$ corresponding to the CV of Fc-h shift to less positive potentials in the presence of 1.1 equiv CB6 is the same as in Fc-b.

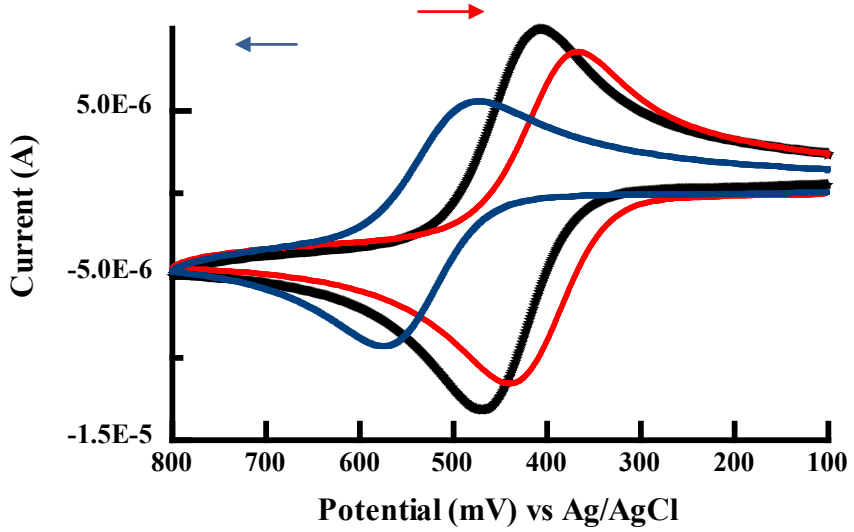

Figure 2.10 CV response on glassy carbon (0.071cm^2) of 1.0 mM Fc-h in the absence (black) and in the presence of 1.1 equiv. CB6 (red) and in the presence of 1.1 equiv. CB7 (blue). The aqueous solution also contains 0.1M NaCl. Scan rate=0.1V·s^{-1}

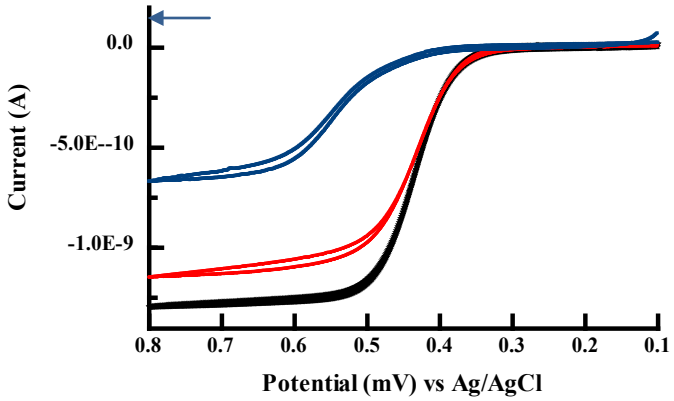

Figure 2.11 Steady-state voltammetry of 1.0 mM Fc-m in the absence (black) and in the presence of 1.1 equiv. CB6 (red) and in the presence of 1.1 equiv. CB7 (blue). The aqueous solution also contains 0.1 M NaCl. Scan rate=0.1V·s^{-1}

Interestingly, Fc-m shows very little difference of the $E_{1/2}$ in the absence or in the presence of CB6 although the current level decreases as that of Fc-b and Fc-h with CB6 complexes (**Figure 2.11**). It indicates that the interaction between Fc-m and CB6 is different compared to Fc-b or Fc-h with CB6.

We conclude that Fc-b and Fc-h both have an aliphatic chain with reasonable length, which is able to interact with CB6. The trimethyl ammonium group on Fc-m is different compared to the secondary amines of Fc-b and Fc-h.

2.4 Electrochemical kinetic studies of free guests Fc-m, Fc-b and Fc-h and their CB complexes

We also recorded electrochemical data of Fc-m, Fc-b and Fc-h cations binding with CB6 or CB7 assemblies and demonstrated that a considerable decrease in their rates of heterogeneous electron transfer takes place. With the diffusion coefficient (D_o) values obtained from Pulsed Gradient Spin Echo (PGSE) NMR spectroscopy and voltammetric

experiments we determine approximate values for the heterogeneous rate constants of electron transfer. [33] The inclusion effects mentioned in **2.3** will be demonstrated by the electrochemical behavior of 1.0 mM free guest Fc-m, Fc-b and Fc-h, and guest mixed with 1.1 equiv. CB6 host or mixed with 1.1 equiv. CB7 host. Each solution was investigated in aqueous 0.1 M NaCl by using a glassy carbon working electrode and Ag/AgCl reference electrode at variable scan rate in the range between 0.05 and 3.0 $V \cdot s^{-1}$.

2.4.1 Diffusion coefficient (D_o)

Diffusion coefficients are an effective method for probing molecular volumes and effective molecular radii. The diffusion coefficients of guests Fc-m to Fc-h and their complexes with CB6 or CB7 are measured by PGSE NMR experiments and from steady state voltammograms by using ultramicroelectrodes. The steady state voltammograms of Fc-b and its CB6 complex and CB7 complex are shown in **Figure 2.12**.

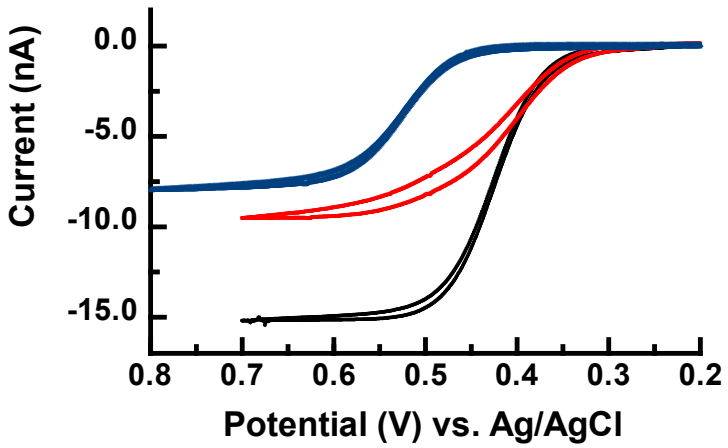

Figure 2.12 Steady-state voltammograms of 1.0 mM Fc-b in 0.1 M aqueous NaCl in the absence (black) and in the presence of 1.1 equiv of CB6 (red) and in the presence of 1.1 equiv of CB7 (blue) recorded using a 5-μm radius glassy carbon UME at a scan rate of 10 $mV \cdot s^{-1}$.

Figure 2.12 shows the steady-state voltammetric behavior of Fc-b in the absence of any cucurbituril and in the presence of 1.1 equiv CB6 (red) and 1.1 equiv CB7 (blue). The overall level of current is diminished by both CB hosts, due to the formation of guest-host complex, which increases the size of the molecular assembly and decreases its diffusion ability in aqueous media. We determined the D_o values using two separate techniques: (1) Voltammetric measurements with ultramicroelectrodes (UMEs) and (2) Pulse Gradient Stimulated Echo (PGSE) NMR measurements.

With 1.1 equiv CB6 (red) or CB7 (blue) present in the solution, the current levels for oxidation of Fc-b are substantially reduced, in agreement with the D_o values determined in the PGSE NMR experiments. In 0.1 M NaCl/D_2O solution and 0.1 M NaCl/H_2O solution for each technique, the difference of D_o values obtained can be taken into account by using the Stokes-Einstein equation:

$$D_o = k\,T\eta^{-1}/(6\pi r_h) \qquad \textbf{(1)}$$

Where r_h is the hydrodynamic radius of the diffusing species, k is Boltzmann's constant and T is the absolute temperature. Assuming that the hydrodynamic radius and temperature remain constant, we can write

$$(D_o)_1\eta_1 = (D_o)_2\eta_2 \qquad \textbf{(2)}$$

While the solution viscosity can be simply calculated as

$$\eta = B\rho t \qquad \textbf{(3)}$$

Where B is a calibration constant and ρ is the density of the solution and t is the flow time of the solution in an Ostwald capillary viscometer. We introduce the correction factor A

which can give the calibration on these diffusion coefficient data obtained from both measurements.

$$[A] = (\eta_2/\eta_1) = (\rho*t)_2 / (\rho*t)_1 = (\rho_2/\rho_1) * (t_2 / t_1) \quad \textbf{(4)}$$

As we know the ratio of the density of D_2O to that of water is 1.09:1.00, and the average flowing time ratio for them is 68.1:63 (5 ml solution @ 298 K), thus [A] = 1.09*(68.1/63) = 1.178

We can generally write that

$$D_o^{UME} = (1.178) \times D_o^{NMR} \quad \textbf{(5)}$$

It is shown that both techniques correlate well with one another, provided that viscosity corrections (to take into account viscosity differences in the two types of solutions used in these measurements) are properly applied. The measured diffusion coefficient values are given in **Table 2.1**.

The values in **Table 2.1** show all the expected trends. For instance, the D_o values decrease as the length of the aliphatic *N*-substituent increases, although this effect is more pronounced in going from methyl to butyl (Fc-m to Fc-b) than from butyl to heptyl (Fc-b to Fc-h). The CB7 complexes exhibit values considerably smaller than the free guests, reflecting the larger molecular volume and hydrodynamic radii of the former. The partial encapsulation of the guest by the CB7 host is also evidenced by the smaller dispersion of D_o values observed in the CB7 complexes as compared to the values measured with the free guests. Finally, the relative proximity of the values in the fourth column of the table to the experimentally determined ratio of viscosities [η(NMR)/η(UME) = 1.18] for the solutions used in both types

of experiments provides further validation to the internal consistency of the data set. From **Table 2.1**, we can conclude that the diffusion coefficients from both measurements are quite close after applying the correction factor [A] (1.178).

Table 2.1
Diffusion coefficients (D_o) ($\times 10^{-6}$ $cm^2 \cdot s^{-1}$) measured using UME steady state voltammetry and PGSE NMR spectroscopic techniques at 25°C.

Sample	D_o(UME)[a]	D_o(NMR)[b]	D_o(UME)/D_o(NMR)[c]
Fc-m	7.99	6.76	1.17
Fc-m+CB6	6.97	5.80	1.19
Fc-m+CB7	4.01	3.29	1.21
Fc-b	6.82	5.60	1.21
Fc-b+CB6	4.7	3.97	1.17
Fc-b+CB7	3.56	2.86	1.23
Fc-h	6.35	5.27	1.19
Fc-h+CB6	4.28	3.63	1.17
Fc-h+CB7	3.42	2.80	1.21

[a]Measured in 0.1 M NaCl from the voltammetric steady state current $i = 4nFD_oCr$, where $n = 1$ and $r = 5$ μm. (error ± 0.02-0.51)

[b]Measured in 0.1 M NaCl/D_2O. (error ± 0.04-0.20)

[c]Assuming identical hydrodynamic radii in both media, D_o(UME)/D_o(NMR) = η(NMR)/η(UME). Experimentally, the solution viscosity ratio was found to be 1.18 at 25°C.

2.4.2 The standard rate constants (k^o)

While the CV behavior of the free guests is clearly reversible (**Figure 2.9** and **Figure 2.10**) as evidenced by the peak-to-peak potential splitting (ΔE_p ~60 mV), the CV response of the CB7·Fc-b and CB7·Fc-h is clearly quasi-reversible (ΔE_p ~90 mV) at the relatively slow

scan rate used (100 $mV \cdot s^{-1}$). As a result of this observation, we decided to concentrate our attention on the determination of the standard rate constants (k^o) for the heterogeneous electron transfer reactions of the CB7 complexes.

$$\text{Fc-m} - e^- \rightleftharpoons \text{Fc}^+\text{-m}$$

$$\text{CB7}\cdot\text{Fc-m} - e^- \rightleftharpoons \text{CB7}\cdot\text{Fc}^+\text{-m}$$

Scheme 2.1 Electrochemical reactions involved in the one-electron oxidation of Fc-m and Fc-m in the presence of host CB7 (CB7·Fc-m).

The study of rates of electron transfer reactions is a fundamental issue in electrochemistry. Information on the kinetics of the reaction is of great importance for a basic understanding of the kinetics of heterogeneous electron transfer reactions. In this work, free Fc-m undergoes redox process to form Fc^+-m reversibly. Fc-m is oxidized to become Fc^+-m, while Fc^+-m is reduced to Fc-m at equilibrium. Meanwhile, CB7 complexed Fc-m (CB7·Fc-m) also undergoes a similar process. The schemes for such processes are shown in **Scheme 2.1**.

In order to address this matter we started with the simplest cationic guest, Fc-m, and carried out a scan rate study of its cyclic voltammetric response. Cyclic voltammogram experiments are performed with free Fc-m and CB7·Fc-m complex, respectively, at scan rates of 0.05, 0.1, 0.2, 0.5 and 1.0 $V \cdot s^{-1}$. The corresponding voltammetric results are shown in **Figure 2.13** and **Figure 2.14**.

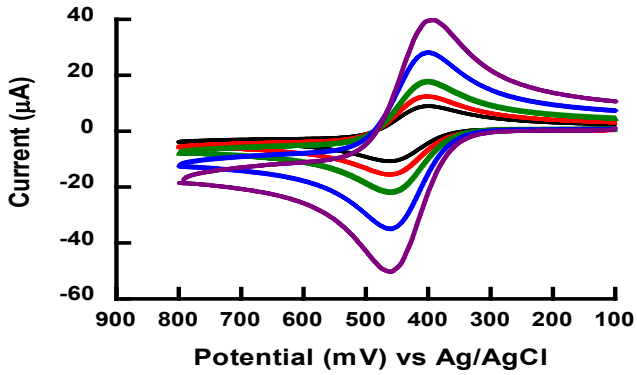

Figure 2.13 Cyclic voltammetric responses of 1.0 mM Fc-m on a glassy carbon electrode (0.071 cm^2) at scan rate of 0.05 (black), 0.1 (red), 0.2 (green), 0.5 (blue), 1.0 (purple) $V \cdot s^{-1}$ in 0.1 M $NaCl/H_2O$.

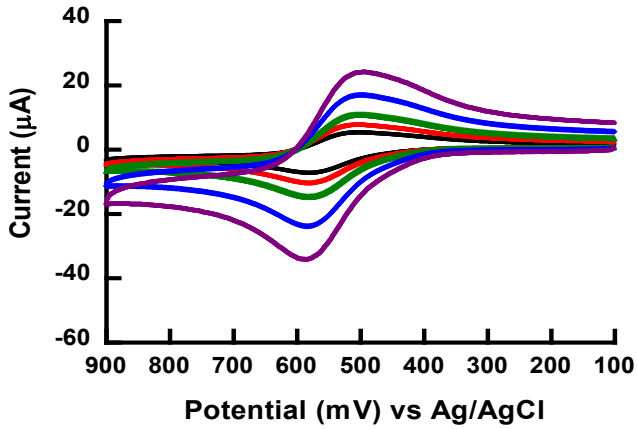

Figure 2.14 Cyclic voltammetric responses of 1.0 mM Fc-m with 1.1 equiv. CB7 on a glassy carbon electrode (0.071 cm^2) at scan rate of 0.05 (black), 0.1 (red), 0.2 (green), 0.5 (blue), 1.0 (purple) $V \cdot s^{-1}$ in 0.1 M $NaCl/H_2O$.

In agreement with previous findings, the free guest shows perfectly reversible behavior as evidenced by the invariance of the anodic and cathodic peak potentials as the scan rate increases from 50 $mV \cdot s^{-1}$ to 1.0 $V \cdot s^{-1}$ (**Figure 2.13**). In clear contrast with this behavior, the CB7·Fc-m complex shows quasi-reversible behavior, as the ΔE_p peak-to-peak splitting increases with the scan rate.

Clearly, these data indicate that encapsulation of the ferrocenyl unit in the CB7 cavity leads to a measurable attenuation of the electrochemical kinetics, that is, a decrease in the k^o

value. Nicholson's method can be utilized to measure the k^o values using data sets of the type shown in **Figure 2.13** and **Figure 2.14**. The voltammetric data show the comparative results of a scan rate study on the Fc-m/Fc^+-m and CB7·Fc-m/CB7·Fc^+-m redox couples. The electrochemistry of the inclusion complex CB7·Fc-m is slowed down compared to that of the free Fc-m. In the cyclic voltammetric experiments, the observed anodic and cathodic peak potentials corresponding to CB7·Fc-m/CB7·Fc^+-m are invariant as the scan rate is increased from 0.05 $V{\cdot}s^{-1}$ to 1.0 $V{\cdot}s^{-1}$. It reveals that free Fc-m undergoes electrochemical reversible characters while CB7·Fc-m is quasi-reversible process. We conclude that CB7 inclusion of Fc-m by CB7 affects its electrochemical kinetics.

Nicholson evaluated numerically the mathematical relationship between the dimensionless function Ψ and the potential difference between the anodic and cathodic peak potentials (ΔE_p). Therefore, from the experimentally determined ΔE_p value at a given scan rate (v), one can obtain the corresponding Ψ value and compute the standard rate constant k^o using equation 6

$$\psi = \frac{(D_o / D_R)^{\alpha/2}(RT)^{1/2}k^o}{(\pi nFDo\upsilon)^{1/2}} \qquad \textbf{(6)}$$

where D_o and D_R stand for the diffusion coefficients of the oxidized and reduced species, α is the charge transfer coefficient and the remaining terms have their usual meaning. As it is rather customary, we took $D_o = D_R$, $\alpha = 0.5$ and used the diffusion coefficients determined in the steady state voltammetric experiments to determine the k^o values. The resulting values are listed in **Table 2.2**.

Table 2.2 Standard rate constants for heterogeneous electron transfer (k^o in $cm \cdot s^{-1}$) and half-wave potentials ($E_{1/2}$ in V vs Ag/AgCl) measured in 0.1 M NaCl at 25°C.

k^o	Free guest	$E_{1/2}$ (V)	k^o (+CB6)	k^o (+CB7)	$E_{1/2}$ (V)
Fc-m	>0.8[a]	0.432	>0.8[a]	4.1×10^{-2}	0.542
Fc-b	>0.8[a]	0.437	3.8×10^{-2}	1.2×10^{-2}	0.527
Fc-h	>0.8[a]	0.440	2.4×10^{-2}	2.2×10^{-2}	0.523

[a]Reversible behavior was observed, with ΔE_p values in the range 57-62 mV.

k^o (+CB6) and k^o (+CB7) (error $\pm$ 0.002-0.005)

$E_{1/2}$ (error $\pm$ 0.002-0.008)

On the basis of the corresponding results in **Table 2.2**, the rate constant, k^o, could not be determined for any of these three guests and Fc-m mixed with CB6 in aqueous solution as expected. However, upon addition of 1.1 equiv. CB7 in 1.0 mM Fc-m aqueous solution, there was a noticeable decrease in k^o to 4.1×10^{-2} $cm^2 \cdot s^{-1}$. This is also in agreement with the conclusion obtained that the interaction of guest The k^o values in **Table 2.2** confirm that encapsulation of the ferrocene centers leads to a pronounced attenuation of electrochemical kinetics in this system. Clearly, inclusion inside CB7 decreases the value of k^o by a factor of 20 or more. This finding can be rationalized as the result of inclusion complexation keeping the ferrocene center further away from the electrode surface, due to the presence of a physical barrier between the two. In other words, the electroactive species diffuses towards the electrode surface and typically undergoes electron transfer from or near the so-called Outer Helmholtz Plane (OHP). The increase in the hydrodynamic radius of the ferrocene center upon encapsulation is thus equivalent to a displacement of the OHP away from the electrode surface, which is thought to be the key factor leading to the decreased rate for the

heterogeneous electron transfer process.

In summary, we have investigated the binding interactions between three different ferrocene compounds Fc-m, Fc-b, Fc-h and two CB hosts (CB6 and CB7). It provided a detailed description of these complexes behavior in an aqueous solution. These results lead to the conclusion that, the ferrocene centers are incorporated inside the cavity of CB7, and the alkyl chains are favorable to bind with CB6. Another important finding in this work is that their heterogeneous rates of electron transfer slow down when the ferrocene residue is included inside the CB7 cavity.

2.5 Neutral ferrocenyl guests

Ferrocene and its derivatives are well-known guests for complexation by CB7.[5] Electrochemical and NMR spectroscopic data demonstrated that CB7 binds preferentially to the ferrocene residue.[5] Here we extend this investigation to the complexation of CB7 and ferrocene derivatives with one or two 2-(2-methoxyethoxy)ethoxy chains.

In this part of the work, we use four neutral ferrocene derivatives M1, M2, D1 and D2 to investigate the effect of encapsulation by CB7 on the kinetics of heterogeneous and homogeneous electron transfer of the ferrocene center.

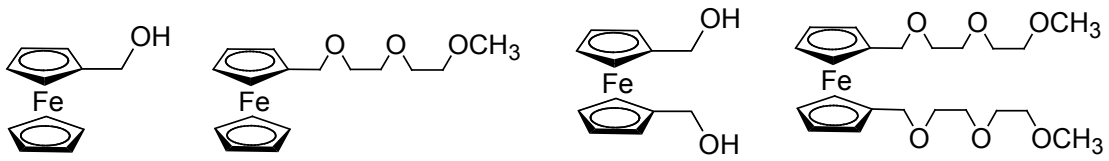

M1 M2 D1 D2

M1--Ferrocene methanol

M2--2-(2-methoxyethoxy)ethoxy]methyl-ferrocene

D1--Ferrocene dimethanol

D2--1,1'-Bis[[2-(2-methoxyethoxy)ethoxy]methyl]-ferrocene

M1 and D1 are commercial available, M2 and D2 are synthesized from M1 and D1 according to the reported procedures.[34]

2.6 Binding studies from ^{1}H NMR spectroscopic analysis

Complexes of M1 and CB7 were characterized by ^{1}H NMR spectroscopic analysis. To 2.0 mM M1 solution in 0.1 M NaCl D_2O, 0.5, 1.0 and 1.5 equiv CB7 were added and subsequent ^{1}H NMR analysis of the complex was performed after each addition. Compound M1 is anticipated to form an inclusion complex with CB7. The ^{1}H NMR spectra of M1 with increasing amount of CB7 in 0.1 M NaCl aqueous solution verifies this hypothesis.

As shown in **Figure 2.15** (a), The ^{1}H NMR spectrum of free M1 in 0.1 M NaCl-D_2O solution only contains a very broad resonance at ca. 4.25 ppm while there should be three proton signals corresponding to ferrocene residue protons, labeled as α, β and γ. This is a relatively unexpected result that probably reflects the slow rotating motions of the CH_2OH-bearing cyclopentadienyl ring around the main molecular axis. Upon addition of 0.5 equiv CB7 to this solution, we observe that proton resonance of signals α, β and γ all shifted to ca. 3.5 ppm in **Figure 2.15** (b), and the peak is even broader. The considerable CB7-induced upfield shift is consistent with inclusion binding of this guest by the CB7 host. Proton signals

corresponding to 1 shifted to ca. 3.95 ppm, showing that the methylene protons are also affected by the host CB7. We also observed that there is no splitting of the host signals at 0.5 and 1.0 equiv added, but in the presence of 1.5 equiv CB7 in the solution, CB7 signals at ca. 5.8 ppm split. This is due to the presence of excess host CB7. In one word, the binding between M1 and CB7 is strong, forming a stable complex in the presence of 1.0 equiv CB7.

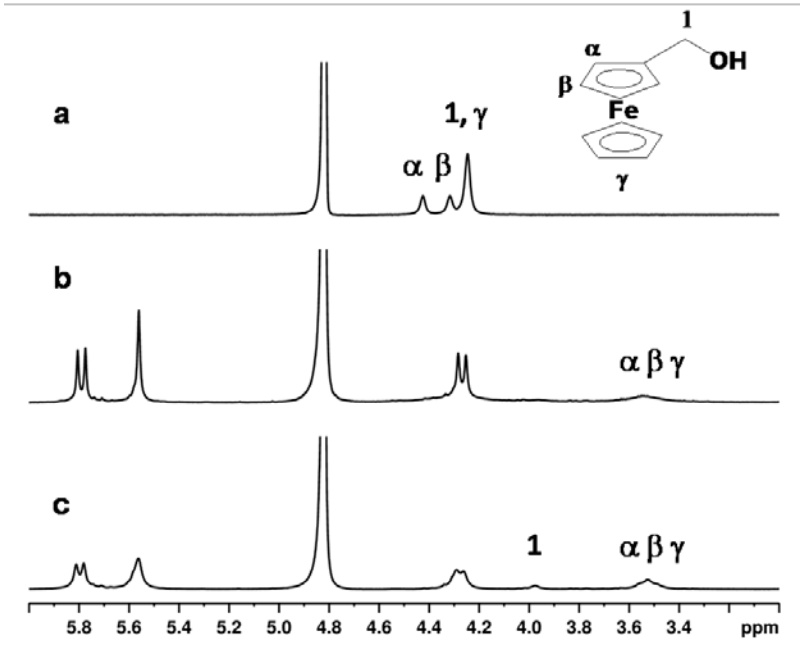

Figure 2.15 ^{1}H NMR spectra (400 MHz, 0.1 M NaCl/D_2O) of 2.0 mM M1 (a) in the absence and in the presence of (b) 0.5 equiv and (c) 1.0 equiv CB7.

Based on the titration study of M1 with CB7, we carried out similar titration experiments for M2 with increasing amount of CB7. M2 is synthesized from M1 with 1-bromo-2-(2-methoxyethoxy)ethane in the presence of base. With a longer chain covalently attached to the cyclopentadienyl ring of the ferrocene unit, M2 behaves similarly although the resonances are less broadened than in the case of M1. It is also anticipated to be strongly encapsulated in CB7 cavity with 1:1 host:guest ratio.

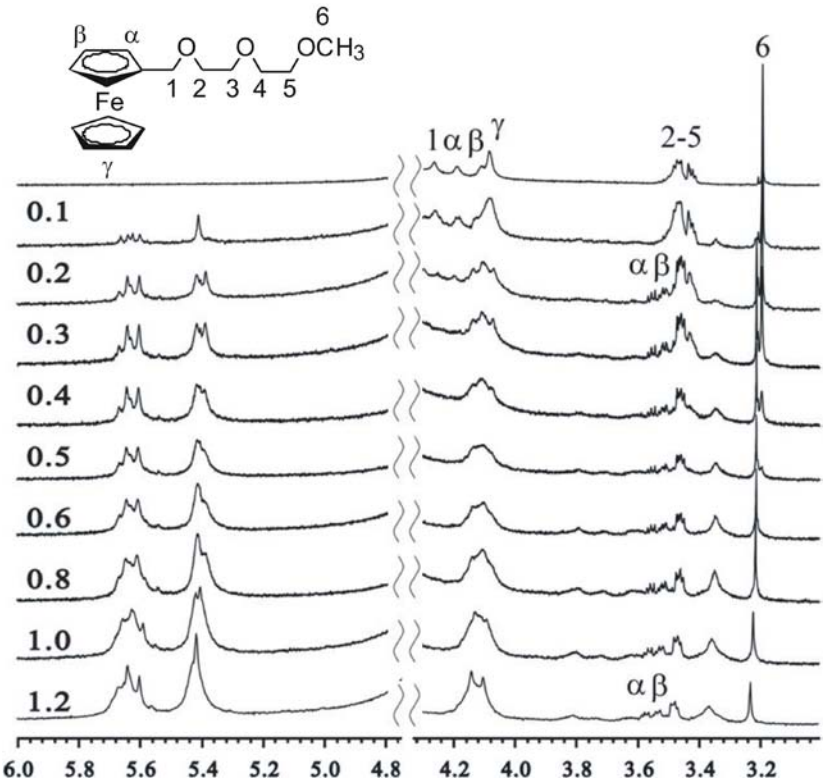

Figure 2.16 ^{1}H NMR spectra (400 MHz, 0.1 M NaCl/D_2O) of 2.0 mM M2 (a) in the absence and in the presence of (b) 0.5 equiv, (c) 1.0 equiv, and (d) 1.5 equiv CB7.

In **Figure 2.16** the CB7 induced upfield shifted proton signals corresponding to α,β and γ on the ferrocene residue disappeared upon addition of 1.0 equiv. CB7 in the solution. The guest ferrocene residue is fully encapsulated inside host CB7 cavity.

Ferrocene dimethanol, D1, is also a good guest molecule to interact with CB7 on the ferrocene residue and form a highly stable complex. We performed titration experiments of 2.0 mM D1 in 0.1 M NaCl solution by ^{1}H NMR spectroscopy. All conditions and parameters are the same as the experiments for M1 and M2 with CB7.

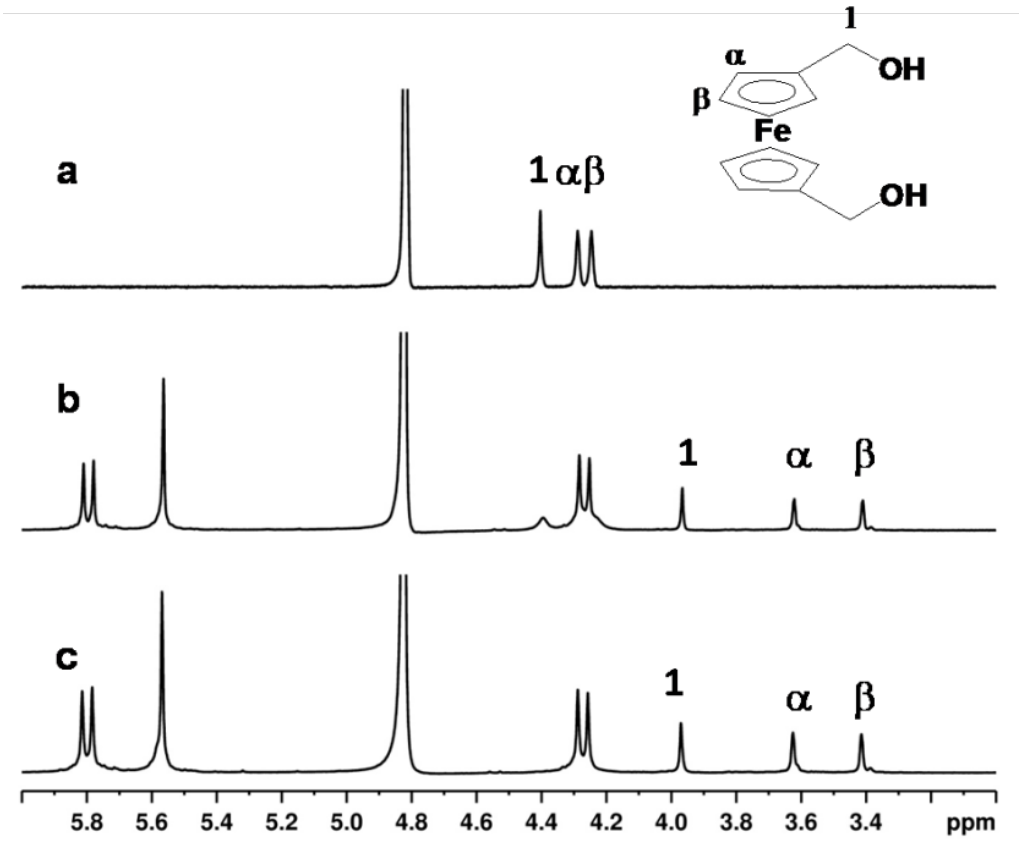

Figure 2.17 ^{1}H NMR spectra (400 MHz, 0.1 M NaCl/D_2O) of 2.0 mM D1 (a) in the absence and in the presence of (b) 0.5 equiv, (c) 1.0 equiv, and (d) 1.5 equiv CB7.

Compared to the result obtained from M1 with CB7 in ^{1}H NMR analysis, D1 also binds with CB7 strongly. In **Figure 2.17** we observe that proton signals α, β and 1 combined as one broad peak, this is due to the flexibility of the ferrocene residue. The proton signals all shift upfield from ca. 4.2 ppm to ca. 3.6 ppm, 3.4 ppm and 4.0 ppm, respectively. The binding stoichiometry is also 1:1 (host:guest) and in **Figure 2.17** (d) when extra amount of CB7 is added, both of the bound and free CB7 peaks appeared.

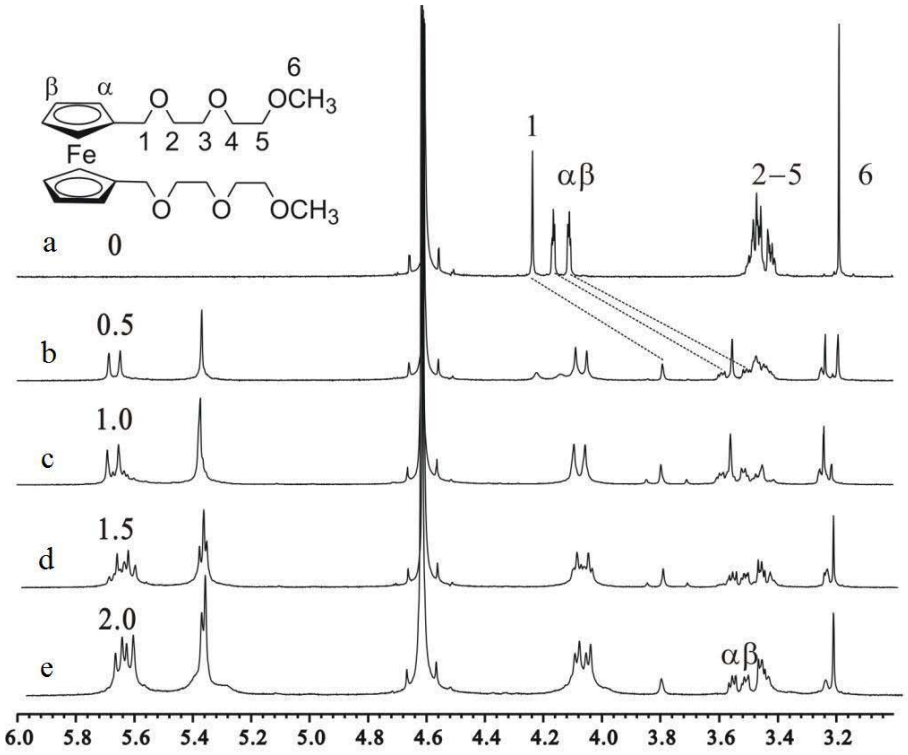

Figure 2.18 ^{1}H NMR spectra (400 MHz, 0.1 M NaCl/D_2O) of 2.0 mM D2 (a) in the absence and in the presence of (b) 0.5 equiv, (c) 1.0 equiv, and (d) 1.5 equiv CB7.

Upon addition of 0.5 equiv CB7 to free D2 aqueous solution [see **Figure 2.18** (a) and (b)] proton signals 1, α and β show significant complexation induced upfield shifts. The bound peaks start to grow at ca. 3.8 ppm, 3.55 ppm and 3.45 ppm respectively. The free peaks disappear as 1.0 equiv. CB7 is added to fully encapsulate D2 [**Figure 2.18** (c)]. However, proton signals corresponding to protons 2-5 at ca. 3.5 ppm do not shift too much, and the signal for proton 6 signals shifts slightly to lower field. These data demonstrated that the encapsulation between CB7 and D2 takes place on the ferrocene residue, and the chain is not affected a lot. We also observe that the proton signals corresponding to CB7 at 0.5 and 1.0 equiv does not show any splitting, which demonstrated that the molecular structure of such

supramolecular assembly is symmetric. In other words, the two hydroxyl chains are on different sides of the CB7 cavity.

2.7 Electrochemistry studies

To study the electrochemical kinetic behavior of these four guests and their complexes with CB7, we run a series of electrochemistry experiments of guests M1-D2 and their CB7 complexes by using voltammetric techniques, in aqueous solution containing 0.1 M NaCl as supporting electrolyte.

2.7.1 Free guests

All of these four guests contain a ferrocene residue. It is well known that ferrocene can undergo reversible one-electron redox behavior in cyclic voltammetry (CV). To investigate the electrochemical behavior, we run CV of M1-D2 under the same conditions. The CV plots are shown in **Figure 2.19**.

As seen in **Figure 2.19** (a), the anodic peak potential (Epa) and cathodic peak potential (Epc) of M1 do not shift significantly as the scan rates increase from 0.1 to 1.0 $V \cdot s^{-1}$ (data also shown in **Table 2.3)**. We conclude that in the absence of CB7, the free guest M1 undergoes a reversible redox process in the CV experiment. The heterogeneous ET kinetics of free M2, D1 and D2 are very fast, similar to that of M1. The potential data are shown in Table 1 for each of them.

Table 2.3 Epa, Epc and ΔEp of free M1 (a), M2 (b), D1 (c) and D2 (d), from top to bottom.

scan rate ($V \cdot s^{-1}$)	Epa (mV)	Epc (mV)	ΔEp (mV)
0.1	319	260	59
0.2	319	260	59
0.5	321	259	62
1	319	258	61

scan rate ($V \cdot s^{-1}$)	Epa (mV)	Epc (mV)	ΔEp (mV)
0.1	345	285	60
0.2	345	284	61
0.5	346	283	63
1	349	286	63

scan rate ($V \cdot s^{-1}$)	Epa (mV)	Epc (mV)	ΔEp (mV)
0.1	359	299	60
0.2	360	302	58
0.5	361	300	61
1	361	298	63

scan rate ($V \cdot s^{-1}$)	Epa (mV)	Epc (mV)	ΔEp (mV)
0.1	405	347	58
0.2	406	347	59
0.5	410	349	61
1	406	349	57

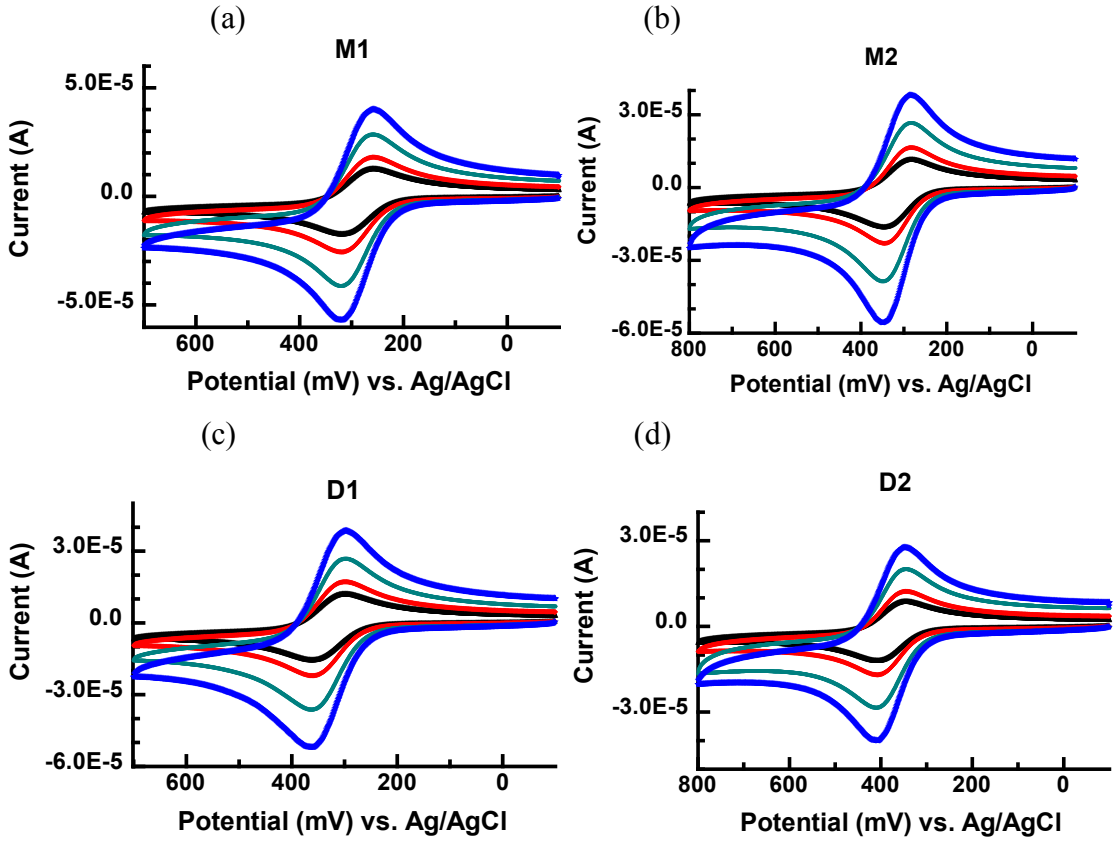

Figure 2.19 Cyclic voltammetric reponse of 1.0 mM M1 (a), M2 (b), D1 (c) and D2 (d) at scan rates of 0.1 (black), 0.2 (red), 0.5 (green), 1.0 (blue) $V \cdot s^{-1}$

2.7.2 CB7 complexes

We performed identical voltammetric experiments with M1-D2 in the absence and in the presence of host CB7, with 0.1M NaCl/H_2O as the supporting electrolyte. In **Figure 2.20**, at a scan rate of 0.1 $V \cdot s^{-1}$, CV of 1.0 mM M2 with increasing amount of CB7 essentially remains electrochemically reversible. The steady state voltammetry of M2 also demonstrated that the $E_{1/2}$ does not shift significantly. We calculated the diffusion coefficient (D_o) values from the steady-state voltammetric experiments.

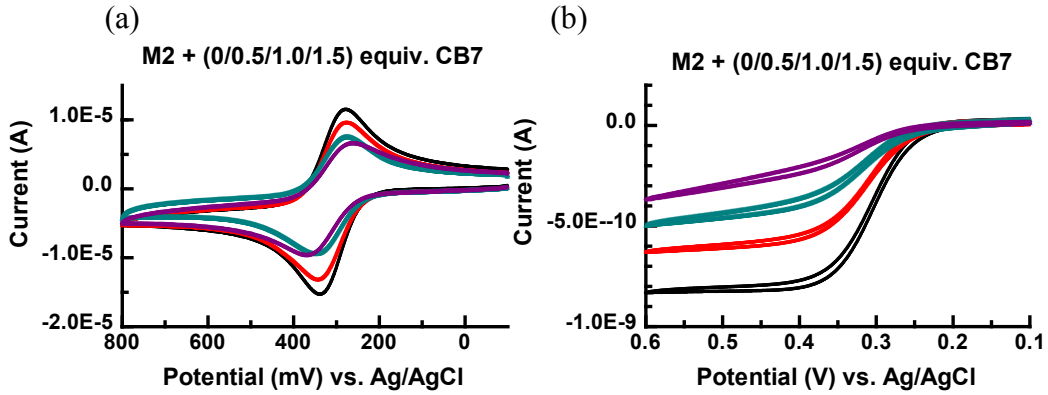

Figure 2.20 (a) Cyclic voltammetric repsonce and (b) steady state voltammetry of 1.0 mM M2 in the absence (black), and in the presence of 0.5 (red), 1.0 (green) and 1.5 equiv. (purple) CB7 in 0.1 M NaCl/H_2O.

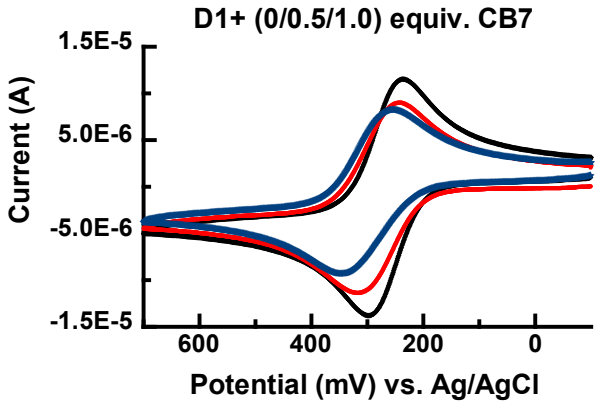

Figure 2.21 Cyclic voltammetric response of 1.0 mM D1 with 0 (black), 0.5 (red) and 1.0 equiv. (blue) CB7 in 0.1 M NaCl/H_2O at a scan rate of 0.1 $V \cdot s^{-1}$

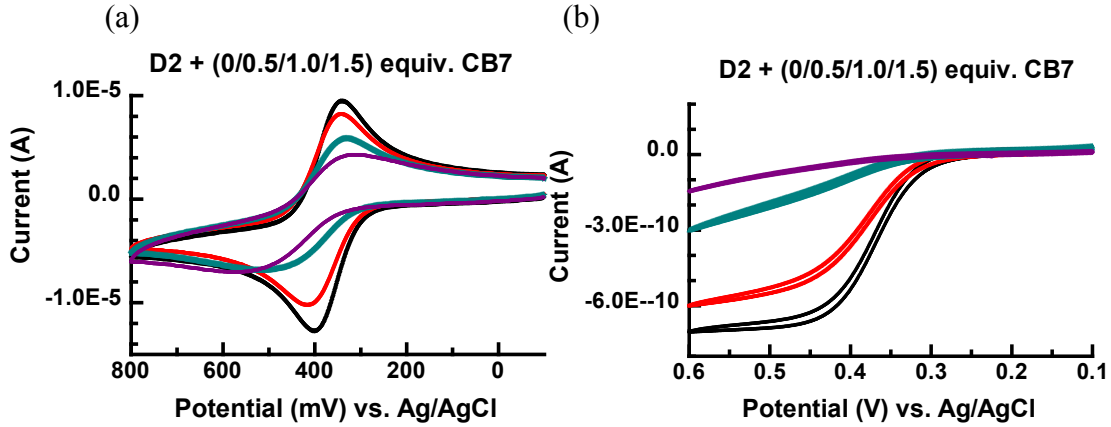

Figure 2.22 (a) Cyclic voltammetry and (b) steady state voltammetry of 1.0 mM D2 (black), with 0.5 (red), 1.0 (green) and 1.5 (purple) equiv. CB7 in 0.1 M NaCl/H_2O.

However, the electrochemical behavior of D1 is affected more clearly by the presence of CB7, as shown in **Figure 2.21**. The $E_{1/2}$ of the D1·CB7 complex (blue) is at more positive potential position compared to that of free D1 (black). While the small molecule D1 is observed being stabilized by CB7 as the $E_{1/2}$ shifted to more positive potential positions, the CV and steady-state voltammetry of D2 in **Figure 2.22** is very similar to that of M2.

It is interesting to compare the difference between the CV of CB7 complexed guests M1-D2 and that of the free guests. CV experiments were performed to analyze the electrochemical kinetics.

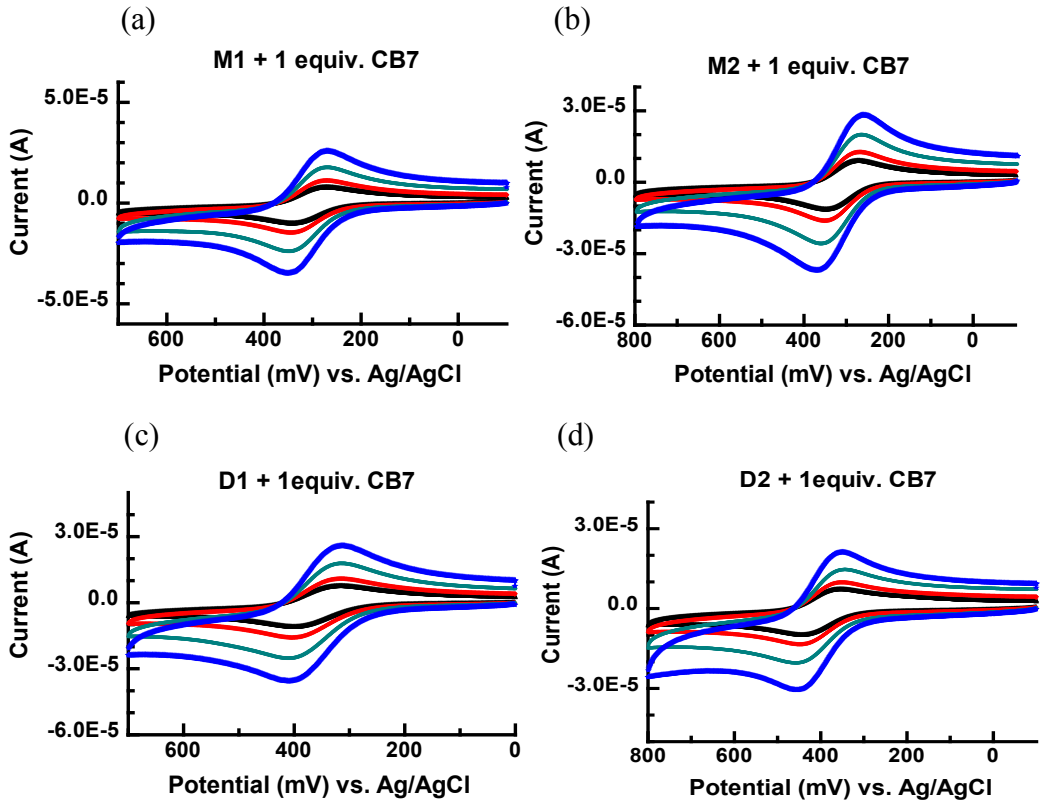

Figure 2.23 Cyclic voltammetric response of 1.0 mM M1 (a), M2 (b), D1 (c) and D2 (d) with 1.0 equiv. CB7 complexes at scan rate of 0.1 (black), 0.2 (red), 0.5 (green), 1.0 (blue) $V \cdot s^{-1}$

Table 2.4

(a) Kinetics data of 1.0 mM M1 with 1.0 equiv. CB7 at scan rate 0.1, 0.2, 0.5, 1 $V \cdot s^{-1}$.

scan rate ($V \cdot s^{-1}$)	**Epa (mV)**	**Epc (mV)**	**ΔEp (mV)**	**ψ**	**k^o ($cm \cdot s^{-1}$)**	**Do ($cm^2 \cdot s^{-1}$)**
0.1	341	275	66	4	2.69×10^{-2}	
0.2	341	274	67	3.5	3.32×10^{-2}	
0.5	347	274	73	1.96	2.94×10^{-2}	
1	347	274	73	1.96	4.16×10^{-2}	
					0.032785	3.65×10^{-2}

(b) Kinetics data of 1.0 mM M2 with 1.0 equiv. CB7 at scan rate 0.1, 0.2, 0.5, 1 $V \cdot s^{-1}$.

scan rate ($V \cdot s^{-1}$)	**Epa (mV)**	**Epc (mV)**	**ΔEp (mV)**	**ψ**	**k^o ($cm \cdot s^{-1}$)**	**Do ($cm^2 \cdot s^{-1}$)**
0.1	348	273	75	1.83	1.20×10^{-2}	
0.2	353	272	81	1.33	1.23×10^{-2}	
0.5	361	269	92	0.75	1.10×10^{-2}	
1	372	268	104	0.52	1.08×10^{-2}	
					0.01151	3.47×10^{-2}

(c) Kinetics data of 1.0 mM D1 with 1.0 equiv. CB7 at scan rate 0.1, 0.2, 0.5, 1 $V \cdot s^{-1}$.

scan rate ($V \cdot s^{-1}$)	**Epa (mV)**	**Epc (mV)**	**ΔEp (mV)**	**ψ**	**k^o ($cm \cdot s^{-1}$)**	**Do ($cm^2 \cdot s^{-1}$)**
0.1	400	321	79	1.5	1.00×10^{-2}	
0.2	404	319	85	0.96	9.07×10^{-2}	
0.5	410	318	92	0.75	1.12×10^{-2}	
1	409	317	92	0.75	1.58×10^{-2}	
					0.01153	3.61×10^{-2}

(d) Kinetics data of 1.0 mM D2 with 1.0 equiv. CB7 at scan rate 0.1, 0.2, 0.5, 1 $V \cdot s^{-1}$.

scan rate ($V \cdot s^{-1}$)	**Epa (mV)**	**Epc (mV)**	**ΔEp (mV)**	**ψ**	**k^o ($cm \cdot s^{-1}$)**	**Do ($cm^2 \cdot s^{-1}$)**
0.1	440	361	79	1.5	7.27×10^{-2}	
0.2	446	358	88	0.87	5.96×10^{-2}	
0.5	457	363	94	0.71	7.69×10^{-2}	
1	454	353	101	0.58	8.89×10^{-2}	
					0.007451	1.90×10^{-2}

In **Figure 2.23**, cyclic voltammetry experiments were performed of M1-D2 in the presence of 1 equiv. CB7 at variable scan rates. The electrochemical kinetics for each of them is much slower compared to that corresponding to the free guests, since the cyclic voltammetric response are not reversible (> 60 mV). These complexes have larger sizes and their mobility is limited. While the free guests with a ferrocene (Fc) moiety undergo fast one-electron oxidation to its cationic form, we found that the voltammetric behavior of the complexes is quasi-reversible, while it is fully reversible for the free guests. The half-wave potentials of complexes shift slightly to more positive values. This voltammetric behavior reveals that CB7 stablize the ferrocene through the complexation process. By Nicholson method we measured the heterogeneous rate constants, k^o, for each complex. The data are listed in **Table 2.4**.

The average k^o value of CB7·M1 complex is 0.033 $cm^2 \cdot s^{-1}$, which means the kinetics of such reversible process is much faster than that of CB7·M2 complex, 0.011. Meanwhile the k^o value of D2 is also lower than that of D1. Guest molecules M2 and D2, compared to the model molecules M1 and D1, has one or two 2-(2-methoxyethoxy)ethoxy]methyl chains. The molecular structure of CB7·M2 and CB7·D2 is less spherical compared to CB7·M1 and CB7·D1. The increased size of CB7·M2 and CB7·D2 leads to the slower kinetics behavior and lower value of heterogenous rate constants.

D and k^o of all these four CB7 complexes

sample	Avg k^o value($cm \cdot s^{-1}$)
M1	N/A
CB7·M1	3.28×10^{-2}
M2	N/A
CB7·M2	1.15×10^{-2}
D1	N/A
CB7·D1	1.15×10^{-2}
D2	N/A
CB7·D2	7.45×10^{-2}

Table 2.5 Electrochemical data of M1-D2 and their CB7 complexes at scan rate of 0.1, 0.2, 0.5, 1 $V \cdot s^{-1}$ in 0.1 M NaCl at 25°C.

compound	$E_{1/2}$ (V vs Ag/AgCl)	D^o ($cm^2 \cdot s^{-1}$)	k^o ($cm\ s^{-1}$)
M1	0.290±0.004	(7.81±0.29) x 10^{-6}	> 0.8
M1•CB7	0.308±0.002	(3.65±0.17) x 10^{-6}	0.033±0.002
M2	0.315±0.006	(5.41±0.19) x 10^{-6}	> 0.8
M2•CB7	0.311±0.008	(3.47±0.14) x 10^{-6}	0.012±0.002
D1	0.329±0.008	(6.65±0.04) x 10^{-6}	> 0.8
D1•CB7	0.361±0.006	(3.61±0.14) x 10^{-6}	0.012±0.002
D2	0.376±0.004	(3.70±0.28) x 10^{-6}	> 0.8
D2•CB7	0.401±0.002	(1.90±0.16) x 10^{-6}	0.008±0.002

2.8 Guests M2 and D2 binding to α-CD with/without CB7

To investigate how α-CD can affect the binding between CB7 and M2, we also performed voltammetric experiments with of free 1.0 mM M2 and 1.0 mM M2 with 1.0 equiv CB7 complex respectively, adding increasing amount of α-CD. From **Figure 2.24**(a) we observe that the CV curve corresponding to M2 without CB7 remains reversible when α-CD is

introduced in the solution. In **Figure 2.24**(b) the $E_{1/2}$ value of free M2 with 1-10 equiv α-CD clearly shifted to more positive potentials gradually. But in **Figure 2.24**(c), the current of the CV corresponding to M2 with 1.0 equiv. CB7 (orange) sharply decreased to a lower value. The added 1-10 equiv α-CD after adding CB7 has very little effect on the CV curve as shown in **Figure 2.24**(d). We conclude that the interaction between XB7 and M2 takes place on the ferrocene residue and such binding stabilize the complex. α-CD can form inclusion complex on M2's side chian in the absence and in the presence of CB7. However, once M2 is already bound to CB7, the effect from α-CD on CB7·M2 is not so strong. Since α-CD is not binding with M2 strongly, more than 1 equiv α-CD leads to the result that increasing amount of α-CD gradually helps the α-CD with M2 complex to be more stable. Meanwhile, M2 mixed with 1.0 equiv CB7 first and then mixed with more α-CD demonstrated that M2 is stabilized by the CB7 strongly. The ferrocene residue in the complex is shielded from outside so that the α-CD binding on the chain could not lead to any significant changes. The voltammetric results of D2 are similar to that of M2, while the effect of α-CD on D2 is not so strikingly as on M2. The CV and steady-state voltammetry plots are shown in **Figure 2.25**.

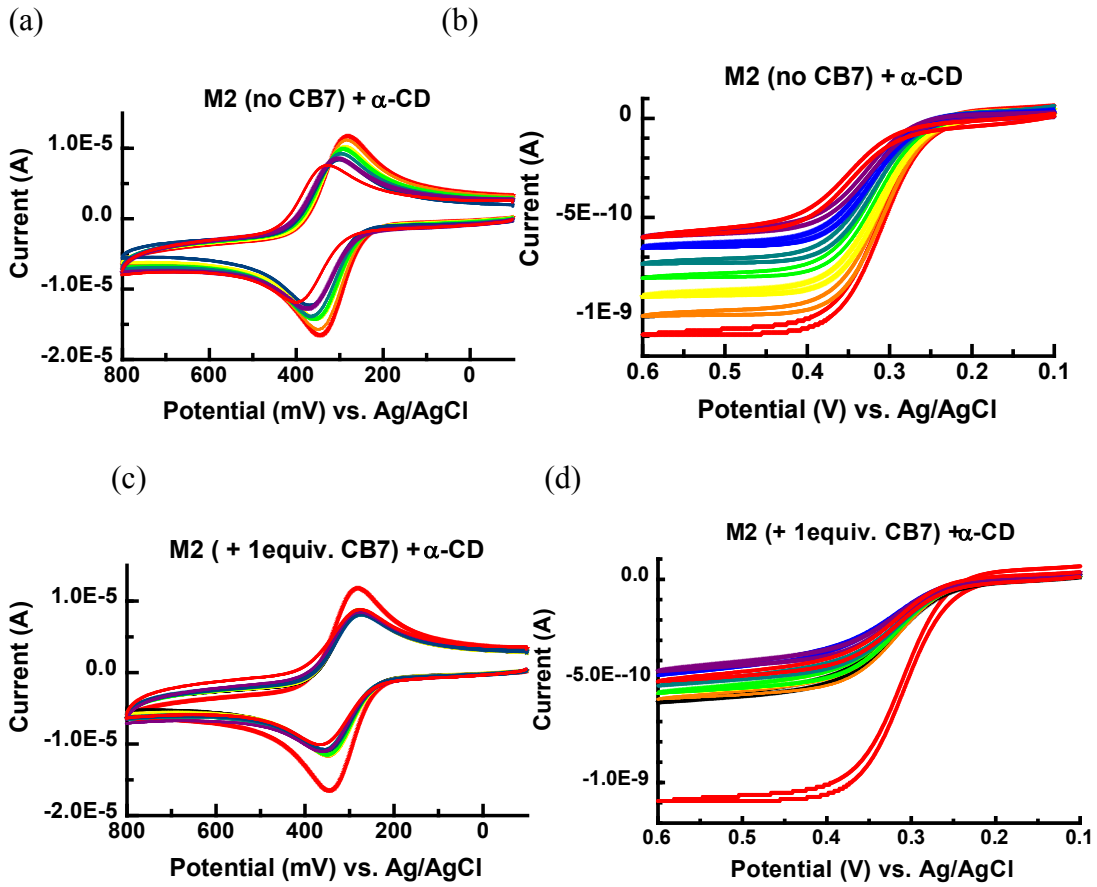

Figure 2.24

(a) CV of 1.0 mM M2 (red) in the presence of 1,2,3,4,5,6,10 equiv. [orange, yellow, light green, dark green, blue, purple, red] α-CD

(b) Steady state voltammetry of 1.0 mM M2 (red) in the presence of 1,2,3,4,5,6,10 equiv. [orange, yellow, light green, dark green, blue, purple, red] α-CD

(c) CV of 1.0 mM M2 (red) in the presence of 1 equiv. CB7(black) and in the presence of 1,2,3,4,5,6,10 equiv [orange, yellow, light green, dark green, blue, purple, red] α-CD

(d) Steady state voltammetry of 1.0 mM M2 (red) in the presence of 1 equiv. CB7(black) and in the presence of 1,2,3,4,5,6,10 equiv [orange, yellow, light green, dark green, blue, purple, red] α-CD

In conclusion, in the presence of 1.0 equiv CB7, $E_{1/2}$ potentials corresponding to M2 (or D2) in CV do not show a notable shift in potentials upon addition of α-CD. While in the absence of CB7, addition of α-CD in free M2 (or D2) can gradually stabilize the complex and lead to positive potentials shift of $E_{1/2}$. CB7 and ferrocene moiety has strong interaction and such

behavior result in the difference on the electrochemical properties analyzed of ferrocenyl group. In the cyclic voltammetric and steady-state voltammetric experiments, free M2 or D2 can be affected by the presence of α-CD gradually. While CB7·M2 or CB7·D2 seems locked by the CB7 host, and very little effect was observed as α-CD is present.

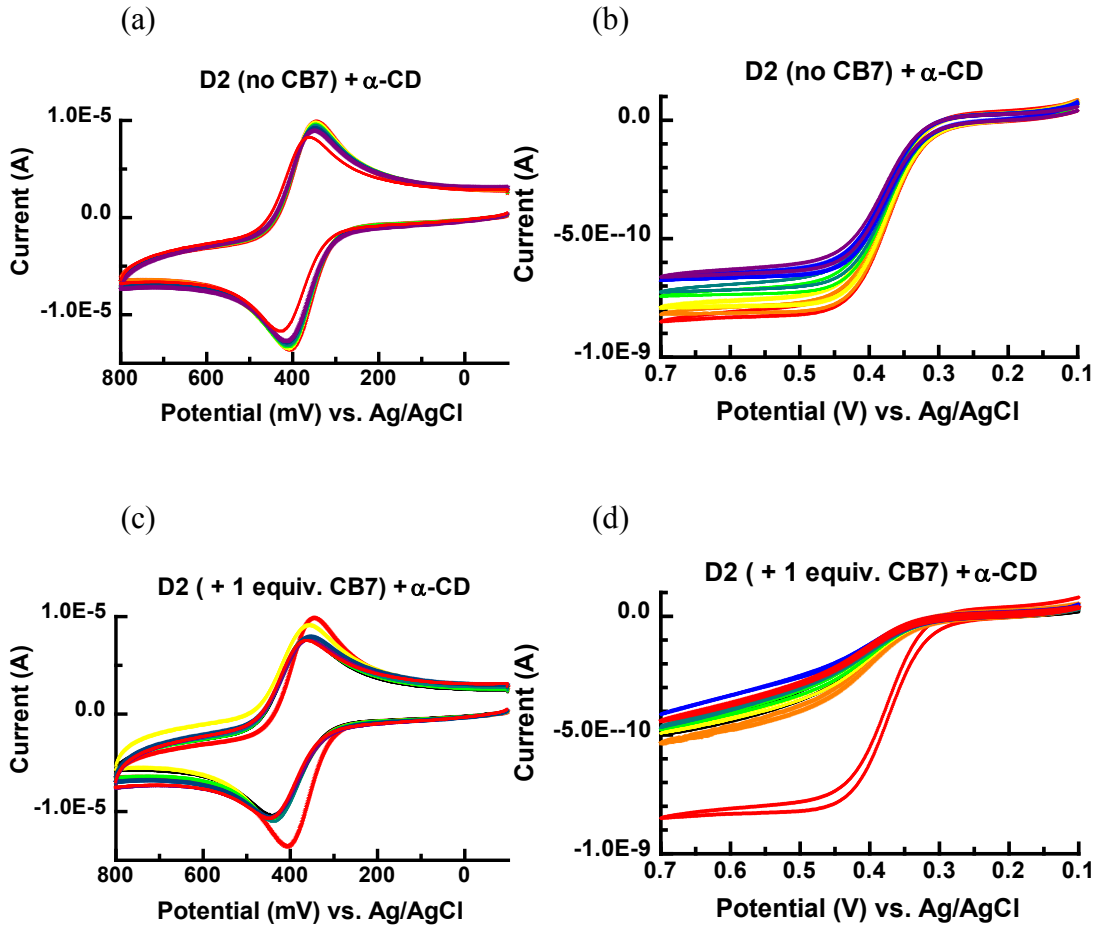

Figure 2.25

(a) CV of 1.0 mM D2 (red) in the presence of 1,2,3,4,5,6,10 equiv. [orange, yellow, light green, dark green, blue, purple, red] α-CD

(b) Steady state voltammetry of 1.0 mM D2 (red) in the presence of 1,2,3,4,5,6,10 equiv. [orange, yellow, light green, dark green, blue, purple, red] α-CD

(c) CV of 1.0 mM D2 (red) in the presence of 1 equiv. CB7(black) and in the presence of 1,2,3,4,5,6,10 equiv [orange, yellow, light green, dark green, blue, purple, red] α-CD

(d) Steady state voltammetry of 1.0 mM D2 (red) in the presence of 1 equiv. CB7(black) and in the presence of 1,2,3,4,5,6,10 equiv [orange, yellow, light green, dark green, blue, purple, red] α-CD

2.9 Competition experiments to measure binding constants (K)

Results from ^{1}H NMR studies on guests M1-D2 allow us to conclude that the main binding site is the ferrocenyl residue in all cases similarly. However, the known *K* value for the CB7·M1 complex in pure water is three orders of magnitude lower than that reported for CB7·Fc-m, and further substitution of the ferrocene center -along with the presence of 0.1 M NaCl in the solution- may lower the *K* values for CB7 complexation of guests M2, D1 and D2 substantially. Therefore, we felt that it was necessary to determine the *K* values with the M2-D2 in order to assess if simple mixing of 1.0 equiv of guest and 1.0 equiv of host at millimolar concentration levels would guarantee quantitative complex formation in the electrochemical experiments. We use ^{1}H NMR spectroscopy to measure values of K for CB7 towards M1-D2. Since K exceeds the experimental accessible range (up to 10^{4} M^{-1}), it is not possible to determine K values for such complexes by direct NMR measurements.[5] To determine the *K* values we resorted to competition experiments with the guest cobaltocenium (Cob^{+}). In the titration experiment of Cob^{+} with CB7, Cob^{+} display fast exchange kinetics relative to the NMR chemical shift time scale. The proton signals corresponding to Cob^{+} shift from ca. 5.58 ppm to ca. 4.91 ppm when Cob^{+} is fully encapsulated in the CB7 cavity, as shown in **Figure 2.26**.

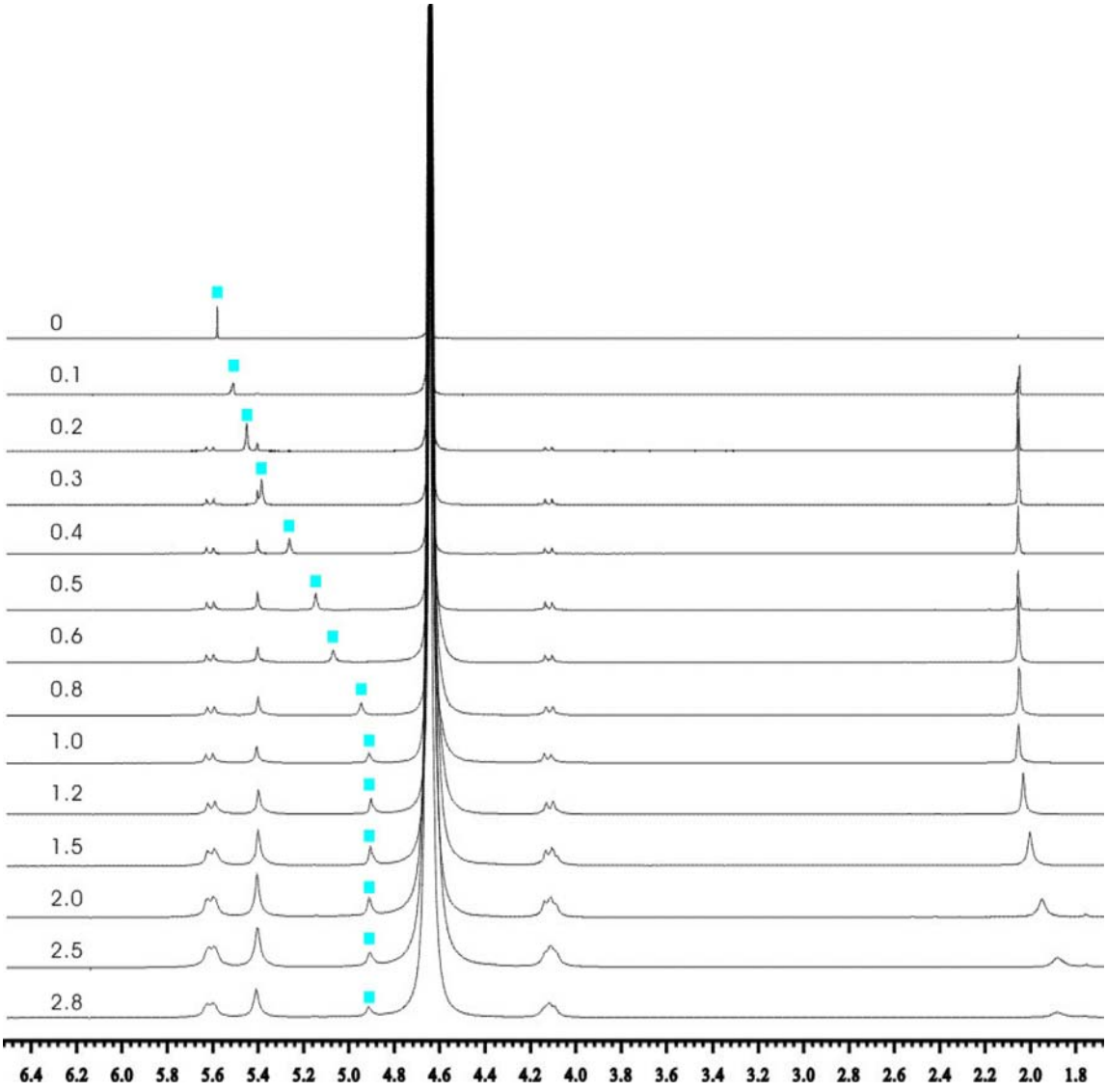

Figure 2.26 ^{1}H NMR spectra of 1.0 mM Cob^{+} with CB7, in 0.1 M $NaCl/D_2O$.

In the competition experiments (**Figure 2.27)**, the concentration of guest (G) Cob^{+} is fixed at 1.0 mM, while the concentration of competing guests (C) M1-D2 is 1-3 mM. Because host CB7 is known to bind strongly to G or C, we add less than 1.0 mM CB7 in the mixture to keep essentially all the CB7 complexed.

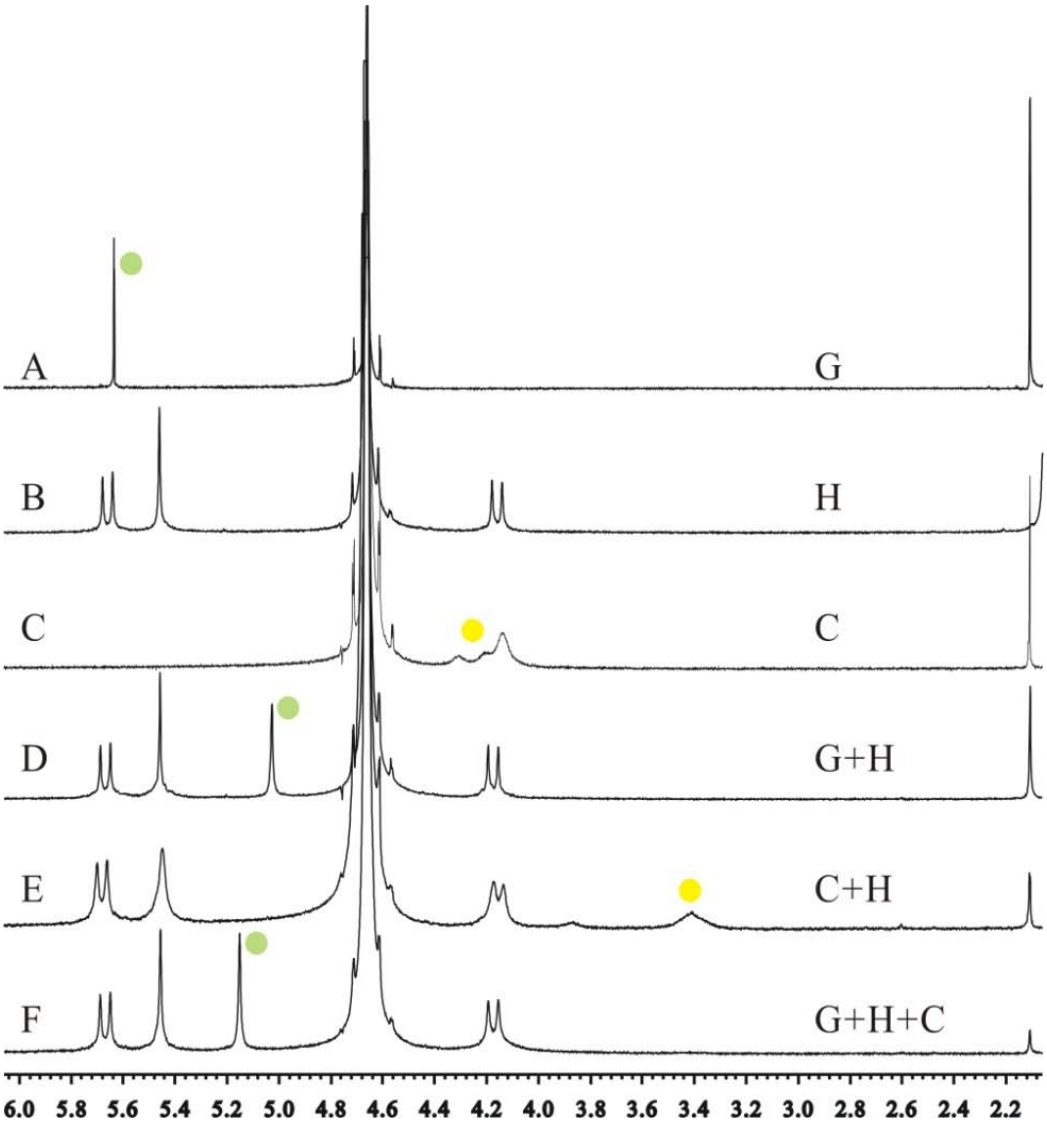

G -- Guest Cob^+; [Cob^+] = 1.0 mM
H -- Host CB7; [CB7] < 1.0 mM
C -- Competition Fc (M1); [Fc] = 1.0/2.0/3.0 mM

Figure 2.27 ^{1}H NMR competition experiment of 1.0 mM M1 and 1.0 mM Cob^+,with 0.72 mM CB7. All in 0.1 M NaCL/D_2O and calibrated with acetone peak at 2.05 ppm (except B, acetone may interact with CB7)
A – 1.0mM G, δ_f (chemical shift of free G) = 5.58 ppm;
B -- 0.72 mM H
C – 1.0mM C, δ_c (chemical shift of complexed G) = 4.97 ppm;
D – 1.0mM G + 0.72 mM H; [Cob^+] = 1.0 mM
E – 1.0mM C + 0.72 mM H
F – 1.0mM G + 0.72 mM H + 1.0mM C; [Cob^+] = 1mM; [CB7] = 0.72 mM.

We observe that the Cob^+ signals shifted upfield from ca. 5.58 ppm to ca. 4.91 ppm in **Figure 2.27**(A) and (D) when 0.72 equiv CB7 is added. However, the proton signals corresponding to Cob^+ shift downfield back to ca. 5.093 ppm as 1.0 mM C (M1) is introduced to compete with Cob^+. The equilibrium association-dissociation process can be written as:

[G and CB7 complexation]: $Cob^+ + CB7 \overset{K_g}{\rightleftharpoons} CB7 \bullet Cob^+$ **(7)**

[C and CB7 complexation]: $Fc + CB7 \overset{K_c}{\rightleftharpoons} CB7 \bullet Fc$ **(8)**

[Binding constant of G with CB7]: $$K_g = \frac{[Cob^+ \bullet CB7]}{[Cob^+] \bullet [CB7]}$$ **(9)**

[Binding constant of C with CB7]: $$K_c = \frac{[Fc \bullet CB7]}{[Fc] \bullet [CB7]}$$ **(10)**

In the mixture of G and C with CB7, the free CB7 concentration is same:

$$[CB7] = \frac{[Cob^+ \bullet CB7]}{[Cob^+] \bullet K_g} = \frac{[Fc \bullet CB7]}{[Fc] \bullet K_c}$$ **(11)**

The single proton resonance of this guest resonates at chemical shifts between 5.58 ppm (free) to 4.91 ppm (CB7-bound) and since this complex typically exhibits fast exchange in the NMR time scale the observed chemical shift, when both free and CB7-bound Cob^+ co-exist, is given by the following equation

$$\delta_{obs} = 5.58\, X_f + 4.91\, X_c$$ **(12)**

where X_f and X_c are the molar fractions of free and complexed guest, respectively. Therefore, if we mix known concentrations of Cob^+ and one of the neutral ferrocene guests M1-D2 with a concentration of CB7 insufficient to fully bind both guests, the observed chemical shift for the Cob^+ protons allows us to determine X_f and X_c, since $X_f + X_c = 1$, and thus the respective concentrations. Assuming that the concentration of free CB7 in equilibrium is negligibly small,

we can calculate the concentrations of free and bound ferrocenyl guest, which we can use to express the ratio of the two relevant equilibrium association constants. For instance, for compound M1 we can write:

$$\frac{K_{M_1}}{K_{Cob^+}} = \frac{[CB7\text{-}M1]\cdot[Cob^+]}{[M1]\cdot[CB7\text{-}Cob^+]} \quad \textbf{(13)}$$

where all the concentrations on the right side are at equilibrium. By using this straightforward procedure we measured the relative *K* values for CB7 binding of guests M1-D2 using K_{Cob}^{+} as a common reference. We determined the values of K_a for a series of competition experiments of M1-D2, using ^{1}H NMR technique, referenced to absolute binding constants of cobaltcenium with CB7 as reported ($K = 5.7\times10^9$ M^{-1}). The calculating procedures are listed below for one experiment and the K values calculated are in **Table 2.6**:

$$5.18 = X_f \cdot 5.58 + (1\text{-}X_f) \cdot 4.91$$

$$X_{freeCob+} = (5.18\text{-}4.91) / (5.58\text{-}4.9) = 0.413$$

$$[FreeCob^+] = X_{freeCob+} * [Cob^+] = 0.413 * 1\ mM = 0.413\ mM$$

$$[Cob\bullet CB7] = [Cob^+] - [Free\ Cob^+] = 1\ mM - 0.413\ mM = 0.586\ mM$$

$$[M1\bullet CB7] = [CB7] - [Cob^+\bullet CB7] = 0.96 - 0.586 = 0.373\ mM$$

$$[FreeM1] = [M1] - [M1\bullet CB7] = 1 - 0.373 = 0.626\ mM$$

$$\frac{0.586}{0.413\cdot K_g} = \frac{0.373}{0.626\cdot K_c}$$

$$\frac{K_c}{K_g} = 0.42$$

We obtained 0.32, 0.24, 0.13 and 0.063 for guest M1, M2, D1 and D2, respectively. We have measured the equilibrium association constant between Cob^+ and CB7 as 5.7 x 10^9 M^{-1} in 50 mM sodium acetate at 25°C. In the medium used in this work (0.1 M NaCl), the

corresponding *K* value should be smaller by a factor of 2-3. This means that the *K* values for guests M1-D2 must all clearly exceed 10^7 M^{-1}, which guarantees quantitative complexation with equal host and guest concentrations at millimolar levels.

Table 2.6 Binding constant of M1, M2, D1 and D2 with CB7 from competition experiments by using ^{1}H NMR technique:

Cob mM	M1 mM	CB7 mM	K/Kcob
1	1	0.96	0.42
1	1	0.72	0.38
1	1	0.48	0.4
1	2	0.96	0.18
1	2	0.72	0.21
1	2	0.48	overlap

Cob mM	D1 mM	CB7 mM	K/Kcob
1	1	0.96	0.17
1	1	0.72	0.18
1	1	0.48	0.23
1	2	0.96	0.06
1	2	0.72	0.08
1	2	0.48	0.05

Cob mM	M2 mM	CB7 mM	K/Kcob
1	1	0.96	0.37
1	1	0.72	0.35
1	1	0.48	0.4
1	2	0.96	0.11
1	2	0.72	0.11
1	2	0.48	0.11

Cob mM	D2 mM	CB7 mM	K/Kcob
1	2	0.96	0.07
1	3	0.96	0.04
1	3	0.72	0.08

2.10 Computational investigation of the CB7•D1 complex

The CB7 inclusion complexation of bi-armed guests **D1** and **D2** is interesting, as it offers two distinct structural possibilities for the resulting host-guest complex. Basically, the two ferrocenyl sidearms can protrude out of the host cavity through the same portal (*syn* 'conformation') or through different portals (*anti* 'conformation'). In principle, one may

anticipate that these two structures can be differentiated by NMR spectroscopy, as the doublet corresponding to the inner methylene bridge protons of CB7, may be sensitive to the two different chemical environments in the *anti* conformation. However, our own NMR spectroscopic data with the CB7•Fc-m, CB7•Fc-b and CB7•Fc-h complexes show that this is not always the case. In all of these complexes, the equatorial plane of symmetry of the CB7 host is lost and this lack of symmetry would be expected to yield nonequivalent inner methylene protons on the two sides of the cavity. While this is observed in the ^{1}H NMR spectrum of the first complex (CB7• Fc-m), it is not observed with the other two cationic complexes, for reasons that are unclear at this point. However, these experimental NMR data prompted us to look for other methods to assess the relative stabilities of the two forms (*syn*/*anti*) of the inclusion complexes of bi-armed guests D1 and D2. We decided to assess the stability of the *syn* and *anti* forms of the CB7•D1 complex using computational Density Functional Theoretical (DFT) methods. The floppy sidearms of guest D2 would create unnecessary complexity in these calculations, which justifies our exclusive computational focus on the CB7•D1 complex.

First, we optimized the *syn* and *anti* forms of CB7•D1 complexes at B3LYP/STO-3G* level in the gas phase. We manually varied the starting positions of the host-guest complexes and run full energy minimizations from each in order to locate the most stable complexes in both forms. After reaching the global minima of the complexes, we performed single point energy calculations, utilizing the same basic conditions but now in water to more accurately determine the binding energies. The completely optimized geometries of the

CB7•D1complexes (*syn* and *anti*) are shown in **Figure 2.28**.

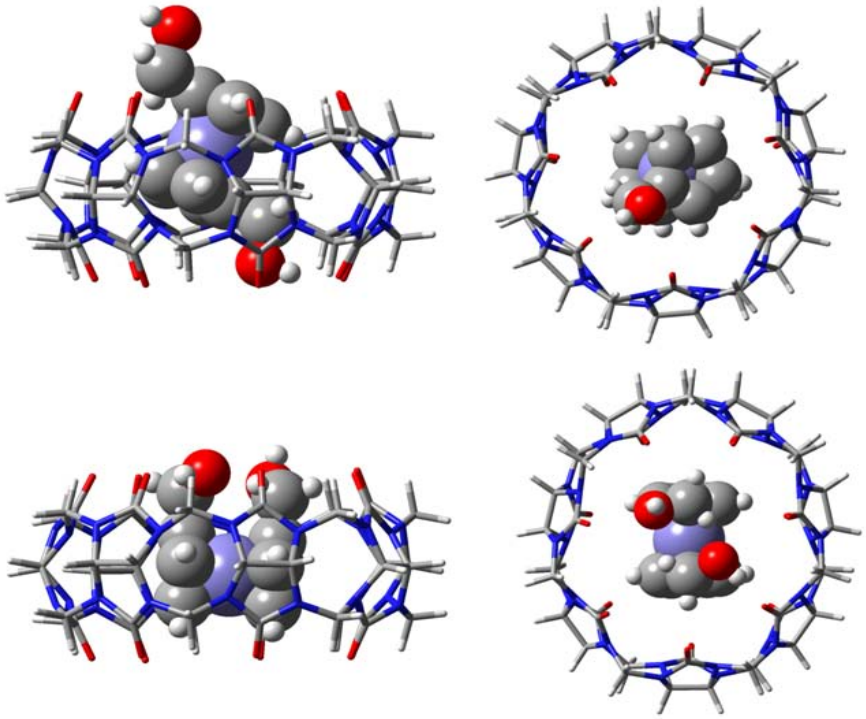

Figure 2.28 Side and top views of the *anti* (top) and *syn* (bottom) conformer minimized structures for the CB7•D1 complex (B3LYP/STO-3G*).

In the gas phase, as well as in water, compound D1 exists in the *syn* form rather than in the *anti* form, the former being more stable than the latter by ~3 kcal mol^{-1}. These results can be explained by possible interactions between the methanolic OH groups in free D1. In contrast, the *anti* form of the CB7•D1 complex is more stable than the corresponding *syn* form. This is mainly due to the possible steric problems arising between the CB7 carbonyl groups and the ferrocenyl methanolic OH groups, as both side arms are projecting out of the host cavity through the same portal in the *syn* form. The distortion of CB7 is more pronounced in the case of the *syn* form, as the host must accommodate both side arms on the same portal, leading to a complex with higher energy content. This is evidenced in the binding energies, as

the formation of the *anti* form of the complex releases -2 kcal mol^{-1}, whereas that of the *syn* form results in positive values. The calculated molecular structure and energy levels of D1 with CB7 are shown in **Figure 2.28** and **Table 2.7**.

First all the calculated data of ΔE is converted to kcal·M^{-1} by multiplying the conversion factor (627,5095), as shown in **Table 2.7**. The energy level between comp-d-p and free host CB7 (CB7-c) and free guest D1 (g-d-opt) are calculated by subtracting the values of comp-d-p with the values of CB7-c and g-d-opt. comp-d-p result -1.57 kcal·M^{-1} while comp-s gives a positive value, 7.29 Kcal/M. These results demonstrated that the comp-d-p has lower energy than the comp-s and comp-d-p is the more stable structure. The computation data is consistent with the ^{1}H NMR result that the guest D1 is inside the host CB7, with the two methyl-hydroxy groups interacting with the carbonyl rims on the cavity portals on each side.

In summary, we have described two different series of ferrocene derived compounds binding to CB6 or CB7. We investigated the noncovalent encapsulation in the cavity of host CBs by ^{1}H NMR measurements, electrochemistry experiments and computation studies. More specifically, we carry out electrochemical studies to investigate heterogeneous electron transfer processes for the free guests and their CB complexes. The results increase our understanding on how the heterogeneous electron transfer rates affected by the different complexes structures.

Table 2.7 Energy of formation data obtained using DFT theoretical computations (B3LYP/STP-3G*) to assess the relative stabilities of the anti and syn forms of the CB7•D1 complex.

B3LYP/ STO-3G*	ΔE, Kcal/mole		$\Delta E_{complex}$, Kcal/mole			
			ΔE_{com} - ΔE_{CB7}-$\Delta E_{7(anti)}$		ΔE_{com} - ΔE_{CB7}-$\Delta E_{7(syn)}$	
	gas	**water**	**gas**	**water**	**gas**	**water**
CB7•D1 (*anti*)	-3775030.32	-3775086.68	-3.84	-2.00	-1.35	1.07
CB7•D1 (*syn*)	-3775033.75	-3775080.62	-7.27	4.05	-4.77	7.12
CB7	-2608938.69	-2608988.24				
7(*anti*)	-1166087.79	-1166096.43				
7 (*syn*)	-1166090.29	-1166099.5				

B3LYP/ STO-3G*	ΔE, Kcal/mole		$\Delta E_{complex}$, Kcal/mole			
			ΔE_{com} - ΔE_{CB7}-$\Delta E_{7(anti)}$		ΔE_{com} - ΔE_{CB7}-$\Delta E_{7(syn)}$	
	gas	**water**	**gas**	**water**	**gas**	**water**
CB7•D1 (*anti*)	-3775030.32	-3775086.68	-3.84	-2.00	-1.35	1.07
CB7•D1 (*syn*)	-3775033.75	-3775080.62	-7.27	4.05	-4.77	7.12

2.11 Experimental

Materials:

CB6 and CB7 were prepared as reported by Day and co-workers. This host hydrates on standing and we found that it is necessary to determine its effective molecular weight before use. This was done by UV-Vis titration with a standard aqueous solution of cobaltocenium.[15]

Preparation of (Ferrocenylmethyl)trimethylammonium bromide:

Guest Fc-m ($FcCH_2N^+(CH_3)_3Br^-$) was prepared according to literature methods.[30] Fc-b and Fc-h is prepared by using the similar synthesis procedure for Fc-m, which was previously reported by our group.

Guests M1 and D1 were commercially available from Sigma Aldrich and M2 and D2 were prepared according to a literature report (**Scheme 2.2**). [34]

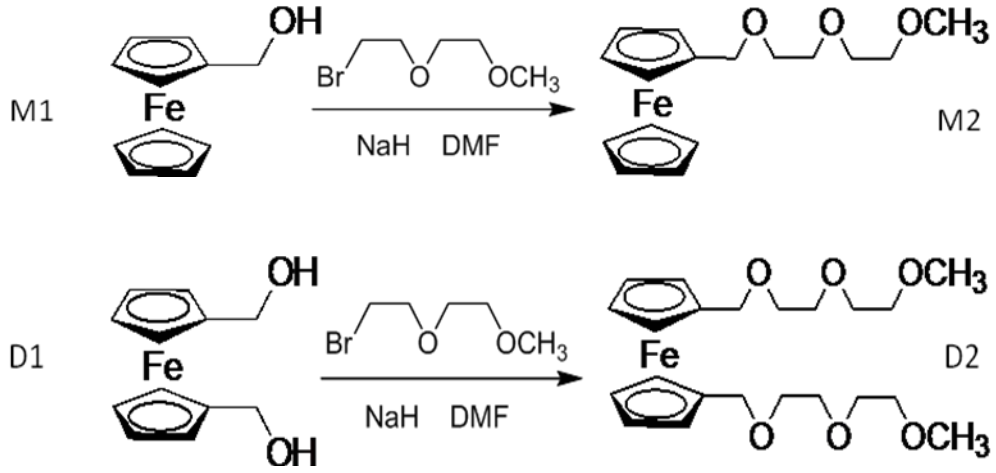

Scheme 2.2 Preparation of M2 and D2.

All other chemicals were of the best commercially available quality and used as received. The anticipated structures of all these compounds were confirmed by ^{1}H-NMR and MS (FAB).

Procedures:

NMR spectroscopic experiments:

Samples for ^{1}H NMR and PGSE NMR spectroscopy were prepared with D_2O (99.99%D) purchased from Cambridge Isotope Laboratories. The sample solutions also contained 0.1 M NaCl to create experimental conditions similar to those employed in electrochemical experiments. In some cases, sodium acetate was added to the sample solution and the methyl acetate protons used to provide calibration to measure the concentration of other species in the D_2O (Cambridge Isotopes) solution. NMR spectroscopic experiments were recorded in Bruker Avance instruments (400 or 500 MHz).

Electrochemical experiments

The electrochemical experiments were recorded with a BAS 100W system. A single compartment glass cell was used for all voltammetric experiments. Typically the cell was fitted with a glassy carbon working electrode (0.071 cm^2), a Pt or W auxiliary electrode, a Ag/AgCl reference electrode and nitrogen inlet Teflon tubing. Nitrogen gas was purified before use and bubbled through the solution to remove oxygen gas before the measurements. During the voltammetric measurements, nitrogen flow was maintained above the solution to minimize re-dissolution of oxygen. The working electrode was polished on a soft, felt surface using

alumina powder (0.05 μm) and water as the lubricant. Before use the working electrode surface was rinsed extensively with water and sonicated to remove any particulate left from the polishing. In some voltammetric experiments we used a 5 μm diameter carbon fiber ultramicroelectrode (BAS) as the working electrode.[10, 33]

Computational experiments:

The computational experiments were performed by using computational density functional theoretical (DFT) methods. The molecular models of *syn* and *anti* forms of CB7 complexes were optimized at the B3LYP/STO-3G* level and were manually adjusted the starting positions to run full energy complexes in both forms. Single point energy calculations were performed after the calculating reached global minima of the complexes, both in gas phase and water.

Chapter 3

REVERSIBLE CONTROL ON THE BINDING AFFINITY BETWEEN CB7 AND FERROCENE GUESTS

3.1 Cucurbit[n]uril binding to ferrocene derivatives

Among the family of cucurbit[*n*]uril (CBn) hosts, cucurbit[7]uril (CB7) is an excellent host for ferrocene and its derivatives as reported in the last few years. The molecular cavity of CB7 can reach high binding affinities with ferrocene guests in aqueous solution. Previous study in our group demonstrated the formation of inclusion complexes between ferrocene and CB7.[15] Two years later, the complexformed by a cationic ferrocene derivative, (ferrocenylmethyl)trimethylamine (**1**), and CB7 was reported to have an equilibrium association constant (*K*) of 4 x 10^{12} M^{-1} in pure water at 25°C.[10] This led to the investigation of the inclusion complex formed between a dicationic ferrocene derivative (**2** in **Figure 3.1**) and CB7. The equilibrium association constant measured between the CB7 host and the dicationic guest is extremely high (10^{15} M^{-1}).

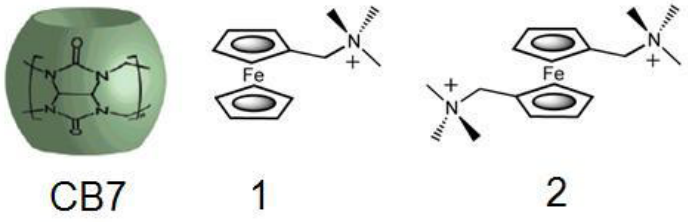

Figure 3.1 Structures of the cationic ferrocene guest (**1**) and dicationic ferrocene guest (**2**) and CB7 (*n* =7) host that partner to form inclusion complexes with high stability.

3.2 Two ferrocene guests with reversible protonated behavior controlled by pH

Ferrocene derivatives are well studied in the supramolecular binding with CB7. Our previous work on these complexes has focused on the determination of structures and thermodynamic stabilities of the CB7 complexes. We have also studied the voltammetric behavior of some water-soluble ferrocene derivatives. The presence of CB7 always results in the shift of half-wave potential ($E_{1/2}$) in cyclic voltammetry corresponding to the ferrocene guests and thus behavior illustrates the formation of the CB7-induced complex.

For instance, the half-wave potential ($E_{1/2}$) for electrochemical oxidation of the ferrocene residue in **1** shifts ca. 100 mV to more positive values in the presence of 1.0 equiv CB7. This means that the one-electron oxidation of ferrocene is thermodynamically hindered by encapsulation inside the CB7 cavity. It also means that the equilibrium association constant of the CB7 complex decreases by 1-2 orders of magnitude upon oxidation of the ferrocene residue. In contrast to this, similar voltammetric experiments with the neutral ferrocene derivative, hydroxymethylferrocene (guest M1 in Chapter 2), revealed that the $E_{1/2}$ value experiences a modest anodic shift of only ca. 10 mV upon complexation by CB7.

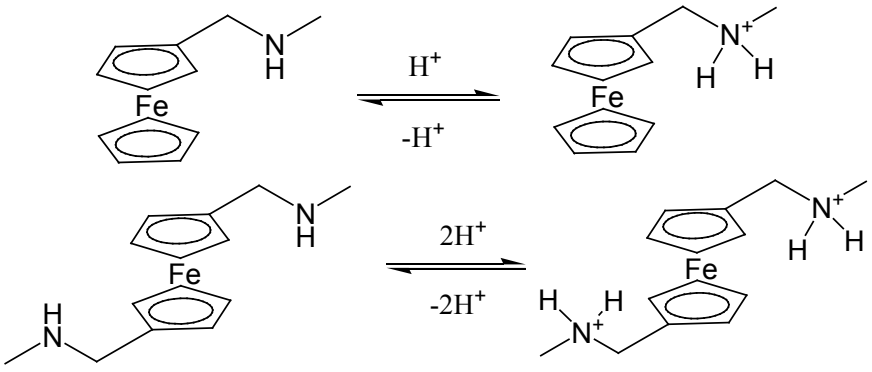

Scheme 3.1 Reversible protonation and deprotonation process of MFc and DFc controlled by pH.

Therefore, to develop methods based on simple chemical transformations to substantially weaken the binding affinity between CB7 and ferrocene guests is becoming of great interest. In order to address this issue, we choose ferrocene derivatives MFc and DFc as guests in our study. As shown in **Scheme 3.1**, both guests are deprotonated in basic solutions, while they are cationic in acidic solutions.

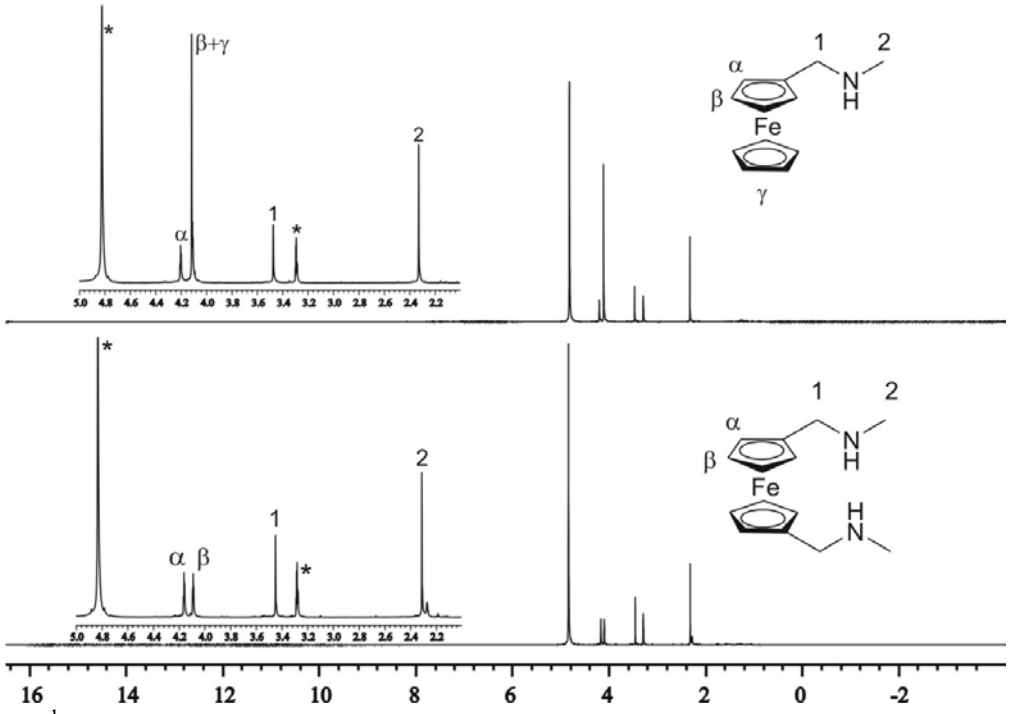

Figure 3.2 ^{1}H NMR spectra (400 MHz) for MFc and DFc in deuterated methanol. [The symbol ***** denotes the signals for the water and methanol protons.]

The ^{1}H NMR spectra of pure guests MFc and DFc are shown in **Figure 3.1**. We anticipated that their binding affinity with host CB7 may be a function of solution pH and this issue will be studied by ^{1}H NMR spectroscopy and voltammetric spectroscopic experiments.

3.3 ^{1}H NMR spectroscopic binding studies

3.3.1 In pH<7 solution

The binding interactions of the cationic ferrocene derivative **1** and **2** with the CB7 host in aqueous solution have already been described in Chapter 2. The resulting inclusion complex is highly stable and CB7 is believed to include the ferrocenyl unit in its cavity, while the positively charged nitrogen is located close to the center of one of the cavity portals, generating favorable ion-dipole interactions with the carbonyl groups at the cavity opening.

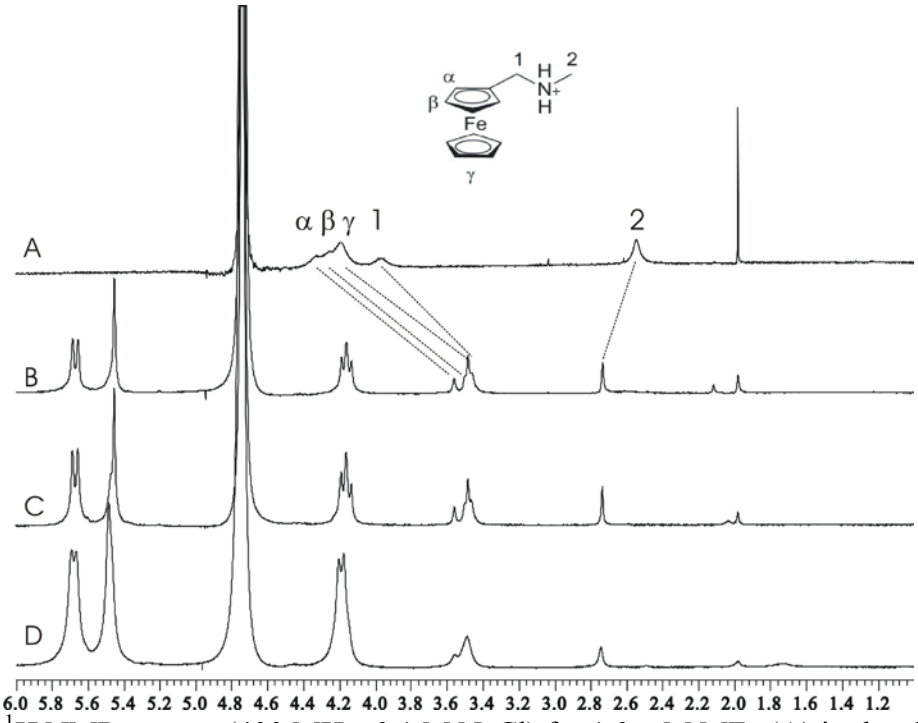

Figure 3.3 ^{1}H NMR spectra (400 MHz, 0.1 M NaCl) for 1.0 mM MFc (A) in the absence and in the presence of (B) 0.5 equiv, (C) 1.0 equiv and (D) 1.5 equiv CB7 in DCl/D_2O solution at pH 1.0. (The sharp peak at ca. 2.0 ppm denotes the signal for the acetone protons as standard reference for calibration.)

In DCl-D_2O solution at pH 1.0, MFc is protonated and thus positively charged, which is very similar to **1** in structure, the corresponding binding constant is expected to approach

10^{12} in pure water at 25°C. Complexes formed between guest MFc and CB7 were characterized by ^{1}H NMR spectroscopy. We performed titration experiments of 1.0 mM MFc upon addition of CB7 at 0.5, 1.0 and 1.5 equiv, respectively. For instance, **Figure 3.3** shows the ^{1}H NMR spectra data of free guest MFc and of the bound complex with CB7 in acidic solution.

In acidic solution, the presence of 0.5 equiv CB7 (**Figure 3.3** B) leads to a pronounced upfield shift of the ferrocene protons (α, β and γ), while the signals corresponding to the protons on the ternary methyl chain (2) shift downfield. This pattern of complexation-induced shifts reveals that the ferrocenyl unit is included by CB7, while the side chain remains outside the cavity. The chemical exchange is slow in the NMR time scale. MFc binds to CB7 with binding strength similar to **1** (Chapter 2). The methylene protons (1) that bridge the ferrocenyl unit to the nitrogen shift upfield along with the ferrocenyl protons, providing clear evidence that they are all fully included by CB7. The 1:1 binding stoichiometry is confirmed by NMR in **Figure 3.3** C. Upon addition of 1.0 equiv CB7 to the solution leads to the disappearance of the free MFc proton signals, corresponding to the ferrocene residue at ca. 4.4 ppm and the methyl protons (2) at ca. 2.5 ppm. The splitting peaks of CB7 at ca. 4.2 ppm in **Figure 3.3** C demonstrated that the inclusion complex structure is unsymmetric.

We also performed similar titration experiments with DFc in acidic solution by ^{1}H NMR spectroscopy (**Figure 3.4**). This guest is anticipated to bind CB7 strongly since both of the amino groups are expected to be protonated. We observed that, similarly to dicationic ferrocene guest **2** (**Figure 3.1**), DFc exhibits remarkably strong binding affinity to CB7.

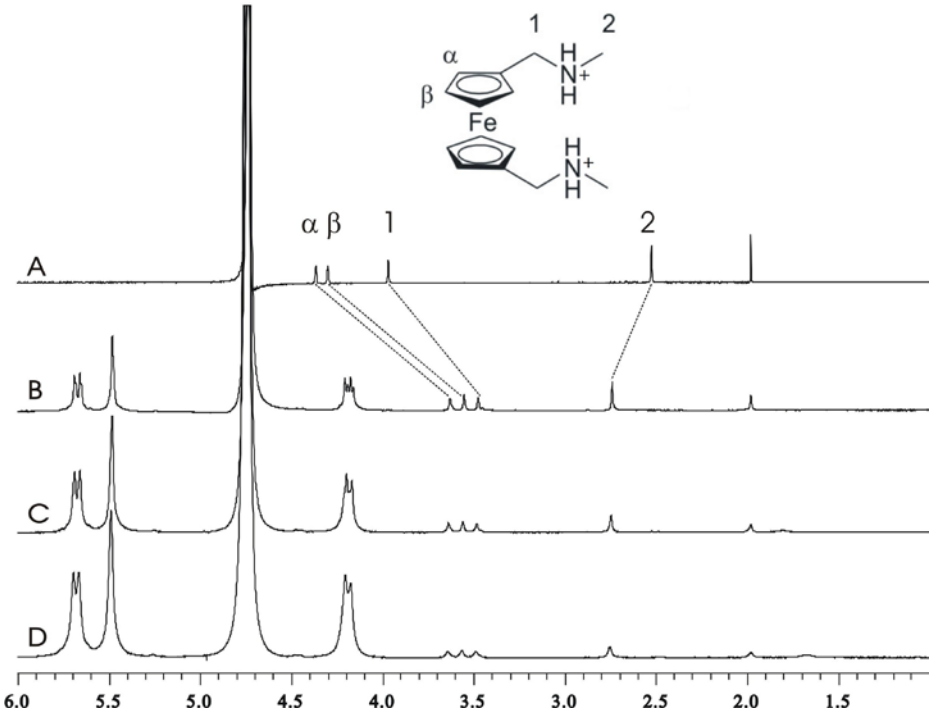

Figure 3.4: ^{1}H NMR spectra (400 MHz, 0.1 M NaCl) of 1.0 mM DFc in the absence (A) and in the presence of 0.5 equiv (B), 1.0 equiv (C) and 1.5 equiv (D) CB7 DCl/D_2O solution at pH 1.0. (The sharp peak at ca. 2.0 ppm denotes the signal for the acetone protons as standard reference for calibration.)

3.3.2 In pH>7 solution

However, at higher pH, once deprotonation of the amine groups is achieved (**Scheme 3.1**), the binding constants are expected to decrease, if ion-dipole interactions between the ammonium groups and the carbonyl portals of the host play a substantial role. ^{1}H NMR spectra of MFc in basic solution, borax buffer at pH 10.0, in the absence and in the presence of CB7 are shown in **Figure 3.5**.

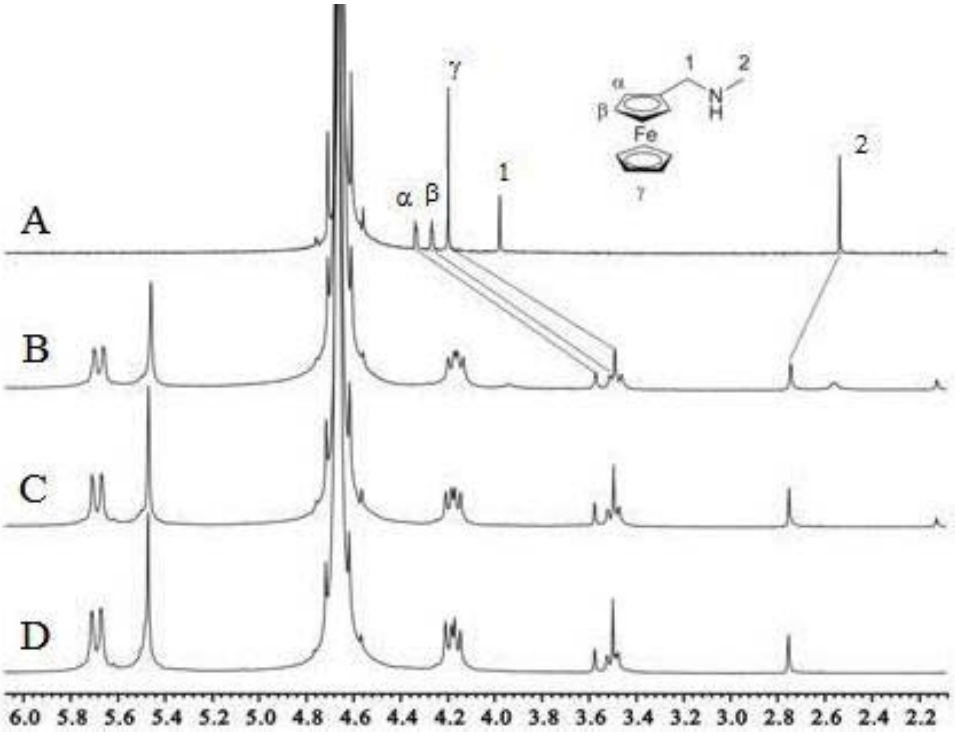

Figure 3.5 ^{1}H NMR spectra (400 MHz, 0.1 M NaCl) for 1.9 mM MFc (A) in the absence and in the presence of (B) 0.5 equiv, (C) 1.0 equiv, and (D) 1.5 equiv CB7 in borax buffer pH = 10.0.

Here we also investigated the binding interactions of the MFc and DFc with CB7 in basic solution and found very similar results as those in acidic solution (**Figure 3.5** and **Figure 3.6**). For instance, **Figure 3.5** shows ^{1}H NMR spectroscopic data on the interaction of CB7 and MFc, which suggests that the binding interactions between the MFc and CB7 in borax buffer are similar to which previously observed in pH 1.0 DCl solution. However, in **Figure 3.5** B, the free proton resonances corresponding to 1 and 2 are not so broadened as in **Figure 3.3** B. However, we can not conclude that the binding interactions of both of them with host CB7 in pH 1.0 solution are stronger than those in pH 10.0 environment from the 1H NMR data.

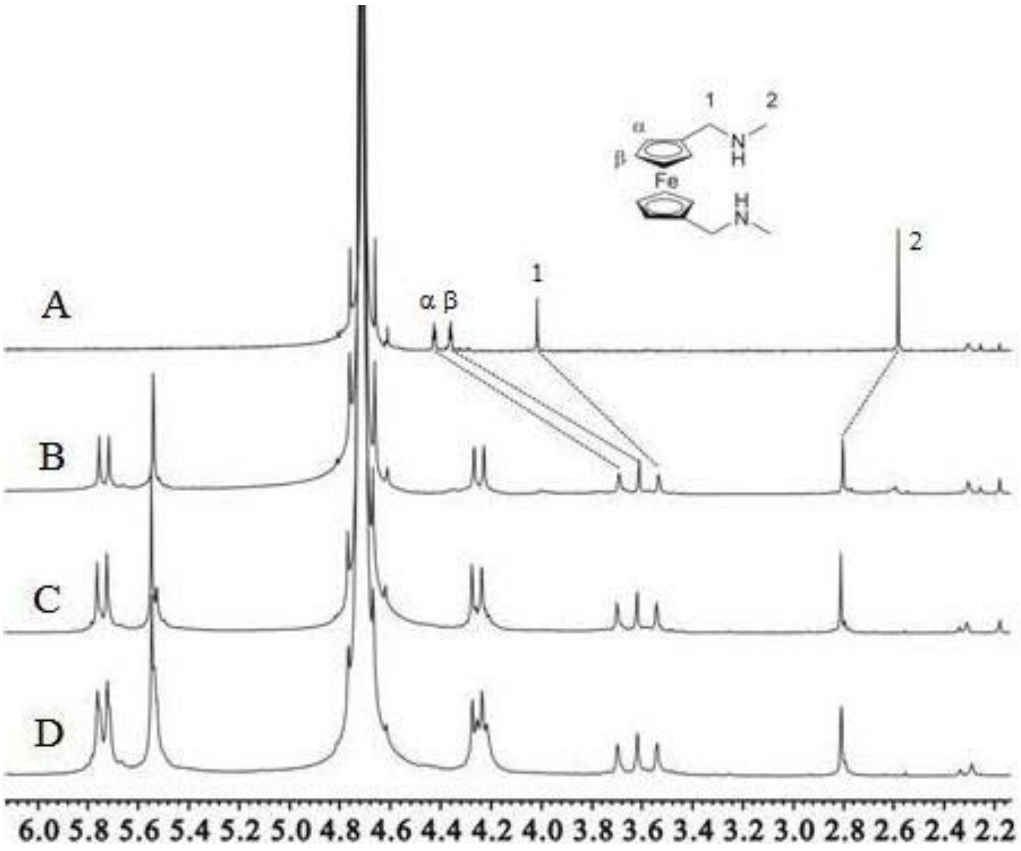

Figure 3.6 ^{1}H NMR spectra (400 MHz, 0.1 M NaCl) for 1.9 mM DFc (A) in the absence and in the presence of (B) 0.5 equiv, (C) 1.0 equiv, and (D) 1.5 equiv CB7 in borax buffer pH = 10.0.

From the ^{1}H NMR spectroscopic data obtained in **Figure 3.6**, we observed that CB7 binds on the ferrocene residue, too. The extremely high association equilibrium constant of the complex formed between guest MFc and CB7 in 0.1 M NaCl water solution and the strong similarities of the NMR spectroscopic data obtained in binding studies between the host and DFc strongly imply that the *K* values in 0.1 M NaCl for both guests are more than high enough to guarantee quantitative complexation of the guest upon mixing with 1.0 equiv of the host at

millimolar concentration levels. Besides, we observed several minor peaks between ca. 2.2 to ca. 2.4 ppm, which may be the proton resonances of the amino protons on the side chains of DFc and trace amount acetone in the basic solution.

Besides, an important issue in the binding of DFc with CB7 is the possibility of obtaining two types of complexes (represented in **Figure 3.7**), which we will refer here as anti and syn, for simplicity. Dicationic guest, **2** (**Figure 3.1**), is known to form anti complexes, as anticipated from the electrostatic repulsions that would be present in the syn form.

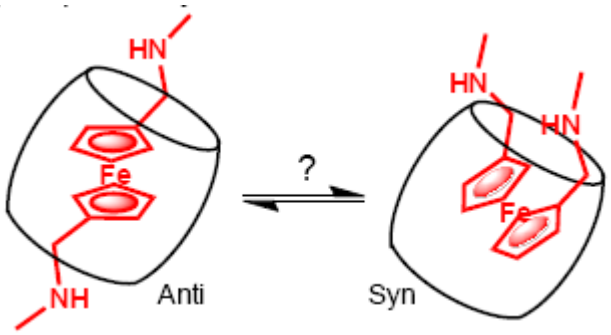

Figure 3.7 Anti and syn forms of the complex between CB7 and deprotonated DFc.

The presence of anti or syn complexes can be readily detected in ^{1}H NMR spectroscopic experiments, as the host's equatorial plane of symmetry is lost in the syn complex. This plane of symmetry remains in the anti complex. Therefore, the observed pattern of ^{1}H NMR resonances for the complex is an excellent diagnostic tool for this purpose. From the data shown in **Figure 3.6** B, we conclude that the only possible complex formed is anti form.

3.4 Voltammetric investigation of the CB7 complexes

The binding system contains another 'handle' (**Scheme 3.2**) that we will also explore as a potential method to decrease the binding affinity. In both CB7·**1** and CB7·**2**, we have shown that the stability of the complexes decreases upon one-electron oxidation of the ferrocene center. Therefore, we will also investigate the voltammetric behavior of CB7·MFc and CB7·DFc as a function of solution pH to asses what is the effect of one-electron oxidation on the stability of these complexes in all their forms, depending on the state of protonation of the guest. We anticipate that the combination of basic conditions and one-electron oxidation may decrease the K value by several orders of magnitude.

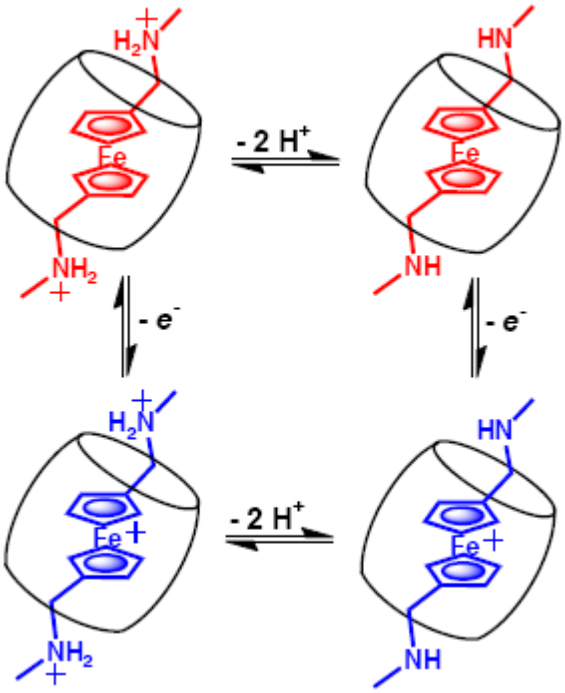

Scheme 3.2: Scheme illustration of DFc protonated and deprotonated in the cavity of CB7 undergoes a two-electrons redox process. Relevant proton and electron transfer equilibria affecting the stability of CB7·DFc.

3.4.1 In acidic buffer or solution (pH=4 for MFc, pH=1 for DFc)

In pH 4.0 acetate buffer, MFc is protonated and therefore the anticipated cyclic voltammetric (CV) behavior of guest MFc is dominated by the one-electron oxidation of the ferrocene residue. As expected this electrochemical process is extremely fast, leading to reversible behavior in the CV experiments as the black curve. (**Figure 3.8**)

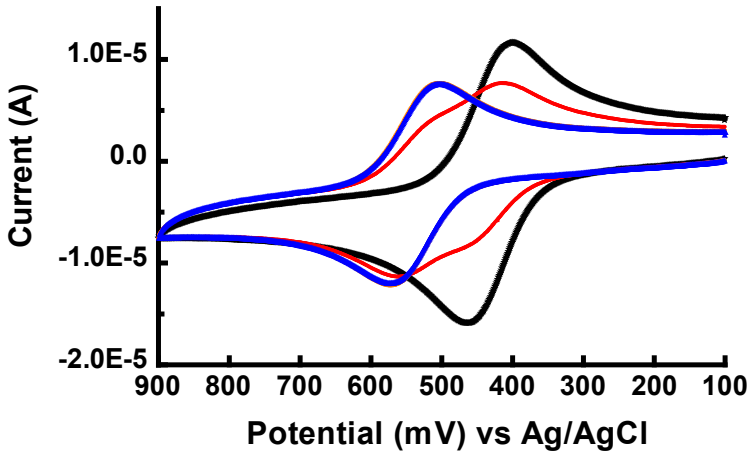

Figure 3.8 CV response on glassy carbon (0.071 cm^2) of 1.0 mM MFc in the absence (black) and in the presence of 0.5 equiv (red), 1.0 equiv (orange), and 1.5 equiv (blue) CB7, in acetate buffer pH = 4.0, in 0.1 M NaCl/H_2O. Scan rate: 0.1 $V \cdot s^{-1}$.

In an acidic acetate buffer solution (pH = 4.0), MFc is protonated and exhibit a fast, reversible, one-electron oxidation process (black curve). The presence of 0.5 equiv of CB7 to the MFc solution converts about 50% of the guest into its CB7 inclusion complex (red curve). Both free and bound peaks corresponding to MFc are observed. In the presence of 1.0 equiv. CB7, the CV response exhibits a more positive half-wave potential for ferrocene oxidation and decreased current levels (orange curve). Further addition of CB7 did not lead to any changes (1.5 equiv CB7, blue curve). This behavior is identical to our reported observations from ^1H

NMR. The CB7 complex is obviously bulkier than the free guests, and its diffusion to the electrode surface is slower, thus yielding smaller currents. The anodic shift in the $E_{1/2}$ value reflects the differential stabilization by CB7 of the reduced (ferrocene) form of the guest as compared to its oxidized (ferrocenium) form. It also means that the stability of the inclusion complex is decreased by oxidation of the ferrocene residue. While the CV behavior of the free guests is clearly reversible as evidenced by the peak-to-peak potential splitting (ΔE_p ~64 mV), the CV response of the CB7·MFc is also almost reversible (ΔE_p ~67 mV) at the relatively slow scan rate used (100 $mV \cdot s^{-1}$).

Cyclic voltammogram is also performed with 1.0 mM DFc in acidic acetate buffer solution at pH 4.0. However, the CV of free DFc is observed with two redox waves, which means DFc is not fully protonated at pH 4.0. Therefore, we run the CV experiments in HCl/H_2O solution at pH 1.0 (**Figure 3.9**).

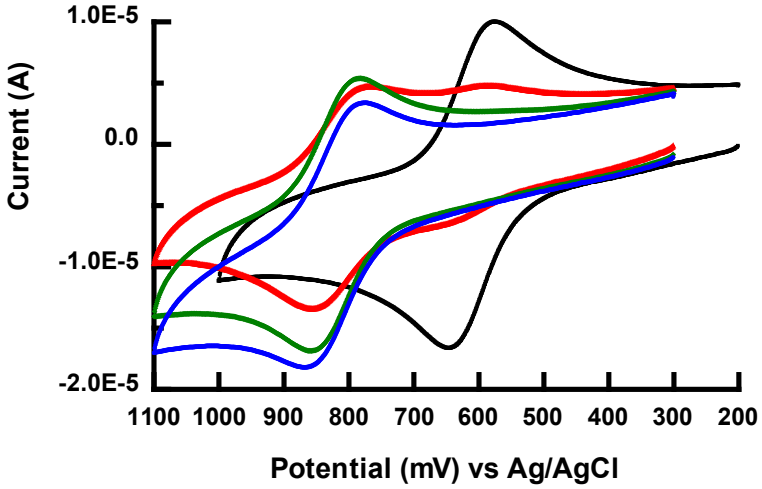

Figure 3.9 CV response on glassy carbon (0.071 cm^2) of 1.0 mM DFc in the absence (black) and in the presence of 0.5 equiv (red), 1.0 equiv (green) and 1.5 equiv (blue) CB7, in HCl aqueous solution pH = 1.0, in 0.1 M $NaCl/H_2O$. Scan rate: 0.1 $V \cdot s^{-1}$.

Our voltammetric data of DFc with its CB7 complexes show that the voltammetric behavior is similar to that of MFc with CB7, which is slower due to the host encapsulation effect. However, the half-wave potential ($E_{1/2}$) value of free DFc in pH 1.0 solution is 611 mV, while $E_{1/2}$ of free MFc in pH 4.0 buffer is at 432 mV. This great difference is due to the dicationic ferrocene guest containing two positive charges in acidic solution, thus it is more difficult to be oxidized.

3.4.2 In basic borax buffer, pH=10.0

To compare the difference between deprotonated guests and protonated ones, CV experiments were also performed of MFc and DFc with their CB7 complexes in a basic buffer, at pH 10.0, with same working conditions and experimental parameters. (**Figure 3.10** and **Figure 3.11**) The data collected are listed in **Table 3.1**.

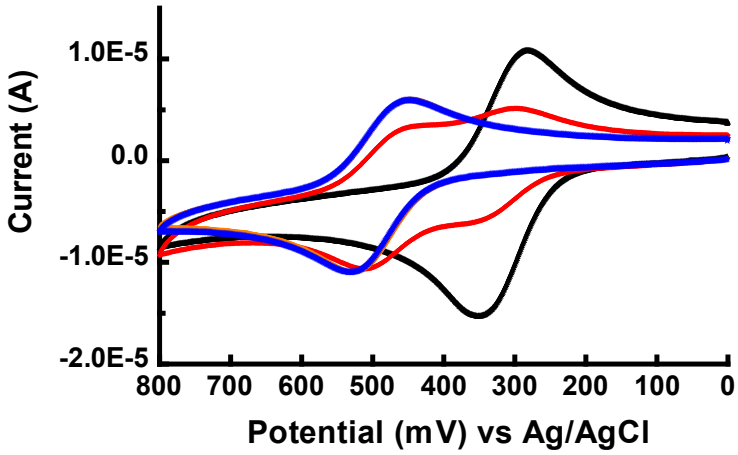

Figure 3.10 CV response on glassy carbon (0.071 cm^2) of 1.0 mM MFc in the absence (black) and in the presence of 0.5 equiv (red), 1.0 equiv (orange) and 1.5 equiv (blue) CB7, in borate buffer pH = 4.0, in 0.1 M NaCl/H_2O. Scan rate: 0.1 $V \cdot s^{-1}$.

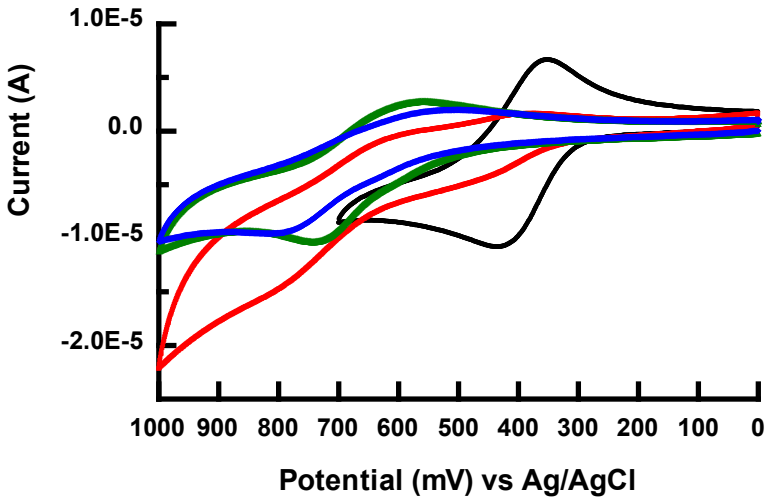

Figure 3.11 CV response on glassy carbon (0.071 cm^2) of 1.0 mM MFc in the absence (black) and in the presence of 0.5 equiv (red), 1.0 equiv (green) and 1.5 equiv (blue) CB7, in borate buffer pH = 10.0, in 0.1 M NaCl/H_2O. Scan rate: 0.1 $V \cdot s^{-1}$.

The values in **Table 3.1** show all the expected trends. For instance, the ΔEp value of each guest is smaller than that of its CB7 complexes, reflecting that the cyclic voltammetric behavior of complexes is less reversible. And all of the $E_{1/2}$ values of CB7 complexes shift to more anodic potentials compared to those corresponding to the free guests, pH<7 and pH>7, due to the host-induced effect. For each guest, in basic and acidic solutions, deprotonated and protonated, the $E_{1/2}$ values also exhibit considerable shift as expected.

Table 3.1 Cyclic voltammetric data obtained for MFc, DFc and their CB7 complexes at different pH. The unit of *E*pa, *E*pc, Δ*E*p and $E_{1/2}$ is mV. (Scan rate: 0.1 V·s^{-1})

	MFc				$E_{1/2}$	MFc+CB7			
pH=4	Epa	Epc	ΔEp	$E_{1/2}$	shift	Epa	Epc	ΔEp	$E_{1/2}$
	464	400	64	432	105	570	503	67	537
	MFc					MFc+CB7			
pH=10	Epa	Epc	ΔEp	$E_{1/2}$		Epa	Epc	ΔEp	$E_{1/2}$
	353	284	69	319	168	526	447	79	487
	DFc					DFc+CB7			
pH=1	Epa	Epc	ΔEp	$E_{1/2}$		Epa	Epc	ΔEp	$E_{1/2}$
	647	574	73	611	211	860	783	77	822
	DFc					DFc+CB7			
pH=10	Epa	Epc	ΔEp	$E_{1/2}$		Epa	Epc	ΔEp	$E_{1/2}$
	428	343	85	386	264	750	549	201	650

3.5 syn and anti of DFc

We also tried to search for experimental conditions required to form syn complexes. For instance, we anticipate that the presence of Ag^{+} with affinity for amine coordination, which may favor the formation of syn complexes with diamine DFc. However, in pH>7 environment Ag^{+} formed precipitate. A relevant work was recently reported that in CH_3CN solution, the presence of Zn^{2+} can operate as a dual-ion-switched molecular brake, which could reversibly interact with the nitrogen atom on side arms and lock them repeatedly.[35] (**Figure 3.12**)

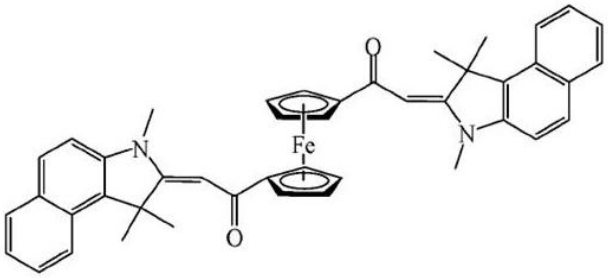

Figure 3.12 Chemical structure of ferrocene derivative with two benzo[e]indoline units which exhibit syn and anti forms at different conditions. (Picture was taken from reference 35)

3.6 Experimental

Materials:

CB7 was prepared as reported by Day and co-workers. This host hydrates on standing and we found that it is necessary to determine its effective molecular weight before use. This was done by UV-Vis titration with a standard aqueous solution of cobaltocenium.[15]

Preparation of MFc and DFc:

According to literature methods, guests N-methylaminomethyl ferrocene (MFc) and 1,1'-Bis(N-methylaminomethyl) ferrocene (DFc) were prepared by the reductive amination of the imines formed from the commercially available ferrocenecarboxaldehyde and ferrocenedicarboxaldehyde.[36]

All other chemicals were of the best commercially available quality and used as received. The anticipated structures of all these compounds were confirmed by ^{1}H-NMR and MS (FAB).

pH 4.0 acetate buffer:

Acetate buffer solution was made by dissolving 1.2 g acetic acid (0.2 moles, 1.143 mL) and sodium acetate 2.72 g (0.2 moles) in 100 mL 0.1 M NaCl water solution.

pH 10.0 borax buffer:

Borate buffer solution was made by dissolving 18.3 mL 0.1 M NaOH in 50 mL 0.025 M Borax, and then dilute to 100 mL.

Procedures:

NMR spectroscopic experiments:

Samples for ^{1}H NMR spectroscopy were prepared with D_2O (99.99%D) purchased from Cambridge Isotope Laboratories. The sample solutions also contained 0.1 M NaCl to create experimental conditions similar to those employed in electrochemical experiments. NMR spectroscopic experiments were recorded in Bruker Avance instruments (400 or 500 MHz). In some cases, sodium acetate was added to the sample solution and the methyl acetate

protons used to provide calibration to measure the concentration of other species in the D_2O (Cambridge Isotopes) solution.

Electrochemical experiments:

The electrochemical experiments were recorded with a BAS 100W system. A single compartment glass cell was used for all voltammetric experiments. Typically the cell was fitted with a glassy carbon working electrode (0.071 cm^2), a Pt or W auxiliary electrode, a Ag/AgCl reference electrode and nitrogen inlet Teflon tubing. Nitrogen gas was purified before use and bubbled through the solution to remove oxygen gas before the measurements. During the voltammetric measurements, nitrogen flow was maintained above the solution to minimize re-dissolution of oxygen. The working electrode was polished on a soft, felt surface using alumina powder (0.05 μm) and water as the lubricant. Before use the working electrode surface was rinsed extensively with water and sonicated to remove any particulate left from the polishing. In some voltammetric experiments we used a 5 μm diameter carbon fiber ultramicroelectrode (BAS) as the working electrode.

Chapter 4

TOWARDS CUCURBITURIL-BASED SUPRAMOLECULAR POLYMERS: A NEW GUEST FOR DIMERIC BINDING INSIDE CUCURBIT[8]URIL

4.1 Cucurbit[8]uril binding to methyl viologen (MV^{2+})

Cucurbit[8]uril (CB8) is one of the most well studied macrocyclic host molecules in the CB family. Like other CB hosts, CB8 favors the binding to positively charged guests at the carbonyl portals. It is characterized by its ability to accommodate two complementary interesting aromatic guests inside its cavity simultaneously. This characteristic makes it a very useful building block in supramolecular architectures. Kim and co-workers first showed that CB8 can bind to dialkyl-*N,N'*-bipyridium (viologen) derivative, methylvilologen (MV^{2+}) with 1:1 stoichiometry, while host CB8 binds the dimer formed by methylviologen radical cations ($MV^{+}\cdot$) when the host-guest complex system is undergoing a reduction process (**Scheme 4.1**).[18]

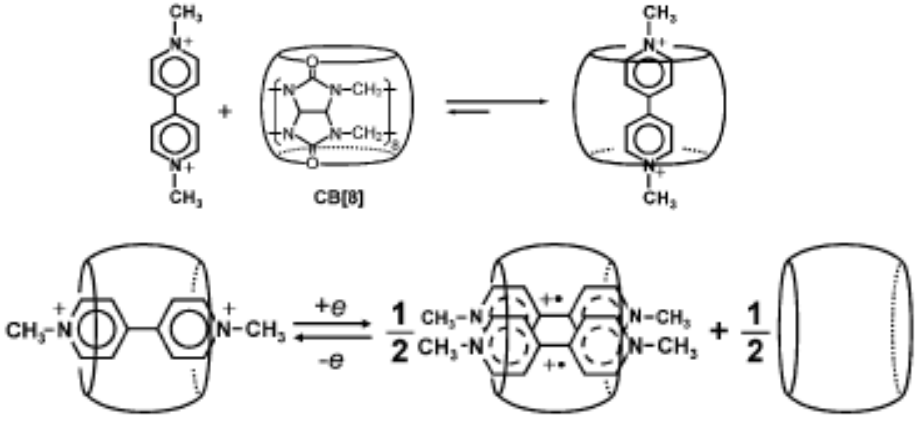

Scheme 4.1: Inclusion process of 1:1 complexation corresponding to MV^{2+} in CB8 cavity and dimerization process of cations $MV^{+}\cdot$ in CB8 cavity (Graphics was taken from reference 24).

The binding constant of CB8 with MV^{2+} is high ($K > 10^5\ M^{-1}$) in aqueous environments. While methylviologen forms stable 1:1 host-guest complexes with CB8, the corresponding one-electron reduced form, $MV^{+}\cdot$, selectively yields 1:2 host-guest complexes with the same host CB8. We reasoned that such 1:2 complexes derive stabilization from the ion dipole interactions between the two positive charges on the cation radical dimer and the rims of carbonyl oxygen atom lining the host cavity portals. Contacts between the aromatic surfaces of the viologen radical cations and between the $MV^{+}\cdot$ dimer and the inner surface of the CB8 cavity, coupled with hydrophobic forces, contribute significantly to the stability of the ternary complex.

In particular, Kim and co-workers first reported the formation of charge transfer complexes -between a π-donor, dihydroxynaphthalene (HN), and a π-acceptor, methyl viologen (MV^{2+})- inside the hydrophobic cavity of CB8.[37] CB8 exhibits a unique ability to stabilize the charge transfer (CT) complexes inside its cavity (**Scheme 4.2**). The corresponding X-ray crystal structure was also obtained as shown in **Figure 4.1**.

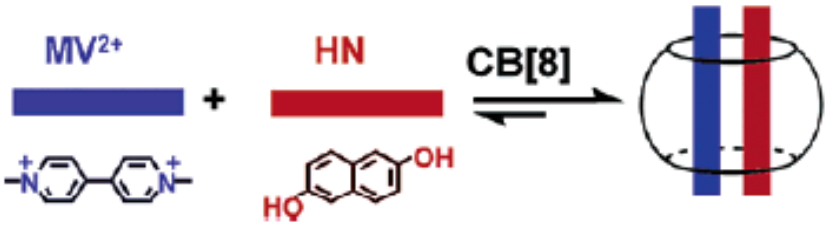

Scheme 4.2: Charge-transfer complex $HN\cdot MV^{2+}$ formation in CB8 illustration at 1:1:1 ratio (Graphics was taken from reference 37).

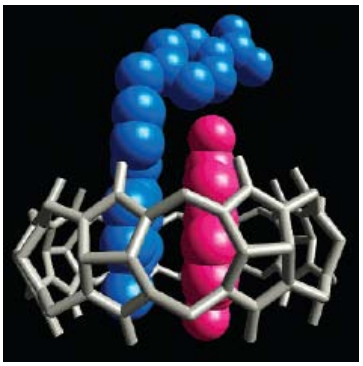

Figure 4.1: X-ray crystal structure of charge transfer complex stabilized in CB8 cavity (Graphics was taken from reference 24).

Kim and co-workers have made extensive use of these unique binding properties of CB8 with charge transfer complex inside the cavity to design and to demonstrate the operation of a number of CB8-based, switchable molecular systems. They have also developed an interesting redox driven molecular machine that behaves as a molecular loop lock utilizing these supramolecular interactions.[38] The guest molecule contains a naphthalen-2-yloxy (Np) unit and a viologen unit linked to each other by a flexible spacer, with a bulky cationic unit at the terminal to make it more soluble in aqueous solution. Treatment of guest with 1 equiv CB8 in water resulted in the exclusive formation of the stable 1:1 complex through the formation of the intramolecular CT complex between the Np and viologen units inside CB8.

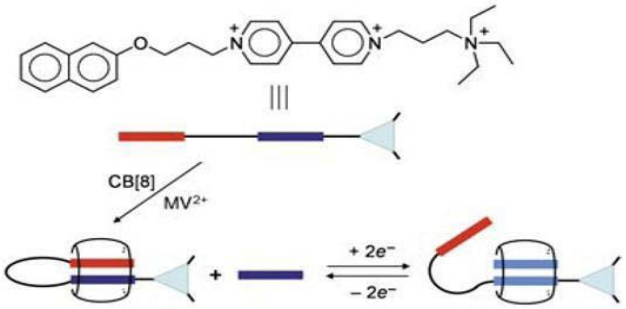

Scheme 4.3: Molecular loop lock based on CB8 mediated charge transfer complex (Graphics was taken from reference 38).

Our group have used CB8 to mediate the redox-controlled dimerization of dendrimers containing viologen residues and extended this concept to the redox control and size selection of dimeric assemblies formed between two types of dendrimers, containing either (π-acceptor) viologens groups or (π-donor) dialkoxybenzene groups.[19]

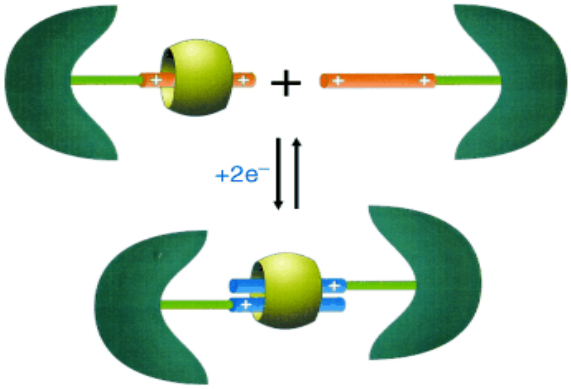

Scheme 4.4 CB8 mediated dendrimer self-assembly (Graphics was taken from reference 19).

Recently, Sherman and co-workers have shown that CB8 can be used to mediate the formation of supramolecular polymers. This entire body of work relies on the pronounced stabilization of aromatic donor-acceptor charge transfer complexes or viologen cation dimers inside the cavity of CB8. [39]

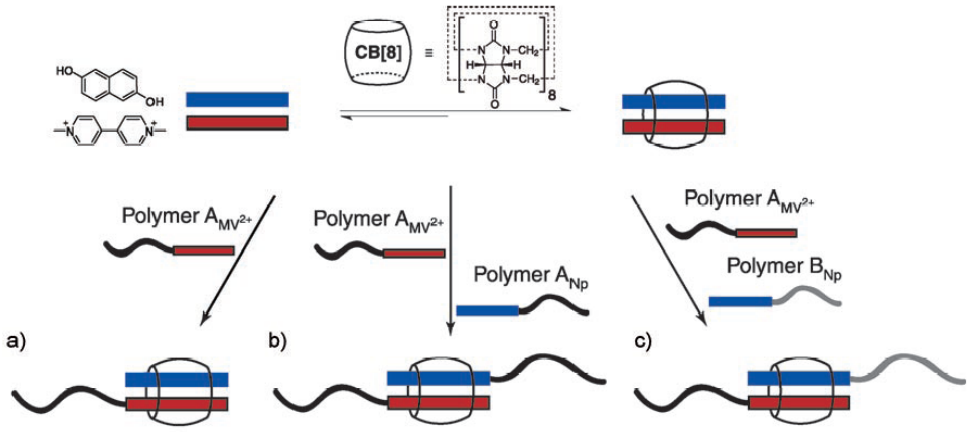

Scheme 4.5 CB8 mediated supramolecular polymer (Graphics was taken from reference 39).

Another CB8·MV recognition on specific amino acids and peptides is reported by Urbach.[40] The size, shape, and hydrophobicity of trypotophan (Trp) are similar and comparable to that of 2,6-dihydroxynaphthalene (HN) which is studied in Kim's work.[18] The interaction between CB8·MV and a series of peptide with Trp groups is observed with high binding affinity and remarkable optical changes. This work demonstrated a novel biomimetic approach to the construction of multivalent receptors via molecular self-assembly. [**Scheme 4.6**]

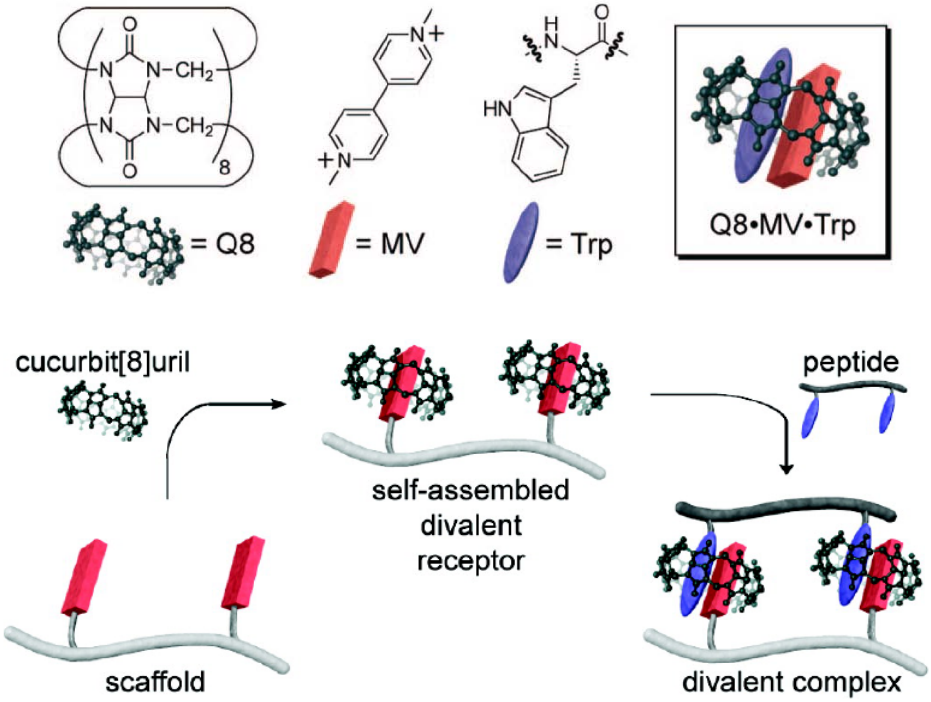

Scheme 4.6 Self-assembling modular receptor of CB8·MV with the binding to a tryptophan peptide. (Graphics was taken from reference 40).

In this chapter, we investigate a series of new guests for CB8 inspired by the considerable stability of the ternary complexes that result from two viologen radical cations forming a π-π dimeric inclusion complex inside the CB8 cavity. The central idea is shown in **Scheme 4.1**. We

propose to replace the viologen radical cation in Kim's work by the 4-phenyl-pyridinium residue, which provides the same overall charge (+1) and a similarly sized aromatic surface.

Our hypothesis is that 4-phenyl-pyridinium (4PP) derivatives will form stable 1:1 or 1:2 host-guest complexes inside the cavity of CB8 with the latter reaching an overall stability similar to that exhibited by the methyl viologen radical cation dimer complex, without any need for reducing conditions.

In order to test this idea we prepared three compounds containing 4-phenyl-pyridinium groups, 4PPOH, 4PPOMe and $(4PP)_2$. The core component of this system is $(4PP)_2$, which is composed of two 4-phenyl-pyridinium units connected by a flexible triethyleneglycol (TEG) linker. Their structures are given in **Scheme 4.6**. The structures of these guests reflect concern on that the effect of different substituent groups on 4-phenyl-pyridinium binding behaviors to CB8.

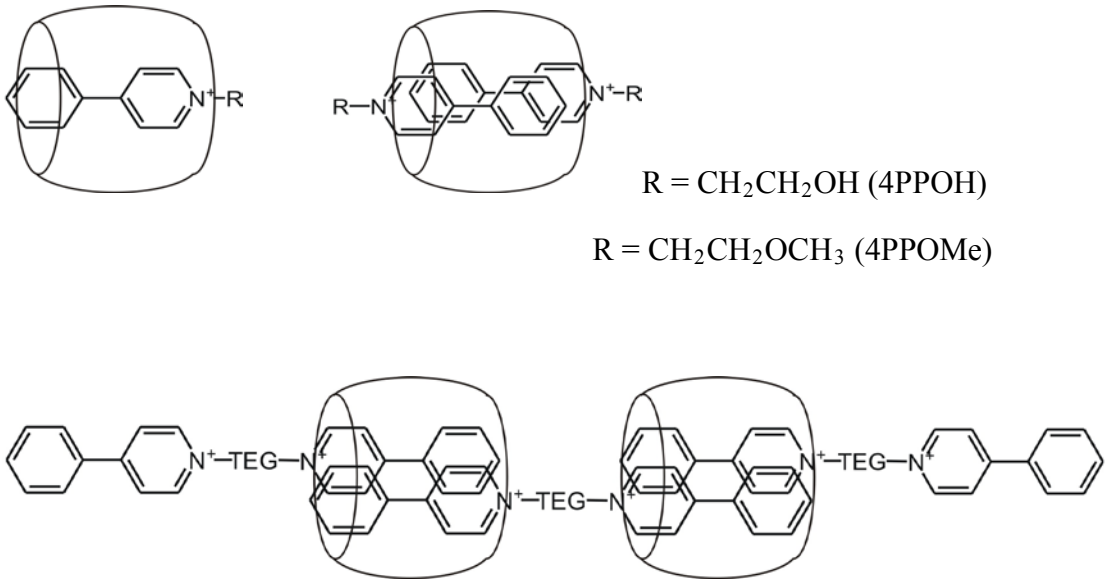

Scheme 4.7 CB8 binding to 4PPOH, 4PPOMe and $(4PP)_2$.

4.2 ^{1}H NMR spectroscopic analysis

^{1}H NMR spectra were obtained for all 4PP compounds in the absence and in the presence of CB8 in 0.1 M NaCl deuterium oxide solution at 25^{o}C. In all cases, the proton signals corresponding to the aromatic proton peaks exhibit an obvious upfield shift upon addition of CB8, which is consistent with the hypothesis that the inclusion complexation takes place on the 4-phenyl-pyridine residue. The binding stoichiometry between CB8 and each 4PP compounds was also studied by ^{1}H NMR spectroscopic analysis in the titration experiments

We performed titration experiments of 0.5 mM 4PPOMe with increasing concentrations of CB8 in 0.1 M NaCl aqueous solution by ^{1}H NMR spectroscopy, since the solubility of 4PPOMe is the best among the three 4PP derivatives.(**Figure 4.1 (a)** and **Figure 4.1 (b)**)

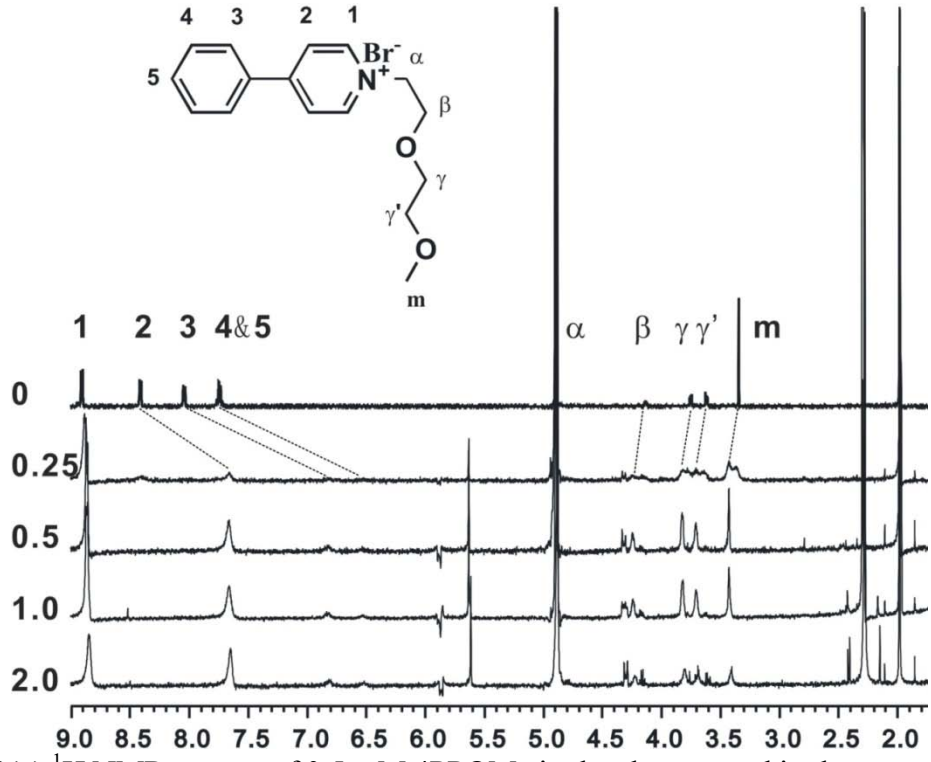

Figure 4.2(a) ^{1}H NMR spectra of 0.5 mM 4PPOMe in the absence and in the presence of CB8 from 0 to 2.0 equiv, in 0.1 M NaCl/D_2O.

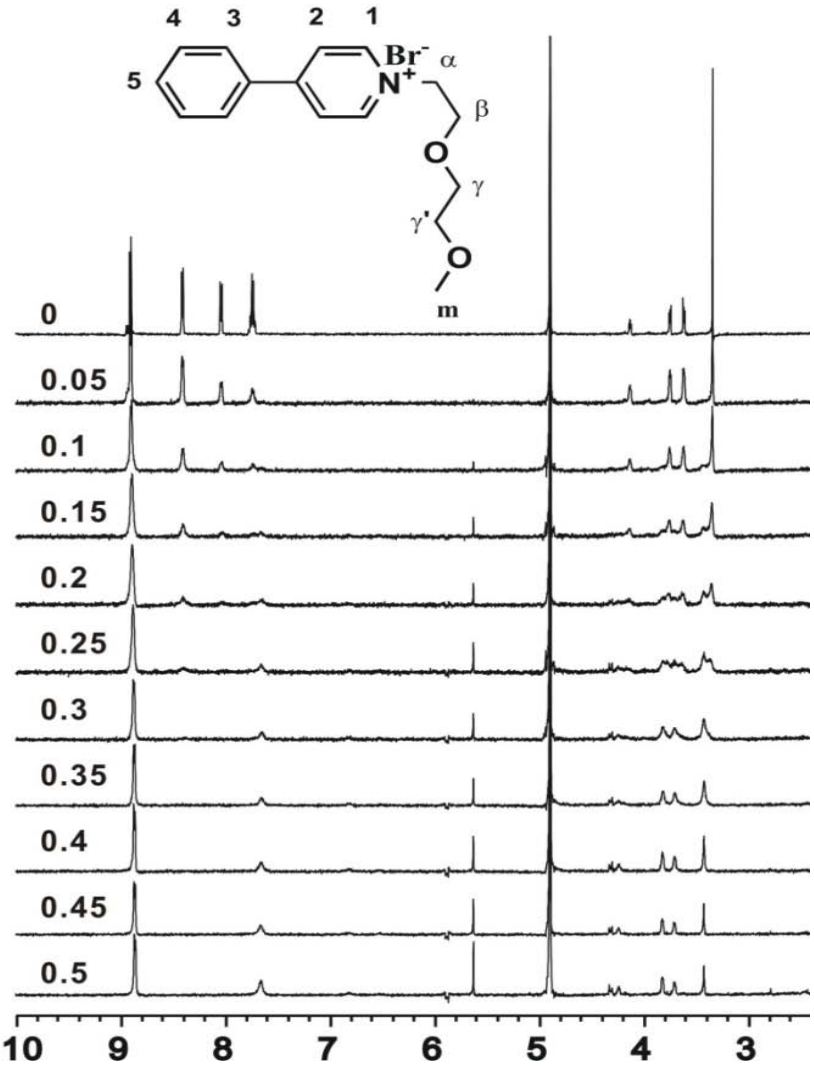

Figure 4.2(b) ^{1}H NMR spectroscopy of 0.5 mM 4PPOMe in the absence and in the presence of CB8, from 0.05 to 0.5 equiv, in 0.1 M NaCl/D_2O.

The general formation of stable inclusion complexes of 4PPOMe in the presence of CB8 was observed from the ^{1}H NMR spectra. **Figure 4.2(a)** clearly evidenced that for the free guest 4PPOMe, proton signals corresponding to aromatic protons 1-5 on the 4-phenyl residue resonate at low field between ca. 9.0 ppm to ca. 7.5 ppm. Proton signals labeled as α, β and γ, γ' and m on the flexible 2-(2-methoxyethoxy)ethoxy]methyl chain are at higher field. The rate of exchange between the free and bound 4PPOMe is slow in the ^{1}H NMR time scale. In the

presence of 0.25 equiv of CB8, the resonances of the 4-phenyl pyridine protons shift upfield, while the proton signals corresponding to the chain shift slightly downfield (**Figure 4.2(a)**). Proton 1 does not shift upfield remarkably, proton 2 shifts upfield by 0.6 ppm, proton 3-5 shift upfield by 1.2 ppm. The remarkable chemical shifts of the 4PP residue protons demonstrate that inclusion complexation takes place on the 4PP residue. Besides, the aromatic protons generally exhibit host-induced chemical shifts accompanied with peak broadening. However, proton signals corresponding to α, β, γ, γ' and m all shift downfield by about 0.1 ppm, a telling sign that they remain outside the cavity.

Upon addition of 0.5 equiv CB8, proton signals corresponding to free guest disappear, which demonstrate that the main compound formed are 1:2 host-guest complexes. In the presence of excess host CB8, the bound 4PPOMe protons do not show any significant changes. Meanwhile a white precipitate starts to come out in the solution, which is probably due to the poor solubility of the 1:2 CB8·4PPOMe complexes at mM concentration level. In other words, whether we can observe the 1:1 CB8·4PPOMe complexes at lower concentration becomes a question. We further our investigation on the binding stoichiometry at much lower concentrations by UV-vis spectroscopy and MALDI-TOF mass spectroscopy, which will be mentioned later in this chapter.

We also performed titration experiments for 0.5 mM 4PPOH and 0.5 mM $(4PP)_2$ with CB8 in 0.1 M NaCl/D_2O solution by ^1H NMR technique. All conditions and parameters are the same as the experiments for 4PPOMe protons with CB8. [see **Figure 4.3** and **Figure 4.4**]

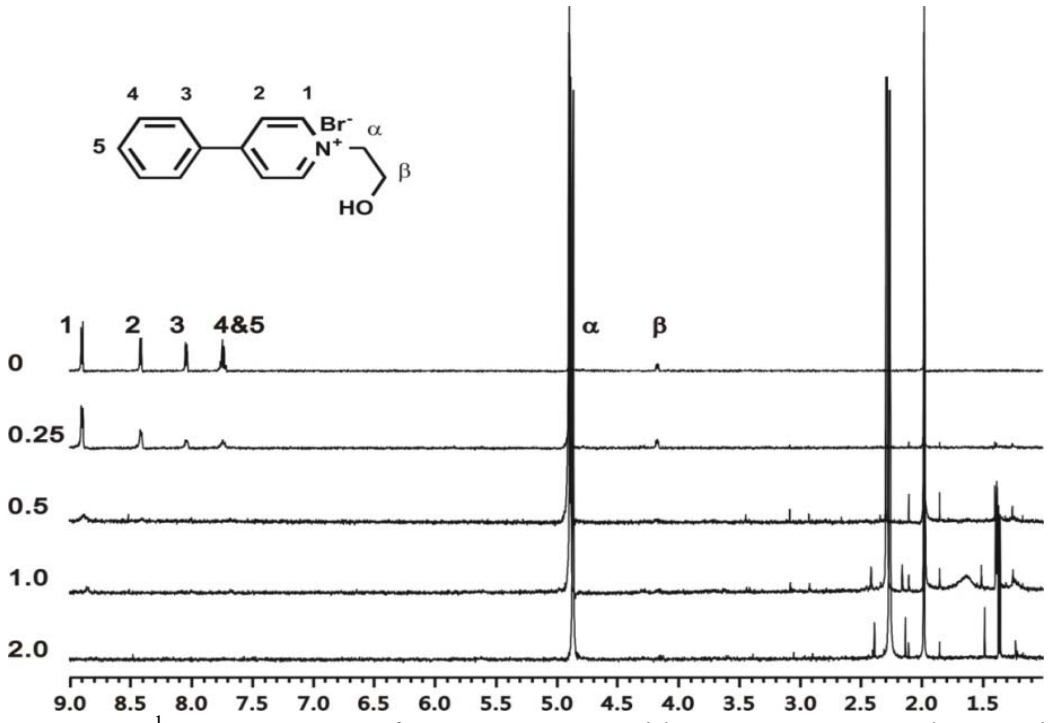

Figure 4.3 ^{1}H NMR spectra of 0.5 mM 4PPOH with 0, 0.25, 0.5, 1.0 and 2.0 equiv CB8 in 0.1 M NaCl/D_2O.

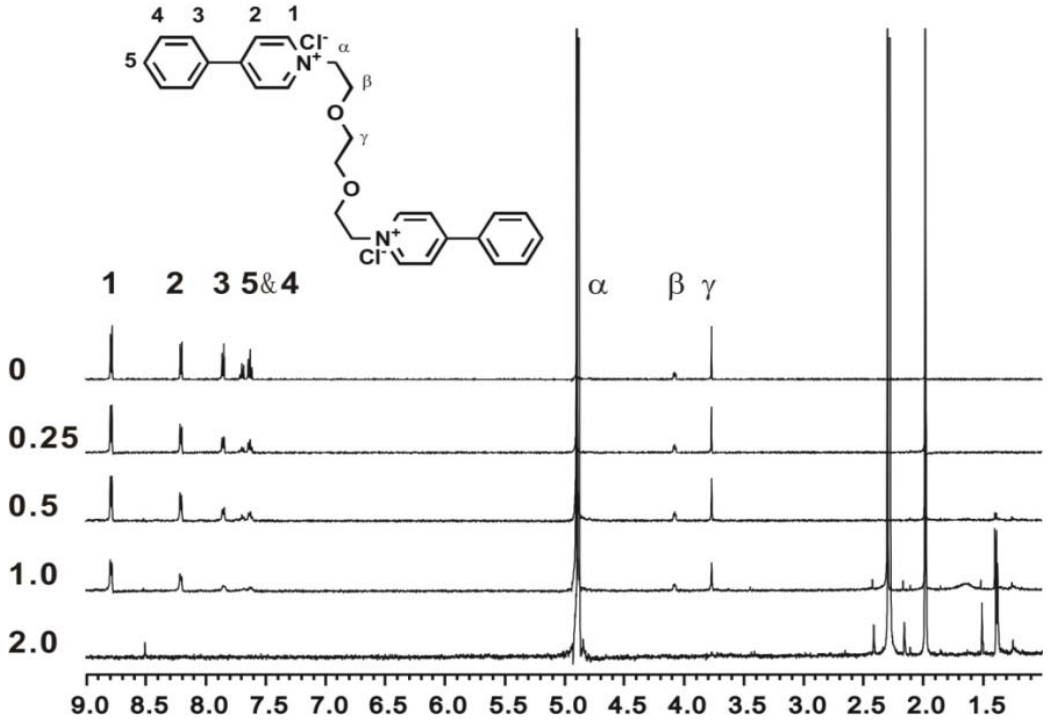

Figure 4.4 ^{1}H NMR spectra of 0.5 mM $(4PP)_2$ with 0, 0.25, 0.5, 1.0 and 2.0 equiv CB8 in 0.1 M NaCl/D_2O.

In **Figure 4.3**, ^{1}H NMR spectroscopic studies in 0.1 M NaCl/D_2O solutions show no CB8-induced changes in the chemical shifts corresponding to the 4-phenyl-pyridine proton resonances. We can not conclude that 4PPOH is not complexed at all by CB8 since it is hard to observe the CB8 proton signals either in the ^{1}H NMR spectra upon addition of CB8. The only changes observed is that 4PPOH signals get broadened and disappear gradually. We suspect that CB8 binds to 4PPOH and the complexes precipitate, which is in agreement with the experimental observation of turbidity and precipitation. Similar results were recorded with $(4PP)_2$ as shown in **Figure 4.4**. The presence of CB8 does not lead to any changes except the broadening and disappearing of the $(4PP)_2$ proton signals. The ^{1}H NMR analysis of 4PPOH and $(4PP)_2$ with CB8 is limited by the low solubility of the complexes in aqueous solution.

4.3 UV-vis spectroscopic analysis

We attempted to determine the binding stoichiometry between CB8 and 4PP derivatives by using UV-vis absorption spectroscopic analysis. Titration experiments of a 20 μM 4PPOH solution with increasing concentrations of host CB8 were performed in 0.1 M NaCl aqueous solution.

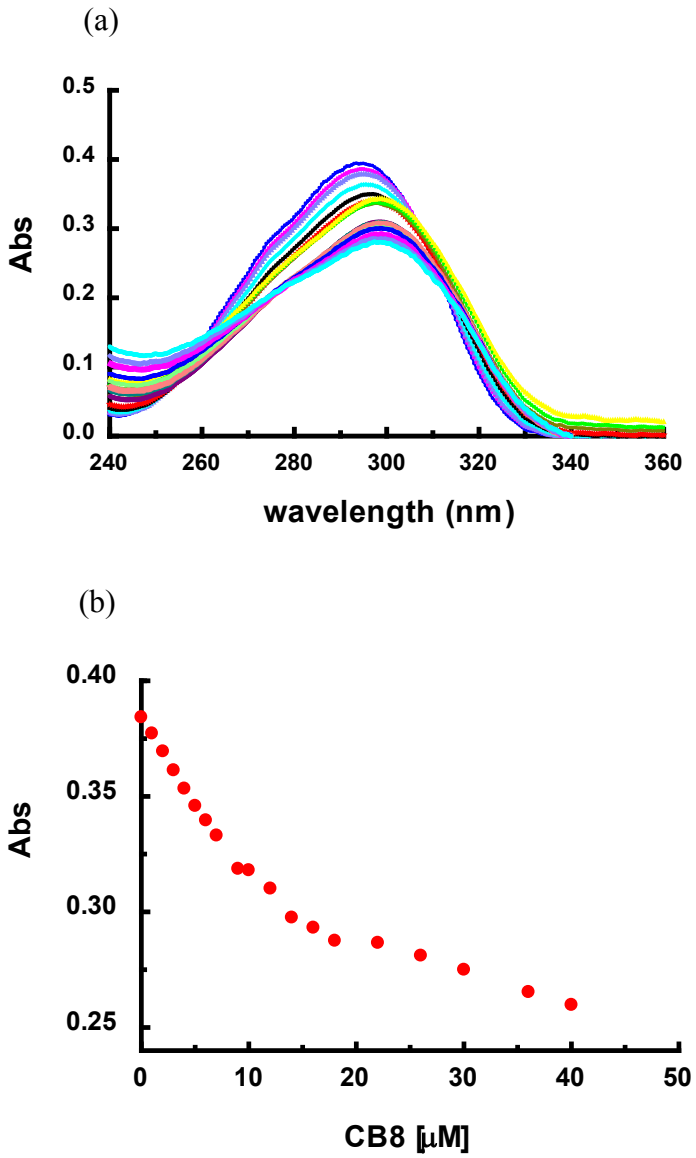

Figure 4.5 (a) UV titration of 20 μM 4PPOH upon addition of CB8 in 0.1 M NaCl/H_2O. (b) Absorbance of 4PPOH at 296 nm.

The UV spectra in **Figure 4.5 (a)** show that the 20 μM 4PPOH solution has an absorbance peak at 296 nm. The peak exhibits a slight red shift upon addition of CB8, which reveals the complexation of 4PPOH by host CB8. The absorbance of 4PPOH solution at 296 nm decreases from ca. 0.38 until CB8 concentration reaches 10 μM, where host CB8 reaches

0.5 equiv to the guest. The curve of absorbance values at 296 nm in **Figure 4.5 (b)** shows a discontinuity between 10 μM and 20 μM. This behavior demonstrated that CB8 binds 4PPOH with different stoichiometry as the host:guest ratio is changed. When less than 0.5 equiv CB8 is introduced in the 4PPOH aqueous solution, the main complex formed is 1:2 (host:guest) due to the large amount of free guest. However, as more than 0.5 but less than 1.0 equiv CB8 is mixed with 4PPOH, another complex, 1:1 (host:guest), is formed. After 1.0 equiv. CB8 is introduced in the solution, excess CB8 leads to very little changes in the absorbance decrease. Since there are two different complexes that exist in the same solution, this UV-vis spectroscopic technique could not afford an accurate value for the corresponding equilibrium association constant. We extended further analysis on the stoichiometry of the CB8·4PPOH inclusion complex by Job's plot using UV-visible spectroscopy. The resulting plot shown in **Figure 4.6** revealed a maximum value at x=~0.6, clearly indicating both 1:2 and 1:1 binding stoichiometries between the host and the guest.

It is observed that in the Job-Plot experiments the guest absorbance decreases and presents a slight-red shift as the percentage of the guest decreases in **Figure 4.6(a)**. **Figure 4.6(b)** shows that from 0 to 40% of guest in the solution, the trend of the binding stoichiometry is nearly 1:1, while in the range between 80 to 100% guest, it is almost 1:2. In the middle range, the top part of the data is flat and we conclude that this is due to the presence of a mixture of 1:1 and 1:2 complexes.

(a)

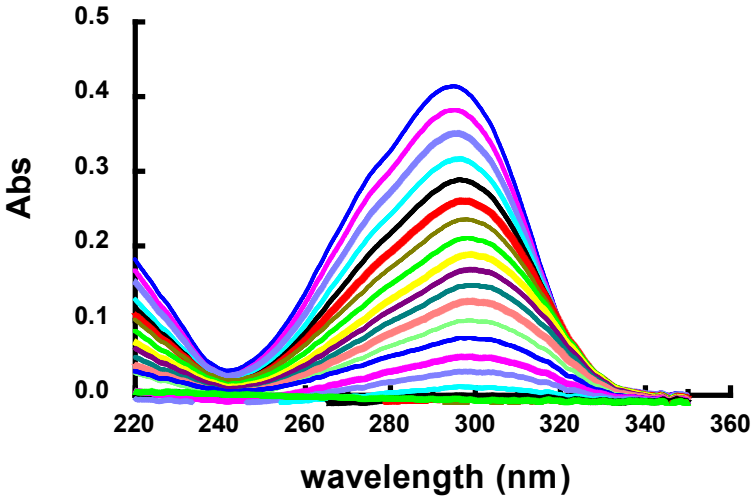

(b)

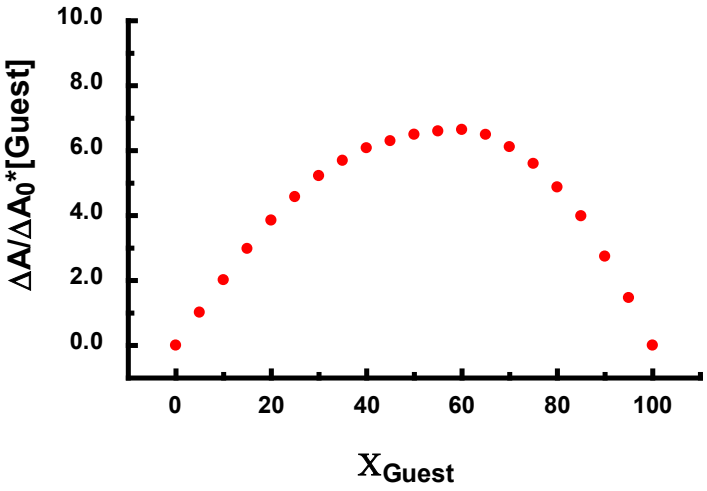

Figure 4.6 (a) Job-Plot of 20 μM 4PPOH with CB8 in 0.1 M NaCl/H_2O. (b) Intensity of 4PPOH at 296 nm.

Very similar to the UV-visible data obtained for CB8 binding to 4PPOH, CB8 binding to 4PPOMe shows similar stoichiometries, 1:1 and 1:2 host:guest complexes together. The UV-vis spectroscopic titration experimental results corresponding to 25 μM 4PPOMe upon

addition of CB8 and Job-Plot data are shown in **Figure 4.7** and **Figure 4.8**. Similar experiments were performed with 15 μM $(4PP)_2$ (**Figure 4.9** and **Figure 4.10).**

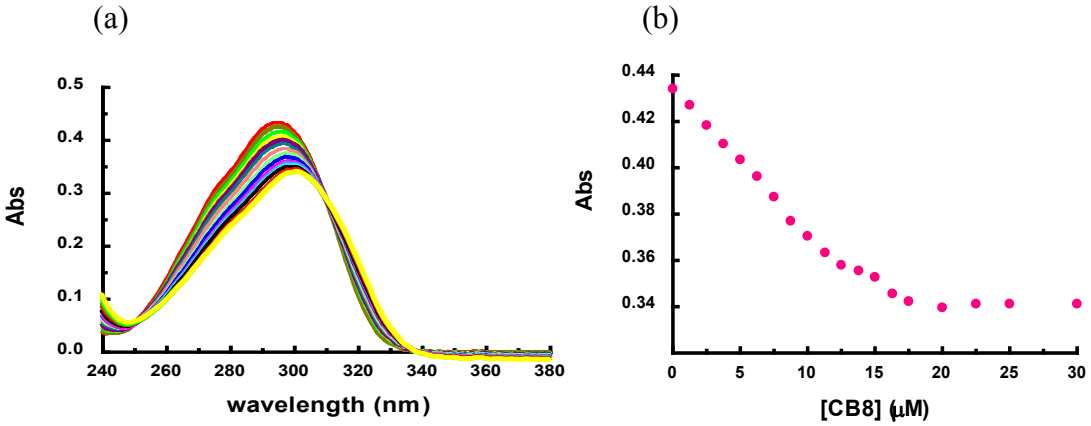

Figure 4.7 (a) UV titration of 25 μM 4PPOMe with CB8 in 0.1 M NaCl/H_2O. (b) Intensity of 4PPOMe at 296 nm.

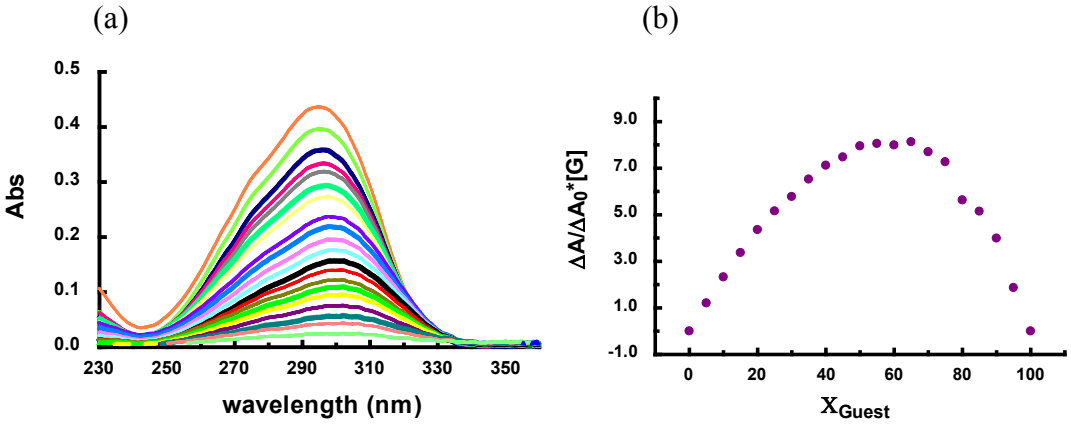

Figure 4.8 (a) Job-Plot of 25 μM 4PPOMe with CB8 in 0.1 M NaCl/H_2O. (b) Intensity of 4PPOMe at 296 nm.

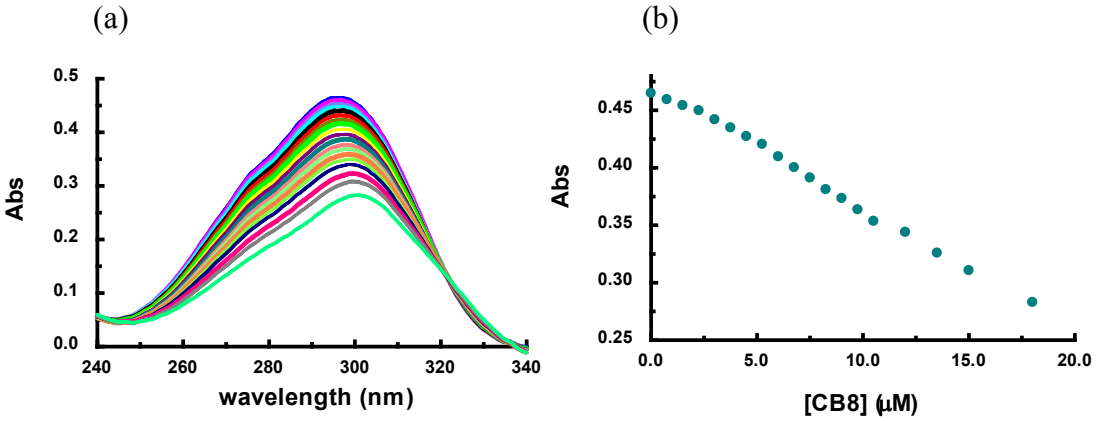

Figure 4.9 (a) UV titration of 15 μM $(4PP)_2$ with CB8 in 0.1 M NaCl/H_2O. (b) Intensity of 15 μM $(4PP)_2$ at 296 nm.

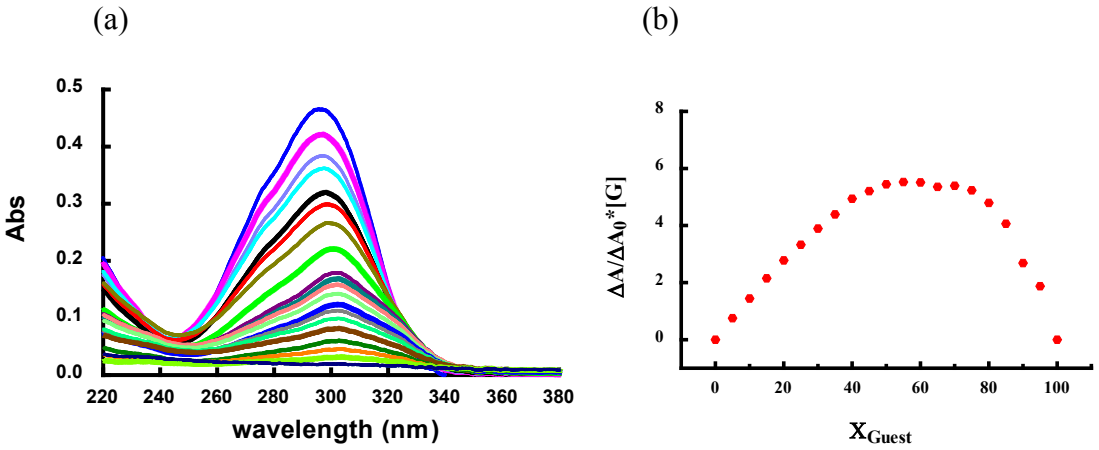

Figure 4.10 (a) Job-Plot of 25 μM 4PPOMe with CB8 in 0.1 M NaCl/H_2O. (b) Intensity of 4PPOMe at 296 nm.

Interestingly, in contrast with the UV-vis spectroscopic data obtained for 4PPOH and 4PPOMe with CB8, the UV titration experiments corresponding to 15 mM $(4PP)_2$ exhibit nearly linear decreasing upon addition of CB8 (**Figure 4.9**). This different curve compared to those of 4PPOH and 4PPOMe represented the different binding stoichiometry with CB8. 4PPOH and 4PPOMe both contain a single aromatic 4-phenyl-pyridine residue, which is

bound by the CB8 cavity, and a side chain. They can form 1:1 and 1:2 host:guest complexes inside CB8 at various concentration. However, the dimerized guest molecule, $(4PP)_2$, contains two 4-phenyl-pyridine residues, and such structure can bind to two CB8 host molecules (**Scheme 4.6**). The UV-vis spectra corresponding to $(4PP)_2$ titrated by CB8 also exhibit a decreased absorbance value at 296 nm and the absorbance decreases linearly. These results suggest that both 4PP groups may be included in CB8 when bound. Besides, when the CB8 concentration increases, there is more chance for CB8 to bind two 4PP residue in the cavity, which can lead to 2:3, 3:4 ··· N: (N+1) host:guest complexation.

4.4 Cyclic voltammetric analysis

The binding interactions between methyl viologen and CB8 have been investigated by Kim and co-workers. They first reported the electrochemical binding behavior between MV^{2+} and CB8 in aqueous solution (**Figure 4.10**).

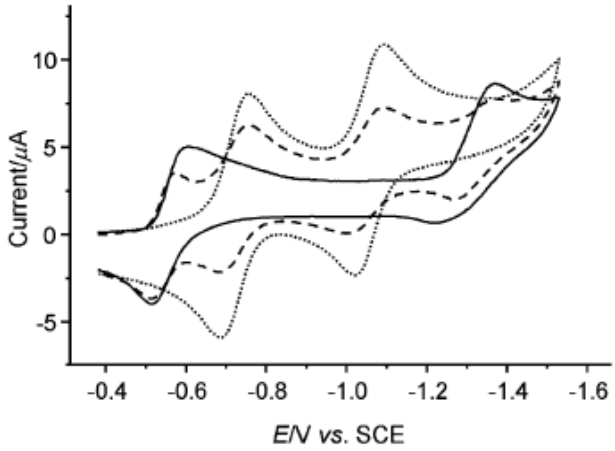

Figure 4.11 Cyclic voltammetric response on a glassy carbon electrode (0.071 cm^2) for a solution containing 0.5 mM MV^{2+} in the absence (dotted line) and in the presence of 0.25 equiv (dashed line) and 1 equiv (solid line) CB8. Medium: pH 7.0 phosphate buffer. Scan rate: 0.1 $V \cdot s^{-1}$. (Graphics was taken from reference 24).

The cyclic voltammetric response of free methyl viologen in the aqueous solution exhibits two reduction waves corresponding to the redox couples $MV^{2+}/MV^{+}\cdot$ and $MV^{+}\cdot/MV^{0}$ (dotted line). Upon addition of 0.25 equiv CB8 (dashed line), two additional redox waves are observed. In the presence of 1.0 equiv CB8 (solid line), the new peaks completely replace the ones corresponding to free MV.[18] It is concluded that the first reduction wave exhibits a large shift which is related to facile formation of the $(MV^{+}\cdot)_2$-CB8, while the second reduction wave becomes quasi-reversible due to a host-induced effect. The redox-controlled interactions in the absence and in the presence of CB8 are shown in **Scheme 4.8**.

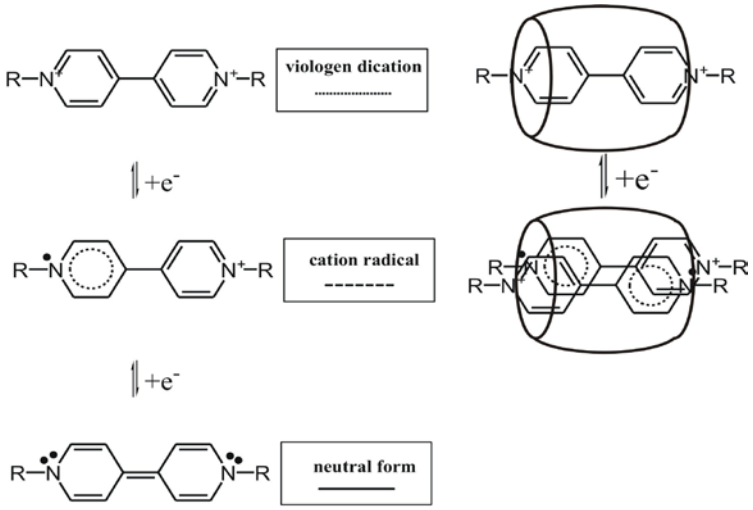

Scheme 4.8 The three reduction states of viologens

We performed competition experiments of guest MV^{2+} and 4PPOMe with CB8 in aqueous solution by using cyclic voltammetry (**Figure 4.12**). A 0.5 mM MV^{2+} in 0.1 M NaCl/H_2O solution shows two reversible waves as reported (black).[18] In the presence of 1.0 equiv CB8 (red), however, the new waves are observed but they do not replace the old waves

completely. Upon addition of 1.0 equiv 4PPOMe, the solution contains 1:1:1 mixture of MV^{2+}, 4PPOMe and CB8 (green).

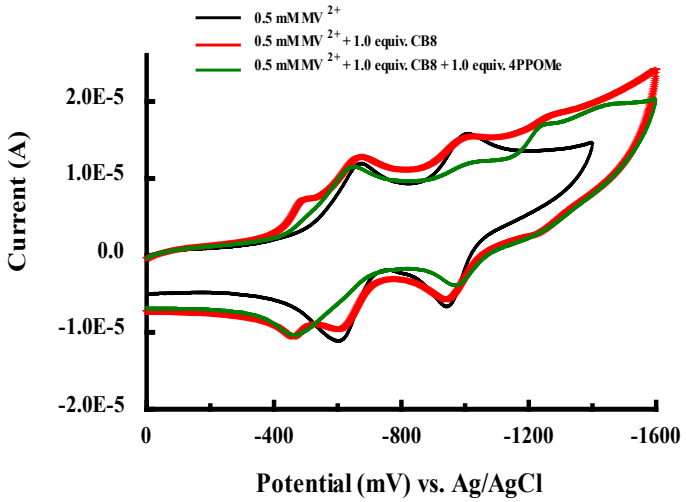

Figure 4.12 Cyclic voltammograms at scan rate 0.1 Vs^{-1} of a 0.5 mM solution of MV^{2+} in the absence (black), in the prescence of 1.0 equivalent CB8 (red) and 1.0 equivalent CB8 and 1.0 equivalent 4PPOMe (dark green) in 0.1 M NaCl/H_2O.

We observe that the new reduction peak corresponding to MV^{2+}/ $MV^{+}\cdot$ in the dimer $(MV^{+}\cdot)_2$ with CB8 at ca. -500 mV disappears upon addition of 4PPOMe. The current level of the second redox wave corresponding to $MV^{+}\cdot/MV^{0}$ decreases significantly. A new wave at ca. -1400 mV is also observed. This wave corresponds to the bound 4PPOMe with CB8. Therefore, we conclude that the presence of 1.0 equiv 4PPOMe affects the binding between CB8 and $MV^{+}\cdot$. The electrochemical behavior of CB8·$(4PPOMe)_2$ reveals that this complex is comparable in stability to CB8·$(MV^{+}\cdot)_2$.

4.5 Diffusion coefficient analysis

The diffusion coefficient (D_o) (D/cm^2·s^{-1}) of free 4PPOMe, free CB8 and their 1:2 host:guest complexes are measured by using pulsed gradient spin-echo nuclear magnetic resonance (PGSE NMR) spectroscopy. The complex formed by 4PPOMe and CB8 (CB8·(4PPOMe)$_2$) is more soluble than complexes formed by 4PPOH or (4PP)$_2$ with CB8. The D_o value of CB8·(4PPOMe)$_2$ complex is much lower than that of free 4PPOMe, the value is also lower than that of the free host. Diffusion coefficient values obtained are listed in **Table 4.1**.

Table 4.1: Diffusion coefficient constants of 4PPOMe, CB8 and their complex:

compound	D_o (D/cm^2·s^{-1})
Free 4PPOMe	6.43×10^{-6}
Free CB8	3.27×10^{-6}
4PPOMe+CB8 (2:1)	3.09×10^{-6}

The D_o values determined by PGSE NMR Echo (PGSE) NMR listed in **Table 4.1.** The D_o value of free guest, 4PPOMe, is 6.43×10^{-6} D/cm^2·s^{-1}. And in the presence of 0.5 equiv CB8, D_o decreased to 3.09×10^{-6} D/cm^2·s^{-1}, which is even a little bit less than that of the free CB8 (3.27×10^{-6} D/cm^2·s^{-1}). It clearly indicated that the formation of the complex. The diffusion of 4PPOMe slowed down when it is bound by host CB8 with a 2:1 ratio.

4.6 MALDI-TOF analysis

We also performed Maldi-TOF experiments to analyze the binding of all three 4PP derivatives to CB8 at low concentration. When these 4PP compounds are mixed with different ratios of CB8, a variety of predetermined self-assembly architectures can be accessed (**Table 4.2**). Interestingly, besides the 1:1 complexes that are observed for each of the 4PP derivatives with CB8, the corresponding 2:1 (host:guest) complexes are all obtained. $(4PP)_2$ forms such complex with two CB8 bound on both 4PP moiety. However, the ability of 4PPOH and 4PPOMe binding to two CB8 hosts adds further interest to this investigation.

Table 4.2 Mass value obtained corresponding to each 4PP guests with CB8 complexes

m/z	1Host:1Guest	2Host:1Guest
4PPOH	1528	2857
4PPOMe	1586	2915
$(4PP)_2$	1756	1575

Conclusion:

In Kim's work, the binding stoichiometry of a CB8- methylviologen dication (MV^{2+}) complex is 1:1. And this binding stoichiometry can be effectively controlled by the redox chemistry. The 1:1 inclusion complex of MV^{2+} in CB8 converts completely and reversibly to a 2:1 inclusion complex of cation radicals ($MV^{+\cdot}$) in CB8, upon the reduction of the guest.

In this chapter, we have described the supramolecular complexation of cationic 4PP compounds by the host CB8, with a strong binding behavior. The experimental results reported in this work clearly indicated that CB8 binds all three 4PP derivatives with host-guest ratio 1:1 and 1:2 at higher concentration in NMR analysis (mM), while at lower concentration the binding stoichiometry of host-guest interactions are 1:1 and 2:1 in MALDI-TOF experiments (μM). However, the UV-vis experiments are also at lower concentrations but the data obtained indicated the binding stoichiometry of host-guest interactions are 1:1 and 1:2.

4.7 Experimental

Materials:

The CB8 host was prepared following a literature method and characterized with MALDI-TOF-MS, ^{1}H-NMR and ^{13}C-NMR methods. Samples for ^{1}H NMR and PGSE NMR spectroscopy were prepared with D_2O (99.99%D) purchased from Cambridge Isotope Laboratories. The UV-visible spectra were recorded using Shimadzu UV-2101PC spectrophotometer. The sample solutions also contained 0.1 M NaCl to create experimental conditions similar to those employed in electrochemical experiments.

Preparation of 4PPOH, 4PPOMe and $(4PP)_2$

1-(2-hydroxyethyl)-4-phenyl-pyridinium, bromide (4PPOH)

4PPOH was synthesized by treating 2 mmols 4-Phenylpyridine (310 mg) with 3.36 mmols (0.238 mL) 2-bromoethanol in 100 mL anhydrous acetone under nitrogen atmosphere. The mixture was stirred and heated to reflux at 56-57^{o}C for 24 hours. The reaction was cooled

down to room temperature then the product was dried under vacuum. The crude product was further purified by column chromatography (SiO_2, 1:1 CH_2Cl_2 and Et_2O). White solid product was obtained (355 mg, 63.3%). ^{1}H NMR (500 MHz, D_2O) δ = 8.90 (d, 2H, CH-pyridinium), 8.42 (d, 2H, CH-pyridinium), 8.04 (d, 2H, CH-benzene), 7.74 (t, 3H, CH-benzene), 4.79 (s, 2H, methylene), 4.17 (s, 2H, methylene) ppm. MS (FAB): 200 $(4PPOH)^+$.

1-(2-(4-phenyl-pyridinium bromide)ethoxy)-2-methoxyethane (4PPOMe)

4PPOMe was synthesized by treating 2.0 mmols 4-Phenylpyridine (310 mg) with 6.0 mmols (2.2 mL) 1-bromo-2-(2-methoxyethoxy)ethane in 100 mL anhydrous hexanes under nitrogen atmosphere. The mixture was stirred and heated to reflux for 24 hours. The reaction was cooled down to room temperature then the product was dried under vacuum. The crude product was further purified by column chromatography (SiO_2, 1:1 CH_2Cl_2 and Et_2O). White solid product was obtained (483 mg, 71.4%). ^{1}H NMR (500 MHz, D_2O) δ = 8.63 (d, 2H, CH-pyridinium), 8.13 (d, 2H, CH-pyridinium), 7.76 (d, 2H, CH-benzene), 7.47 (t, 3H, CH-benzene), 4.58 (s, 2H, 1-O-C), 3.88 (s, 2H, 1-O-C), 3.49 (s, 2H, 1-O-C), 3.36 (s, 2H, 1-O-C), 1.11 (s, 3H, methylene) ppm. MS (FAB): 258 $(4PPOMe)^+$.

1,2 Bis(2-(4-phenyl-pyridinium chloride)ethoxy) ethane ($(4PP)_2$)

$(4PP)_2$ was synthesized by treating5.0 mmols (776 mg) of 4-phenyl-pyridine with 1.0 mmols (0.16 mL) 1,2-Bis(2-chloroethoxy)ethane in 100 mL anhydrous CH_3CN under nitrogen atomosphere. The mixture was stirred and heated to reflux at 96^{o}C for 72 hours. The reaction was cooled down to room temperature for 12 hours then the product was dried under vacuum. The crude product was further purified by column chromatography (SiO_2, 1:1 CH_2Cl_2 and

Et_2O). White solid product was obtained (203 mg, 40.8%). ^{1}H NMR (500 MHz, D_2O) δ = 8.79 (d, 4H, CH-pyridinium), 8.21 (d, 4H, CH-pyridinium), 7.86 (d, 4H, CH-benzene), 7.71 (d, 2H, CH-benzene), 7.64 (d, 4H, CH-benzene), 4.79 (s, 4H, 1-O-C), 4.08 (s, 4H, 1-O-C), 3.77 (s, 4H, 1-O-C) ppm. MS (FAB): 426 $(4PP)_2^{2+}$.

The anticipated structures of all these compounds were confirmed by ^{1}H-NMR and MS (FAB).

Electrochemical experiments:

The electrochemical experiments were performed with a BAS 100B/W workstation from Bioanalytical Systems. The single compartment electrochemical cell was fitted with a glassy carbon working electrode (0.071 cm^2), platinum flag counter electrode, and Ag/AgCl reference electrode. The solution contained ca. 1 mM of MV^{2+} and variable concentrations of CB8 plus 0.1 M NaCl as supporting electrolyte. The working electrode was polished with a 0.05-μm alumina powder/water slurry on a felt surface. The electrolysis solution was purged with purified nitrogen before the voltammetric experiments and kept under a nitrogen atmosphere throughout.

Chapter 5

AN INTRODUCTION OF HYDROGEN BONDING IN SUPRAMOLECULAR CHEMISTRY

5.1 Introduction to hydrogen bonding

5.1.1 Hydrogen bonding

Nature utilizes the cooperative interaction of discrete non-covalent forces, including hydrogen bonding, hydrophobic interaction, metal-ligand coordination, and aromatic stacking, to construct the three dimensional structures and functions of bio-macromolecules.[41] In supramolecular chemistry, hydrogen bonding is one of the most well studied reversible intermolecular interactions used to fabricate self-organized structures.[42,43] Weak interactions between molecules containing hydroxyl groups were already denoted in 1892 by Nernst.[44] A hydrogen bond is a special type of attractive interaction that is usually donated as X-H…Y. Usually X and Y in a hydrogen bond are atoms that have electronegativities larger than a hydrogen atom, such as C, N, O, F, P, S, Cl, Se, Br, and I. The X-H group is called a proton donor and Y is referred to as a proton acceptor (A).

5.1.2 Biological and supramolecular chemical importance of hydrogen bonds

The strength of a hydrogen bond always ranges from 1.0 to 40 kcal·mol^{-1}. In the past many years self-assembly mediated by hydrogen bonding is one of the most well studied approaches to creating structures with nanometer dimensions in biology and supramolecular chemistry field. Hydrogen bonds play an important role in determining the structures and

properties of biological macromolecules.[45] Most natural building blocks have rich sources of hydrogen bonding since life evolves in an aqueous environment, which contains hydrogen bonding. Nucleobases found in DNA and RNA give rise to some of the most familiar hydrogen bond motifs for many years. On the other hand, hydrogen bonding has been described as the "master key interaction in supramolecular chemistry" due to its directionality, specificity, and strength.[46] One of the interesting aspects of hydrogen bonding in supramolecular chemistry is that hydrogen bonds can occur between different parts of a single molecule as well as between molecules. From this, it is possible to produce new well-defined unnatural assemblies selectively.

The typical hydrogen bond is stronger than van der Waals forces, but weaker than covalent or ionic bonds. In the past decade, a large number of artificial supramolecular architectures have been assembled based on single non-covalent force, such as transition metal-ligand interaction, hydrogen bonding, or electrostatic interaction, and hydrophobic interaction.[41] The ability to form and break bonds in response to temperature or stress can confer properties that are not achievable in covalently bonded systems.[47]

5.2 Multiple hydrogen bonds and self assembly

5.2.1 Multiple hydrogen bonds

A single hydrogen bond is useful in some organic functionality, but the relatively low stability on single hydrogen bond limited their utility in non-covalent interactions to prepare new and well-defined structures. Multiple hydrogen-bonded systems have gained great

success in the construction of many superstructures and applications in the field of material science, catalysis, and template synthesis.[46] Compared to other noncovalent interactions, the most significant advantage of hydrogen bonding is that it is directional and reversible. While the strength of single hydrogen bonding is always too weak to stabilize the complex or assemble well-defined structures, the combination of multiple hydrogen bonding motifs can be strong enough to establish more than one bond and build supramolecular assemblies, as well as other non-covalent forces to form highly complex supramolecular aggregates.

Multiple hydrogen bonds play an important role in self-assembly. It is a process that creates structures through a statistical exploration of many possibilities. The application to construct novel supramolecular architechtures requires remarkable bond strength and structural diversity. Owing to the directionality and specificity, multiple hydrogen bonds become particular useful motifs to build self-assembly of smaller molecular components to generate supramolecular features.

5.2.2 The Jorgensen Model

For non-covalent structures formed by two self complementary components through triple hydrogen bond motif, the parameters (like temperature or density) which can affect the dimeric process are consequently studied. Jorgensen and co-workers proved that the number of hydrogen bonds is not the only important parameter leading to the difference of molecular forces in the triple hydrogen bonded dimeric complexes.[48-50]

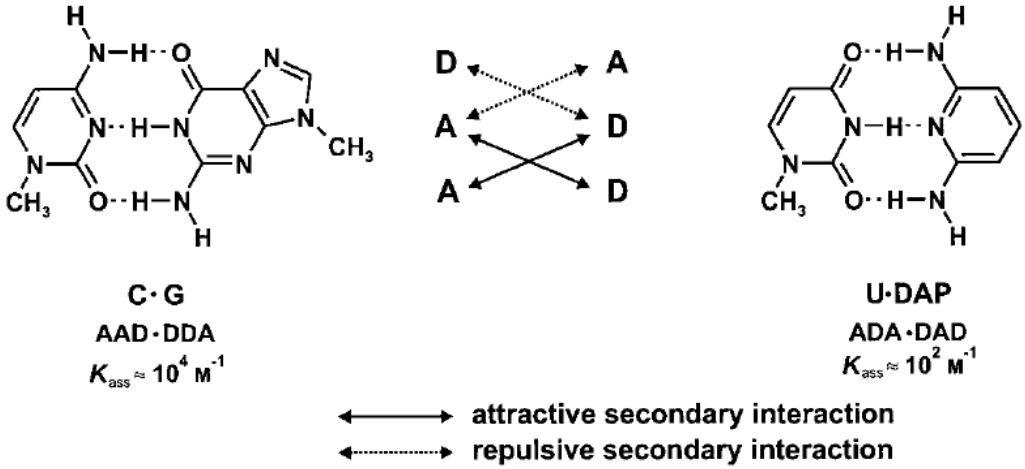

Scheme 5.1 Attractive and repulsive secondary interactions for the 1-methylcytosine·9-methylguanine (C·G) and the 1-methyluracil·2,6-diaminopyridine (U·DAP) dimer.

In **Scheme 5.1** it is shown that the stabilities and strength corresponding to the triple hydrogen bonding motif can be attributed to the attractive and repulsive secondary interactions. The energy of C·G dimer is 10.7 kcal·mol^{-1} lower than that of U·DAP dimer calculated from molecular dynamics simulations. This is because in the C·G complex, two pairs of secondary interactions are attractive and two pairs are repulsive, while in U·DAP complex, they are all repulsive. The computed results are consistant with the experimental binding data.[51,52]

5.3 Complementary quadruple H-bond

5.3.1 Meijer's and Zimmerman's quadruple hydrogen bonded modules

Quadruple hydrogen-bond motifs have been predicted to be much stronger than double or triple hydrogen motifs. Various polar functionalities have been reported to be dimerized through quadruple hydrogen bonds. A close-planar quadruple hydrogen bonding structure can

help to increase the molecular rigidity. Inspired by the hydrogen-bonding capability of nucleobases found in DNA duplexes, quadruple hydrogen-bonded systems are mainly based on functionalized nucleobases, especially urea derivatives. Heterocycle-based quadruple hydrogen-bonded systems developed by the groups of Meijer et al. and Zimmerman et al. are examples of great success.[6] Meijer and co-workers first report the strong self dimerization of a series of 2-ureido-4-[1H]-pyrimidinone(Upy) derivatives that can dimerize through four hydrogen bonds.[53,54]

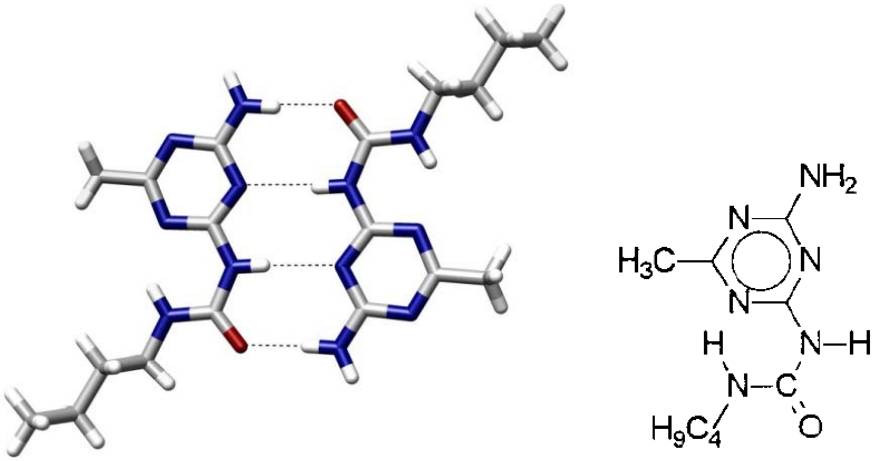

Figure 5.1 An example of intermolecular hydrogen bonding in a self-assembled dimer complex reported by Meijer and coworkers.[53]

The DDAA array that exists in the ureidopyrimidone molecule may tautomerize in different forms and reach equilibrium. The 4-[1H]-pyrimidinone tautomer (DDAA) is in equilibrium with pyrimidin-4-ol tautomer (DADA), as shown in **Scheme 5.2**.

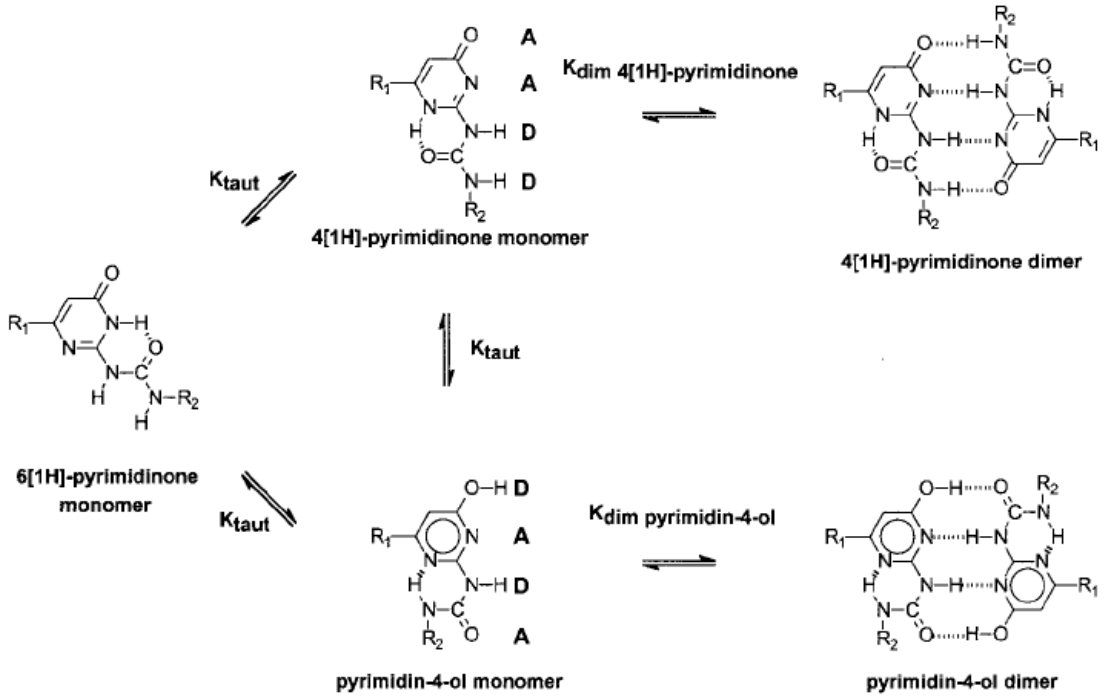

Scheme 5.2 Different tautomeric forms of Meijer and co-workers' ureidopyrimidone derivatives and their dimerization equilibrium constants.

Both species are self-complementary and the dimerization constant of such module is found to be larger than 10^6 M^{-1} in chloroform and 10^7 M^{-1} in toluene. Solvent polarity affects the equilibrium between the two tautomers. Based on the Jorgensen model theory, the secondary interactions in DADA form are predicted to contain three pairs of repulsive interactions while it only contains one pair of repulsive and two pairs of attractive interactions in the DDAA form as shown in **Figure 5.2**.

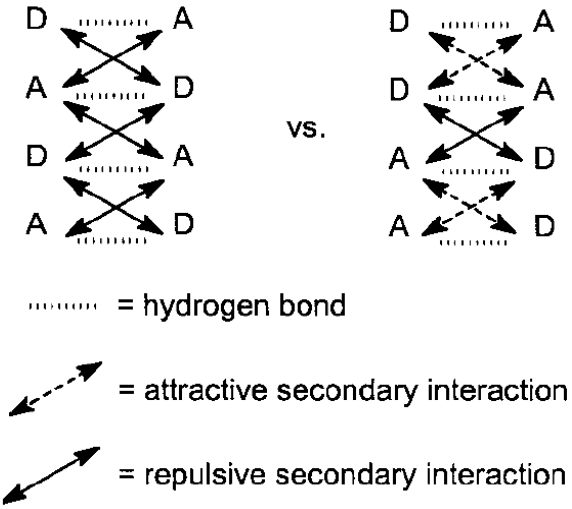

Figure 5.2 Secondary interactions comparison between DADA and DDAA form.[54]

These predicted values are in agreement with the experimental results. Hydrogen bonding strength depends on electron distribution of adjacent atoms strongly in a molecular assembly. In this regard, self-complementary hydrogen bonding motifs containing neighboring donor-donor-acceptor-acceptor (DDAA) groups are more stable than DADA.

5.3.2 Upy dendrimers

Dendrimers are attractive building blocks in supramolecular chemistry. The large size of a dendrimer moiety may play an important role in the self-assembly and self dimerization as the dendrimer generation increases. To apply Upy units in self-assembly of dendrimers, our group developed Newkome-type dendrimers containing a single Upy residue covalently attached to their apical positions. [15] The dendrimers in **Figure 5.3** are designed from generation one (G1) to generation three (G3). From the ^{1}H NMR spectroscopic analysis it is

found that the dendrimers exhibit a pronounced generation effect on the quadruple hydrogen bonded dimer stabilities.

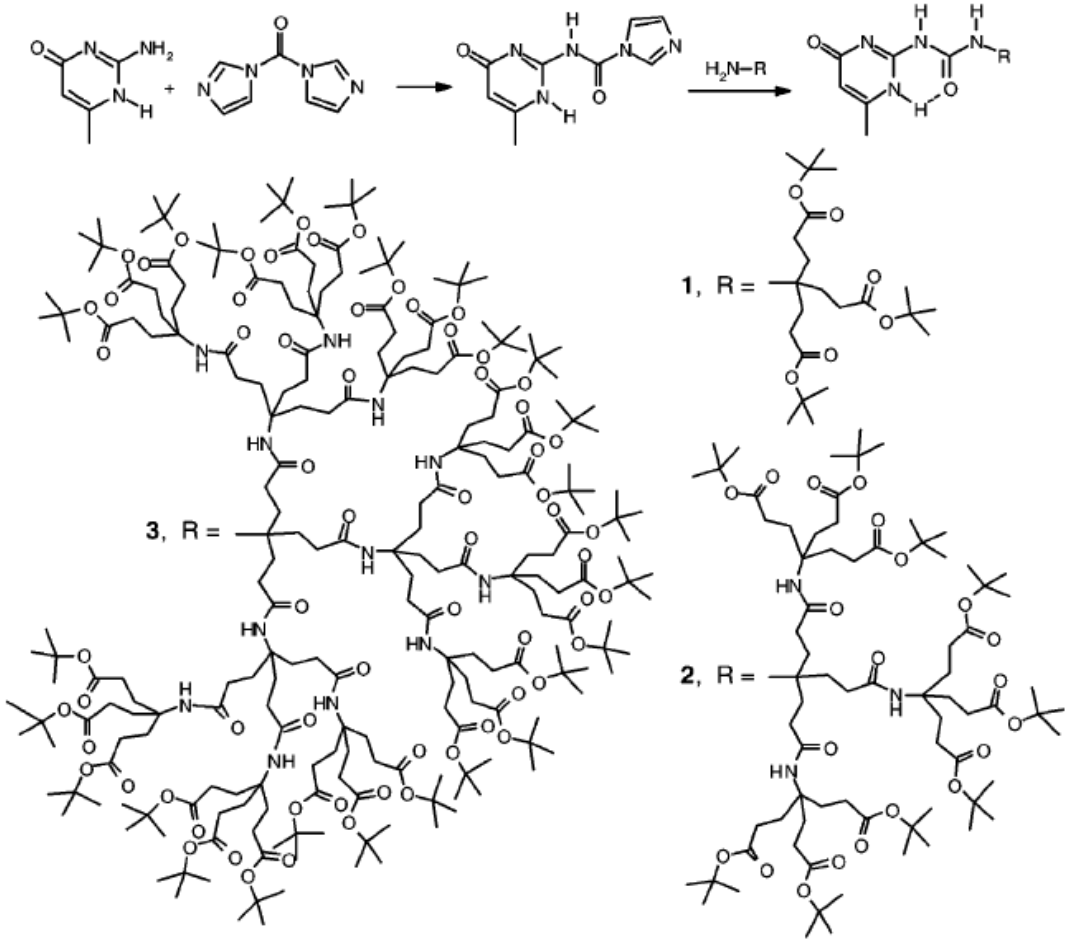

Figure 5.3 Synthesis and structure of uridopyrimidine dendrimers G1-G3.[55]

In low polar solvents, the first and second generation dendrimers form strong hydrogen bonding between the two Upy units. However, the third generation becomes much less dimerized from ^{1}H NMR analysis, vapor pressure osmometry investigation. Interestingly, a similar dendrimer with same Upy backbone but different dendrimer moiety has been reported dimerized with high binding constants.[56] The increasing generation and steric effect could not weaken the hydrogen bonding motif in the center of the self-dimerized dendrimers. The

structures of these dendrimers are shown in **Figure 5.4**.

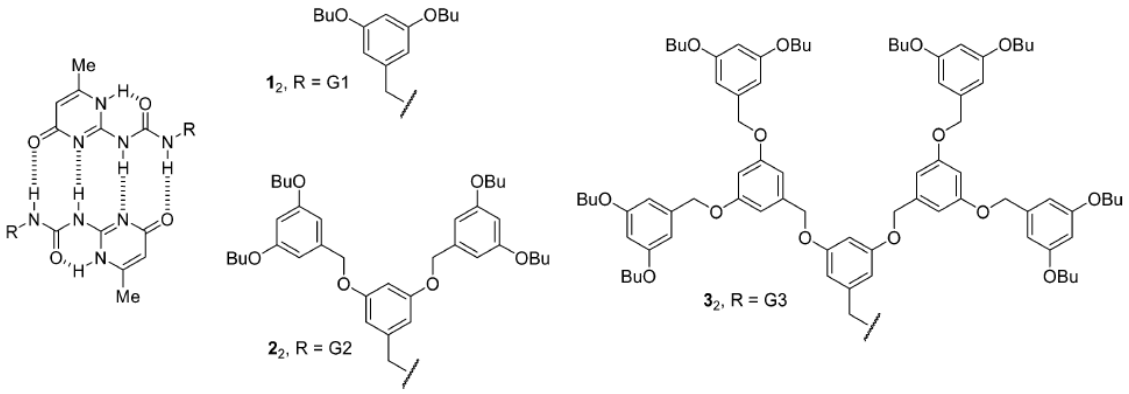

Figure 5.4 Structures of self-assembling dendronized dimers.[56]

5.3.3 Urea-functionalized guanine, 7-deazaguanine and ureidodiaminopurine

To avoid the limitation resulting from the tautomerism from Upy units, there is intense research interest in designing new self-assembling molecules having multiple hydrogen bonding arrays. In recent years, Zimmerman and co-workers have shown that urea-functionalized guanine (UG) and 7-deazaguanine (DeUG), unlike UPy, are tautomerically stable. UG is more favorable to be *anti* while DeUG preferred to be in the *syn* comformation. Such *anti/syn* conformational equilibrium can be controlled by atomic mutation in the fused ring.[57]

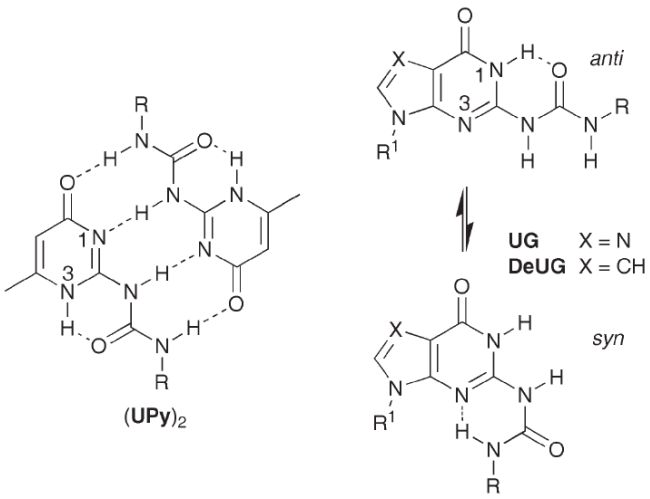

Figure 5.5 Upy dimer and UG and DeUG molecular structures.

As shown in **Figure 5.5**, the structures of UG and DeUG are mostly determined by hydrogen bonds between amide N-H groups of one residue and C=O groups of another. With a preorganized ADDA edge and free from competing tautomeric/conformational equilibria, DeUG is particularly well-suited to forming heterodimeric complexes with DAAD partners with high binding constant value. Likewise, both UG and DeUG are designed to self-associate weakly by various DA motifs in $CDCl_3$. The corresponding intermolecular interactions govern the interplay of order and mobility, as well as the properties and functionality in such systems.

Another self-complementary quadruple hydrogen bonded complex, ureidodiaminopurine (UDAP) has been reported. UDAP can form a well preorganized intermolecular dimer via a DADA hydrogen bonding motif in the *syn* form. The study of UDAP confirms that the dimerization is the predominant mode of assembly so that the mononers of UDAP prefer the *syn* form as in **Figure 5.6**.[58]

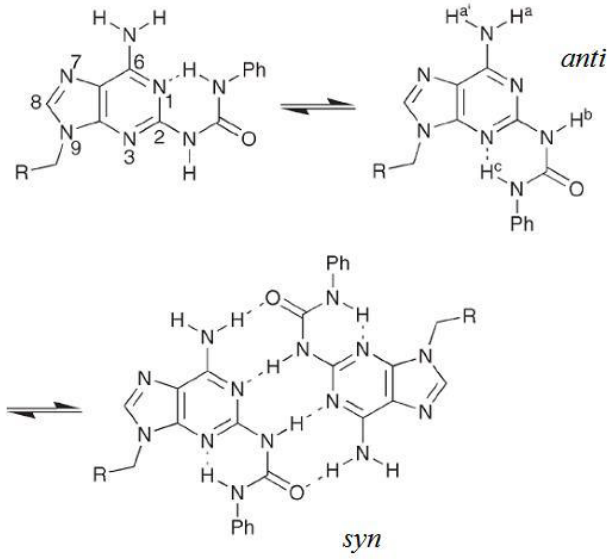

Figure 5.6 Intramolecular and intermolecular hydrogen bonding in UDAP.

5.3.4 Sanjayan's DDAA motif

Among the various self-assembling modules reported above, heterocycle-based AADD-type self-complementary systems have ushered into prominence primarily due to their relatively high dimerization constants coupled with ready synthetic accessibility.[59] Meijer's AADD-type self-complementary arrays are developed and studied in nonpolar solvents in a wide concentration range, making them excellent building blocks for supramolecular architectures. However, despite the many successes outlined of quadruple hydrogen-bonded Upy modules, the tautomeric behavior does have its drawbacks. The study of multiple hydrogen bondings is constantly evolving in supramolecular assembly, but tautomerism limits the further enhance on the strength, directionality, and specificity of hydrogen bonding interactions. The generality of self-assembling systems based on rigid heterocycles is sometimes complicated by prototropy that is often associated with heterocycles. There is a

strong need for the development of new quadruple hydrogen-bonded systems to meet the demand of increasing applications.[46] Meijer's Upy DDAA motif has been modified by Sanjayan and coworkers to avoid the complications arising from keto-enol tautomerism.

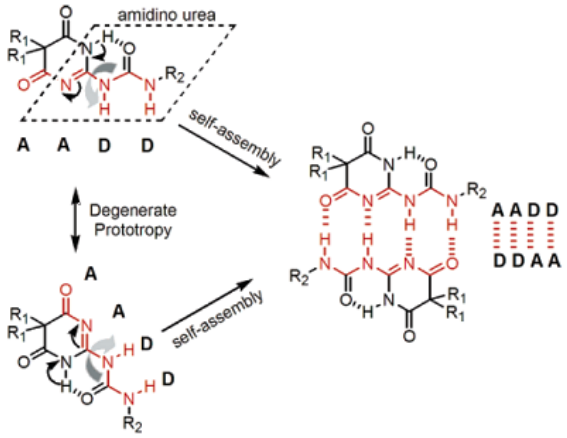

Figure 5.7 Degenerate prototropy in Sanjayan's DDAA.[59]

Figure 5.7 describes the rotation approach of addressing the prototropy-realated urea moiety in heterocycle-based self-dimerized systems. The utility of degenerate prototropy is demonstrated by developing AADD-type self-assembling modules. Their ready synthetic accessibility coupled with the novel property of degenerate prototropy and the great ease of crystal formation would make these novel self-assembling molecules promising candidates for many proposed applications.[59]

5.4 Supramolecular polymer

Stimulated by the potential applications in sensors, molecular electronics, and catalysts, great efforts have been paid to supramolecular polymers, which are polymerized through hydrogen bondings. In general, supramolecular polymers can be classified into two classes, main chain and side chain. In main chain type polymers, crossing networks and linear

main-chain based on bidirectional units with hydrogen bonding motif are two major series. In side chain polymers, the polymers bearing binding motifs are on the main chain or on the side chains are two different types. Systems of multiple hydrogen bonds served as reversible and flexible cross-links in supramolecular polymers.[60] Specific examples of Upy polymers with their polymeric backbone of unique macroscopic properties have been reported.[47] Supramolecular chemistry has focused on the development of the well-defined molecular aggregates through hydrogen bonding interactions between individual building blocks.

Chapter 6

DIMERIZATION OF UREIDO PYRIMIDINEDIONE DERIVATIVES CONTAINING QUADRUPLE HYDROGEN BONDING MOTIF

6.1 Hydrogen bond background and Sanjayan's previous relevant work

Hydrogen bonding is found to play an important role in supramolecular chemistry since 1892, first noted by Nernst. [44] Although single hydrogen bonding is weak and easy to break in all kinds of intermolecular forces, multiple hydrogen bonding motifs exhibit a remarkably higher stability in building supramolecular assemblies. [61,62] The design and characterization of hydrogen bonding arrays is an important research topic within supramolecular chemistry. Furthermore, it is of great interest to investigate the self-assembly of self-complementary modules through four neighboring parallel hydrogen bonds.

Meijer and co-workers first synthesized a series of dimerized ureidopyrimidine derivatives which may form two different tautomers. [53,54] To prevent this keto-enol tautomerism, Sanjayan and co-workers reported a modified quadruple hydrogen bonding system. [59,63-66]

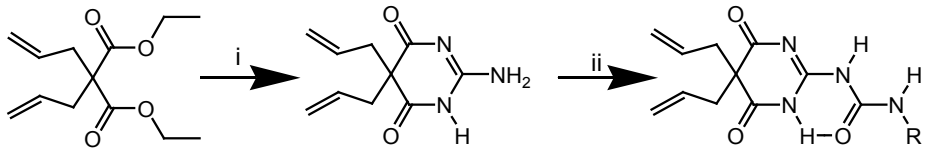

Scheme 6.1 Synthesis of R-DDAA.[59]

6.2 Synthesis and structures of R-DDAA compounds

To understand more on non covalent interactions in molecular self-assemblies and electron transport between these units in nature, our group designed redox active self dimerizing via quadruple hydrogen bonding ferrocene dimer as shown in **Figure 6.1**. The electrochemical studies revealed that there is an excellent communication between the two ferrocene centers through hydrogen bonding. In non polar solvents such as CH_2Cl_2, Fc-DDAA moiety shows two one-electron oxidation waves for the dimer. But in polar solvent like CH_3CN, it shows only one oxidation wave, because the compound is in monomer form due to weak hydrogen bonding. These results show there is good communication between Fc centers upon oxidation in CH_2Cl_2. After oxidation there is a rapid electron transfer or communication via H- bonding between Fe^{II} and Fe^{III} centers resulting one Fe center to be oxidized at higher potentials. The results were supported with inter valence charge transfer (IVCT) bands observed at λ_{max}=1195 nm and also the X-ray crystal structure. Even though the distance between Fc centers is around 13.1 nm, they exhibit a remarkable level of electronic communication mainly due to the quadruple hydrogen bonds.

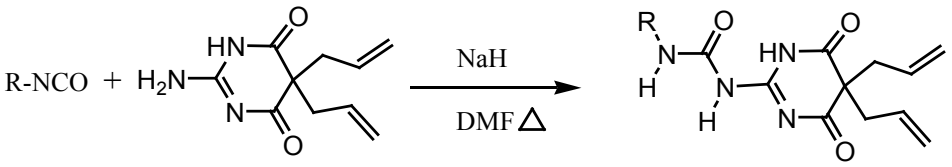

3 4 5 6 7 8 9

Figure 6.1 Synthesis and structures of the self-complementary compounds surveyed in this chapter.

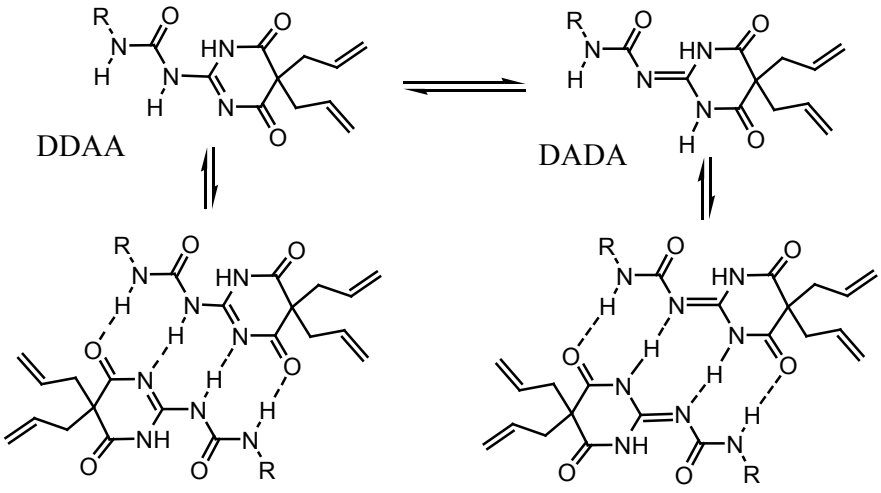

Scheme 6.2 DDAA dimers and DADA dimers and their monomer tautomerization process. The DDAA hydrogen bonding array on the product is indicated by dotted lines.

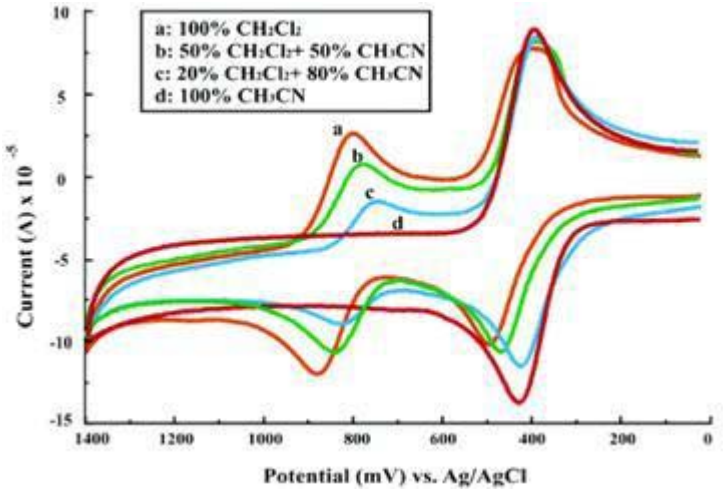

Figure 6.2 Cyclic voltammetric response on glassy carbon (0.071 cm^2) of 1.0 mM Fc-DDAA in 0.2 M $TBAPF_6/CH_2Cl_2$ solution with increasing proportions of CH_3CN. Scan rate: $0.1V{\cdot}s^{-1}$.

In the process of understanding quadruple hydrogen bonds assisted electronic communication in ferrocene moieties and also these electronic communication via non covalent interactions, we have prepared several photo and/or electro active self-complementary quadruple hydrogen bonded compounds. So far, we have prepared

molecules with isopropyl, ferrocene, phenyl, 1-naphthalene or 2-naphthalene, pyrene and fluorene units attached to the DDAA residue. [67,68].

6.3 Self-dimerization by ^{1}H NMR spectroscopic analysis

These DDAA derivatives **3-9** all form self-assembled dimers in non-polar solvent through quadruple hydrogen bonds, which are evident in their ^{1}H NMR spectra with the visible hydrogen-bonded NH peaks. The self-dimerization process of **3-9** can be written as

(A) $\mathbf{3} + \mathbf{3} \overset{K_{dim}}{\rightleftharpoons} \mathbf{3_2}$

(B) $\mathbf{4} + \mathbf{4} \overset{K_{dim}}{\rightleftharpoons} \mathbf{4_2}$

(C) $\mathbf{5} + \mathbf{5} \overset{K_{dim}}{\rightleftharpoons} \mathbf{5_2}$

(D) $\mathbf{6} + \mathbf{6} \overset{K_{dim}}{\rightleftharpoons} \mathbf{6_2}$

(E) $\mathbf{7} + \mathbf{7} \overset{K_{dim}}{\rightleftharpoons} \mathbf{7_2}$

(F) $\mathbf{8} + \mathbf{8} \overset{K_{dim}}{\rightleftharpoons} \mathbf{8_2}$

(G) $\mathbf{9} + \mathbf{9} \overset{K_{dim}}{\rightleftharpoons} \mathbf{9_2}$

Scheme 6.3 Homodimerization process of compounds **3-9**

In order to assess the stability of these dimers we monitored the chemical shifts of the three NH protons as a function of temperature with samples of compound **5** (Ph-DDAA) in $CDCl_3$ solution (**Figure 6.3**).[67]

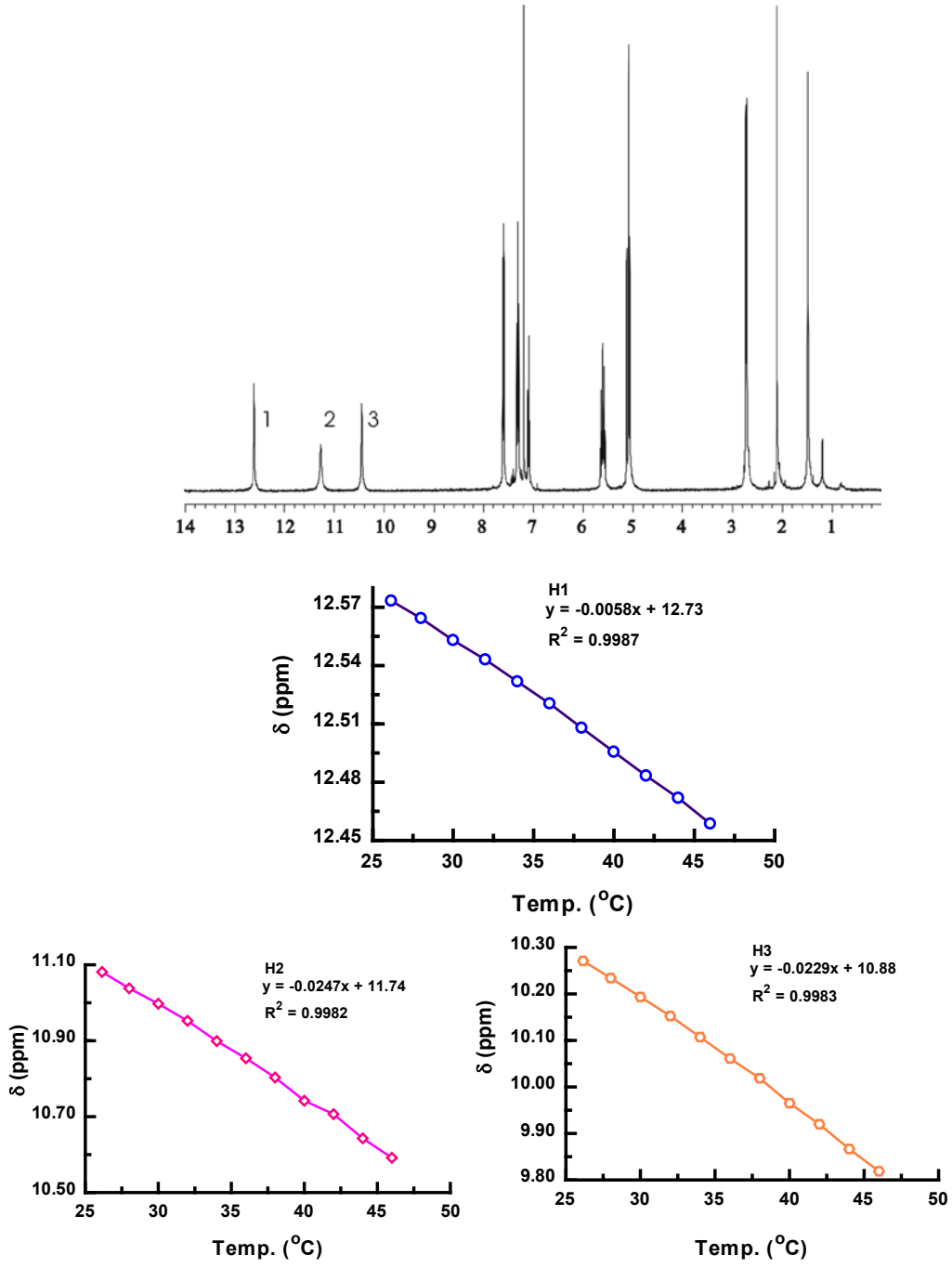

Figure 6.3 ^{1}H NMR spectrum (400 MHz) of compound **5** (Ph-DDAA) self association in $CDCl_3$, and the chemical shift (δ) of H1, H2 and H3 at varibale temperatures.

Each R-DDAA dimer contains three proton signals corresponding to three hydrogen bonds at low field, 14-9 ppm. We found that the chemical shift of the lowest field NH proton (H1) of PhDDAA is not very sensitive to temperature in the range 25–50 ^{o}C [δ (ppm) = 12.73-0.006·T (^{o}C)]. In clear contrast to this, the other two NH protons, H2 and H3 both exhibit greater temperature sensitivity: δ (ppm) = 11.74-0.0247·T (^{o}C) and δ (ppm) = 10.88-0.0229·T (^{o}C). The displacement of all the NH resonances to higher field with increasing temperature is consistent with a decreasing proportion of dimer in the equilibrium mixture. However, the small temperature sensitivity of the lowest field NH proton, H1, reveals that this peak corresponds to the intramolecular hydrogen bond, while H2 and H3 peaks correspond to the intermolecular hydrogen bonds primarily responsible for the formation of the dimer.

In order to investigate the self-complementary dimerization constant of all these DDAA compounds, a series of diluting titration experiments were performed by ^{1}H NMR spectroscopy. A concentrated pure R-DDAA in deuterated $CHCl_3$ or CH_2Cl_2 solution is diluted with pure dry deuterated solvent (dependant on the solubility of R-DDAA in different solvent) from higher concentration at ca. 10-12 mM to 0.5 mM, at constant temperature (26 ^{o}C) with same parameters.

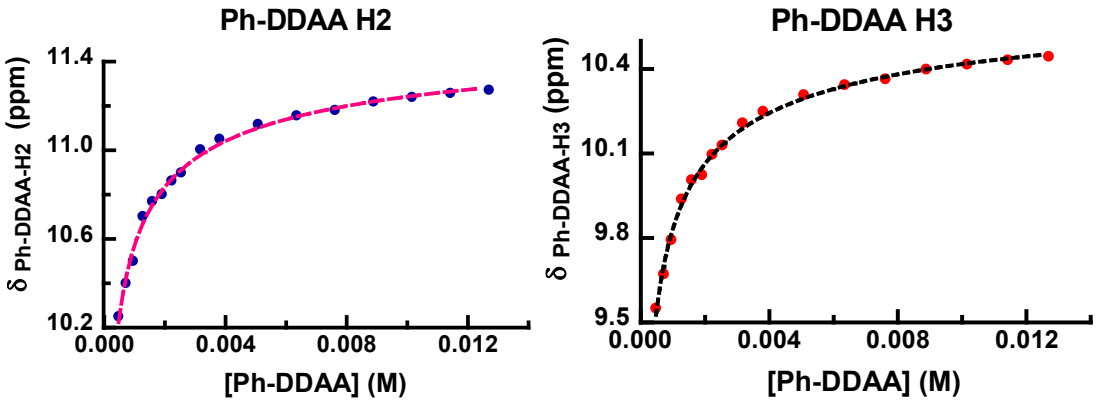

Figure 6.4 Dilution shifts for NH (H2 and H3) protons of compound **5** (Ph-DDAA).

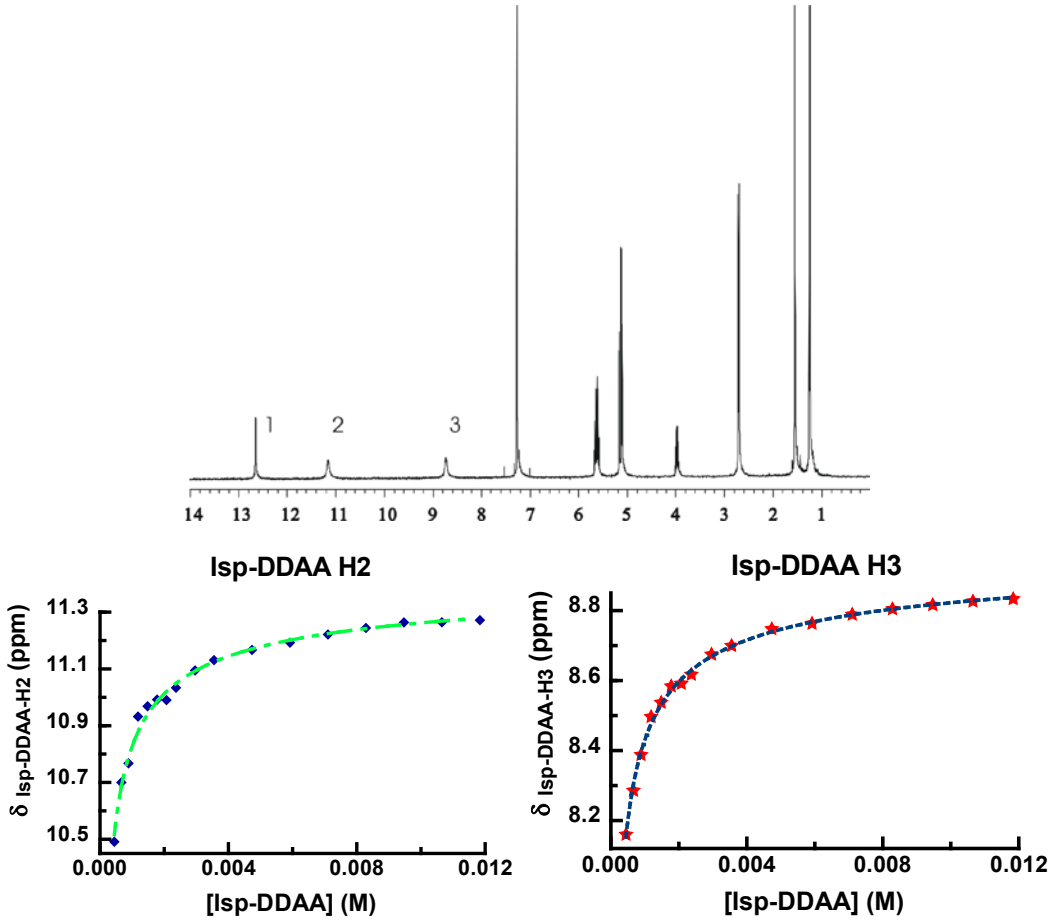

Figure 6.5 ^{1}H NMR spectrum (400 MHz) of compound **3** (Isp-DDAA) self association in $CDCl_3$, and dilution shifts for NH (H2 and H3) protons of compound **3**.

From the results obtained in ^{1}H NMR spectra, the chemical shift values corresponding to the hydrogen bonding recorded at variable concentrations are plotted vs. R-DDAA concentration with a simulation curve to calculate the self dimerizing constant, K_{dim}. Lowering the analytical concentration of the DDAA compound should increase the [monomer]/[dimer] ratio and shift the NH proton resonances to higher field. We did observe upfield shifts for all the NH proton signals on dilution, but the magnitude of the shift was very small in the case of the lowest field NH proton (confirming its engagement in an intramolecular hydrogen bond) and more pronounced in the case of the other two NH protons. Since the chemical shift (δ_{obs}) of the latter protons can be expressed as

$$\delta_{obs} = \delta_m \cdot x_m + \delta_d \cdot x_d$$

where the subscripts 'm' and 'd' refer to monomer and dimer, respectively, we fitted the experimental data using regression analysis to obtain the equilibrium constants for the dimerization process (K_{dim}).

Similar data were obtained in dilution experiments with 3, 4, 6, 7 and 9 in $CDCl_3$ or CD_2Cl_2 solution (**Figure 6.5** – **Figure 6.9**). The resulting values of K_{dim} are given in **Table 6.1**.

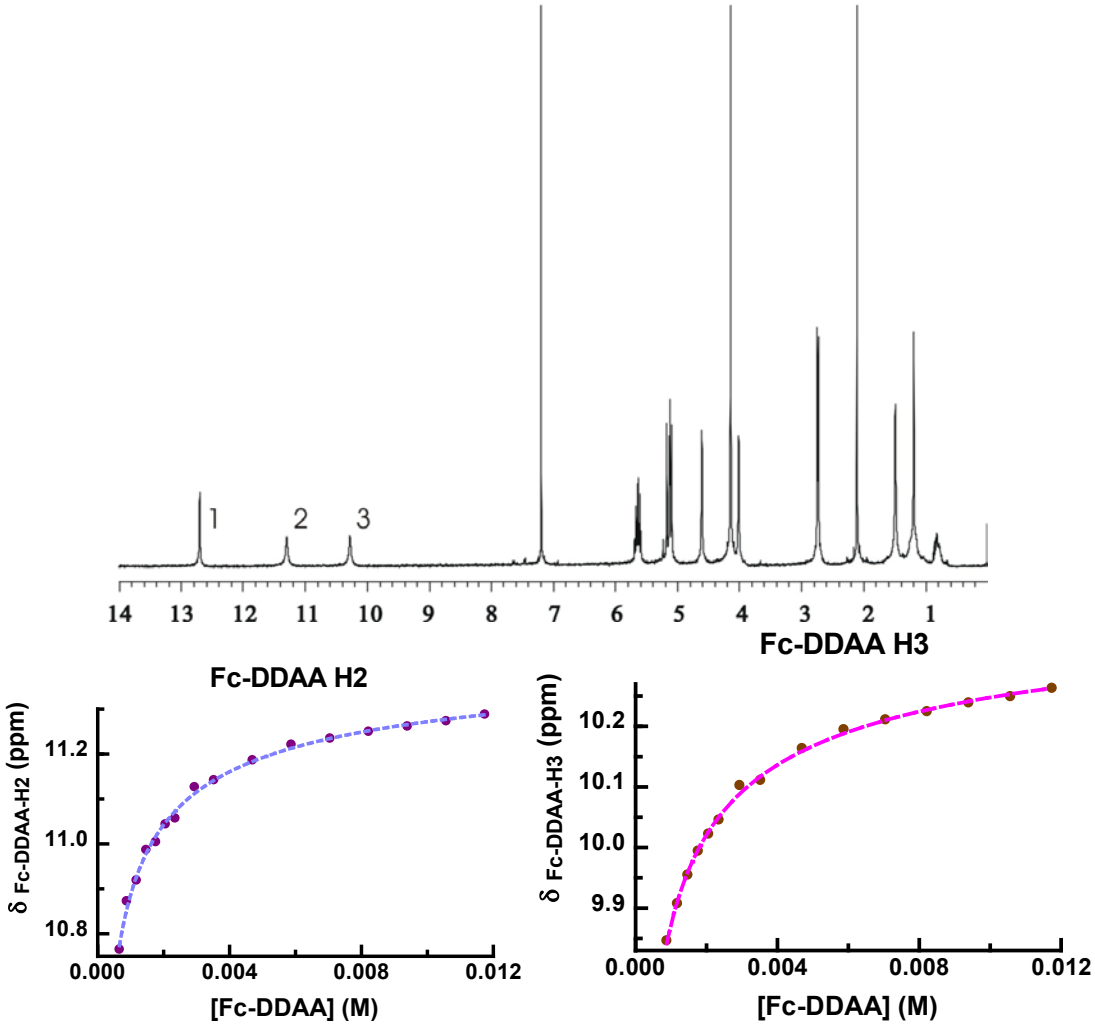

Figure 6.6 ^{1}H NMR spectrum (400 MHz) of compound **4** (Fc-DDAA) self association in $CDCl_3$, and dilution shifts for NH (H2 and H3) protons of compound **4**.

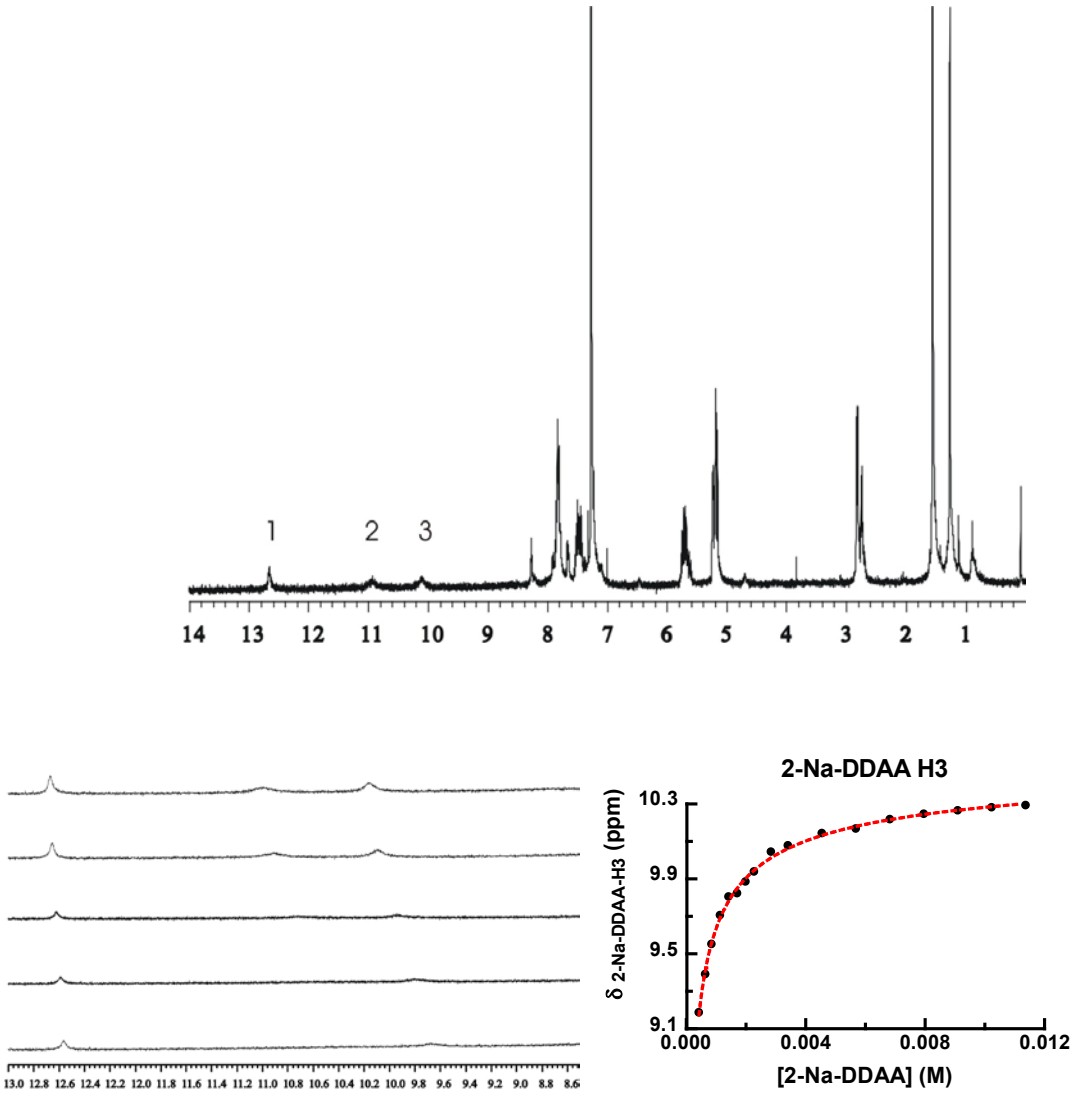

Figure 6.7 ^{1}H NMR spectrum (400 MHz) of compound **6** (2-Naph-DDAA) self association in $CDCl_3$, and dilution shifts for NH (H2 and H3) protons of compound **6**.

In 2-Naph-DDAA solution, the proton signals corresponding to H2 becomes broad and disappear very quickly in the dilution experiments. This behavior leads to limitations to get the simulated results of K_{dim} from H2 chemical shift values. We only obtained the result from H3 data.

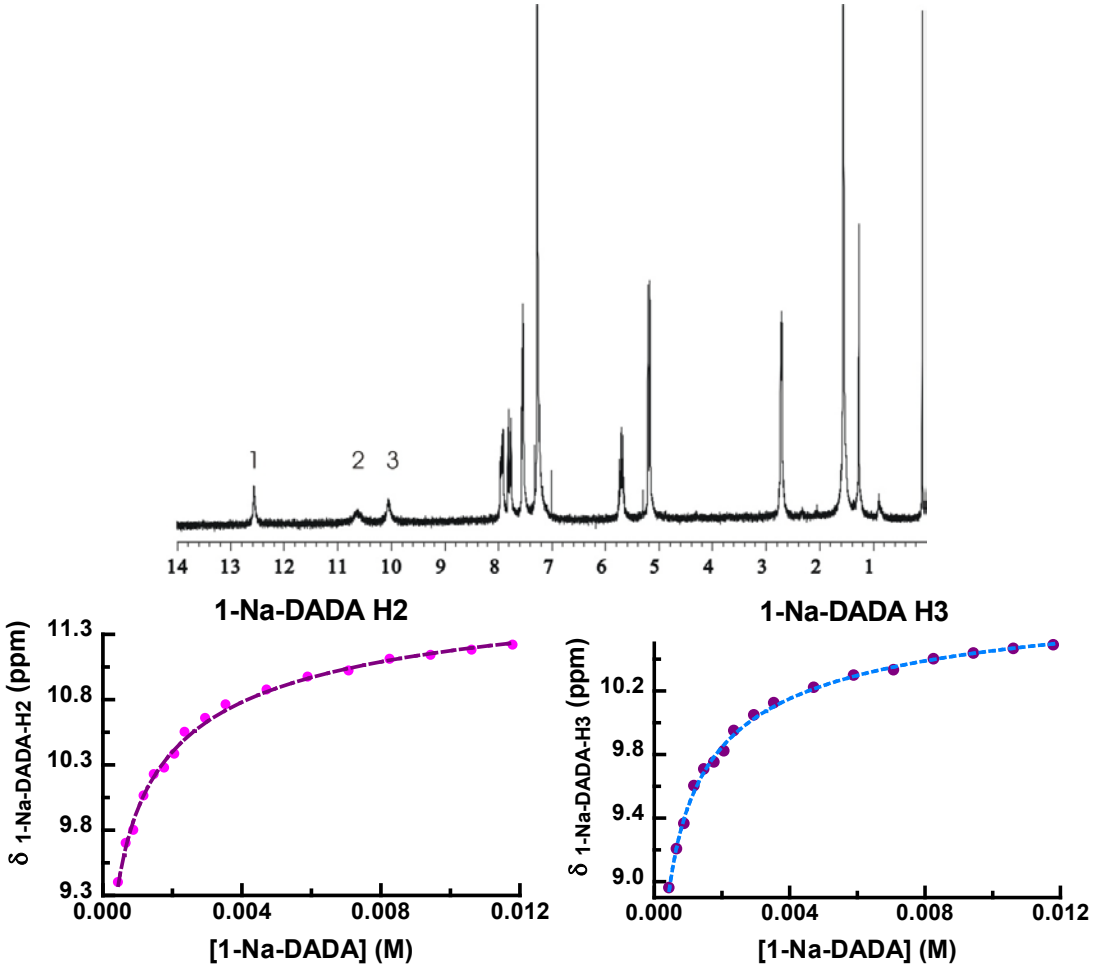

Figure 6.8 ^{1}H NMR spectrum (400 MHz) of compound **7** (1-Na-DADA) self association in $CDCl_3$, and dilution shifts for NH (H2 and H3) protons of compound **7**.

Table 6.1 The calculated equilibrium constants for the dimerization process (K_{dim}).

Compound	K_{dim} (M^{-1}) From δ of H2	K_{dim} (M^{-1}) From δ of H3
Ph-DDAA	1.86×10^{4}	2.11×10^{4}
1-Na-DADA	4.72×10^{3}	1.05×10^{4}
2-Na-DDAA	N/A	2.07×10^{5}
isp-DDAA	2.04×10^{3}	2.54×10^{4}
Fc-DDAA	4.33×10^{4}	2.23×10^{4}
Fl-DDAA	1.90×10^{4}	1.92×10^{4}

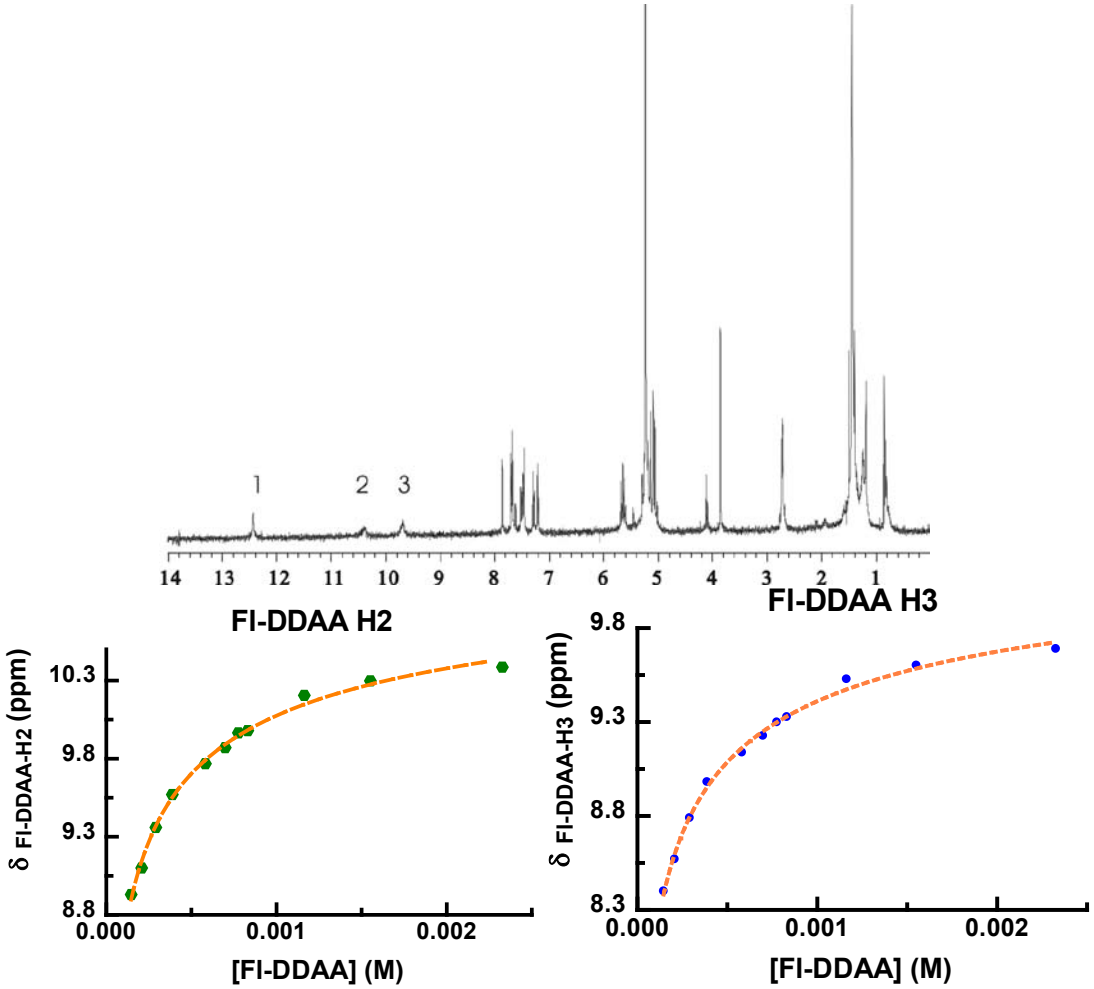

Figure 6.9 ^{1}H NMR spectrum (400 MHz) of compound **9** (Fl-DDAA) self association in CD_2Cl_2, and dilution shifts for NH (H2 and H3) protons of compound **9**.

From the data obtained in **Table 6.1**, we observed that except 2-Naph-DDAA shows a high K_{dim} value (2.07×10^5), all of the other compounds have K_{dim} values in the range 2.04×10^3 - 4.33×10^4, which indicated that these binding are modest in supramolecular chemistry. On the other hand, the H2 proton resonance peaks are always broadened faster than H3 peaks in the dilution process and such behavior may lead to error of K_{dim} calculated from data corresponding to H2. We assume that the K_{dim} values from H3 are more reliable, and most of

these self-dimerized compounds, **3**, **4**, **5**, **8** and **9**, show very close values in K_{dim} (1.92×10^4 – 2.54×10^4) from H3. We anticipate that the different R residue does not affect the self-dimerization too much in these homo-dimers.

However, the K_{dim} obtained for 1-Naph-DADA (1.05×10^4) is the lowest in the values correponding to all DDAA compounds. This lead to our investigation on the crystal structure by X-ray crystal diffraction.

6.4 X-ray crystal structures of DDAA compounds

The extensive dimerization of all DDAA compounds was also verified by X-ray diffraction studies. Single crystals (**Figure 6.10**) suitable for X-ray analysis were obtained by slow diffusion of hexane vapor into chloroform solutions for each of compounds listed below.

All compounds formed single crystals of sufficient quality for X-ray diffraction studies. All five compounds were found to crystallize as hydrogen-bound dimers, and representative dimer structures are shown in **Figure 6.10**. Interestingly compound **4**, **5**, **6** and **9** self-recognize in the solid state, forming dimers through DDAA hydrogen bonding arrays, but compound **7** dimerizes as a tautomeric DADA array.[67] This is a surprising result, not only because these pyrimidinedione derivatives were designed to avoid tautomerization, but also because DDAA dimers are known to be more stable than DADA dimers, due to repulsive secondary interactions between the four parallel hydrogen bonds in the latter case.

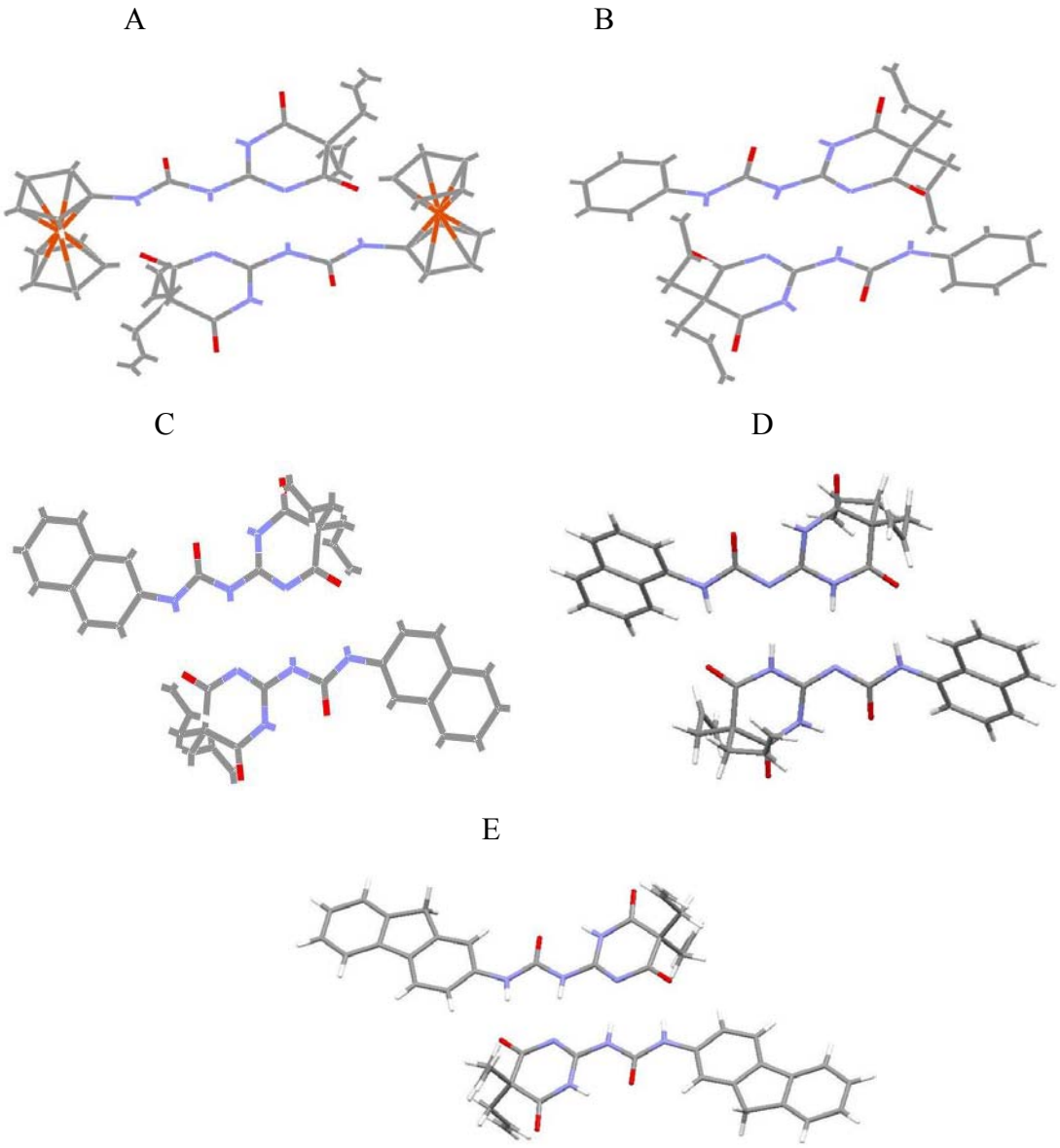

Figure 6.10 Diffraction of X-ray crystal structures of compound (A) **4** (Fc-DDAA), (B) **5** (ph-DDAA), (C) **6** (2-Na-DDAA), (D) **7** (1-Na-DADA) and (E) **9** (Fl-DDAA).

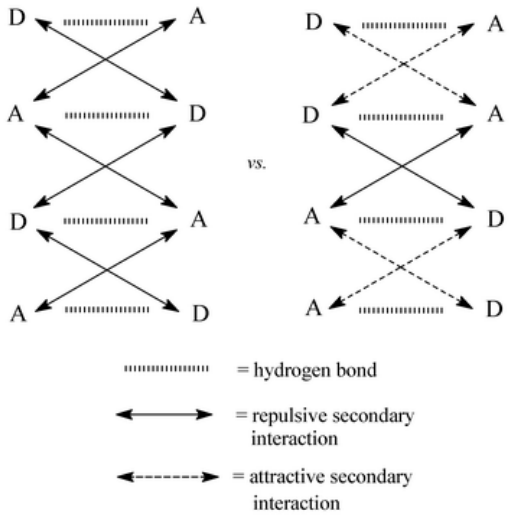

Scheme 6.4 Secondary interactions of DADA and DDAA comparison.

Table 6.2 Representative distances (Å) and angles in the crystal structures of compounds **4**, **5**, **6**, **7** and **9**.

Compound	$d_{H\text{-}O}$[a]	$d_{H\text{-}N}$[b]	$d_{H\text{-}O}$[c]	Angle[d]
4	1.932	2.169	1.912	171.9
5	1.889	2.153	1.842	178.4
6	1.881	2.147	1.765	179.8
7	2.050	2.161	1.742	**143.2**
9	1.882	2.150	1.848	176.2

[a]H-O intermolecular hydrogen bond distance. [b]H-N intermolecular hydrogen bond distance. [c]H-O intramolecular hydrogen bond distance. [d]Dihedral angel between the aromatic residue and the hydrogen bonding plane.

In **Scheme 6.4**, according to the Jorgensen Model, in the DADA dimer, three pairs of secondary interactions are repulsive while only one pair is repulsive and the other two pairs are attractive in DDAA form.

Additionally, it can be noted that, for compounds **4**, **5**, **6** and **9**, the ferrocene and aromatic residues align themselves almost perfectly with the plane formed by the four

hydrogen bonds. Again compound **7** is the exception, as the naphthyl groups are clearly twisted away from the hydrogen bonding plane. Some representative atomic distances in these crystals are listed in **Table 6.2**.

6.5 Computational studies

We also performed DFT calculation by using the B3LYP method with a 3-21G* basis set on the monomeric and dimeric forms of compounds **4, 5, 6, 7 and 9** in an attempt to rationalize the observation of the DDAA and DADA tautomers for each in the crystal structures. These calculations were done for all compounds in their DDAA and DADA tautomers. Starting geometries for the computational work were taken from the X-ray crystal structures data (**Figure 6.10**). A summary of the results is collected in **Table 6.3**.

Table 6.3 Representative distances (Å), angles and energies of formation (kcal□mol^{-1}) calculated for dimmers formed by compounds **5**, **6**, **7** and **9** using DFT methods.

Compound (tautomer)	$d_{H\text{-}O}$ [a]	$d_{H\text{-}N}$ [b]	$d_{H\text{-}O}$ [c]	Angle [d]
4(DDAA)	1.625	1.820	1.665	174
5(DDAA)	1.644	1.826	1.658	179
5(DADA)	1.712	1.870	1.643	179
6(DDAA)	1.642	1.831	1.659	180
6(DADA)	1.707	1.880	1.641	180
7(DDAA)	1.662	1.8125	1.637	154
7(DADA)	1.720	1.856	1.633	153
8(DDAA)	1.651	1.811	1.644	152
8(DADA)[p]	1.942	2.124	1.62	156

A comparision between the hydrogen bonding distances determined experimentally from the X-ray crystal data and those obtained computationally reveals that the latter are uniformly shorter. This finding is easily rationalized by considering that the computational work does not take into account the presence of solvent molecules and, thus, electrostatic attractive interactions, such as hydrogen bonding, are expected to be overemphasized.[67]

In all cases the H-O intermolecular hydrogen bond distances are shorter in dimers formed between DDAA tautomers than in those formed by DADA tautomers. The same trend is observed for the H–N intermolecular hydrogen bond distances. These findings are consistent with the greater stability of dimers formed by self-recognition of DDAA hydrogen bonding arrays vs. those formed by DADA arrays.

Table 6.3 also lists the formation energies obtained from the optimization of these structures. For each of the monomers, more energy is released in the formation of the DADA tautomer than in the formation of the corresponding DDAA form. This is again expected, due to the minimization of electrostatic repulsions in the DADA forms. However, upon dimerization, DDAA dimers are generally found to be slightly more stable than their DADA counterparts. The calculated energy of dimerization is clearly smaller in the case of compound **7** (1-Na-DADA) than for the other three compounds.

6.6 Photochemical studies

Ferrocene (dicyclopentadienyliron) and many of its derivatives were synthesized and characterized since its accidental discovered in 1951. The photochemical behavior of ferrocene

derivative is of great interest. They can be used as excited state quenchers of excited states in fluorescence studies.[69] Compound **4** (Fc-DDAA) has been used as a redox center, in the previous studies of its electrochemical reversible behavior. In the applications of intermolecular or intramolecular quenching **4** is used as a fluorescence quencher in solution.

Considerable interest has focused on electron transfer in hydrogen bonded donor-acceptor supramolecules. To investigate the electron transfer between Fc-DDAA and a fluorophore through quadruple hydrogen bonding motif, we performed the following fluorescence experiments between them. In these photochemical studies, DDAA compounds **6**, **7**, **8** and **9** have been used as photoexcitable electron donors.

Upon addition of one to two drops of DMSO in a 3.5 mL CH_2Cl_2 solution of 30 μM **9** (Fl-DDAA), the fluorescence intensity increases a lot. Since the volume of added DMSO is negligible, solvent polarity is the most significant change. Excitation wavelength is 272 nm. (**Figure 6.11**)

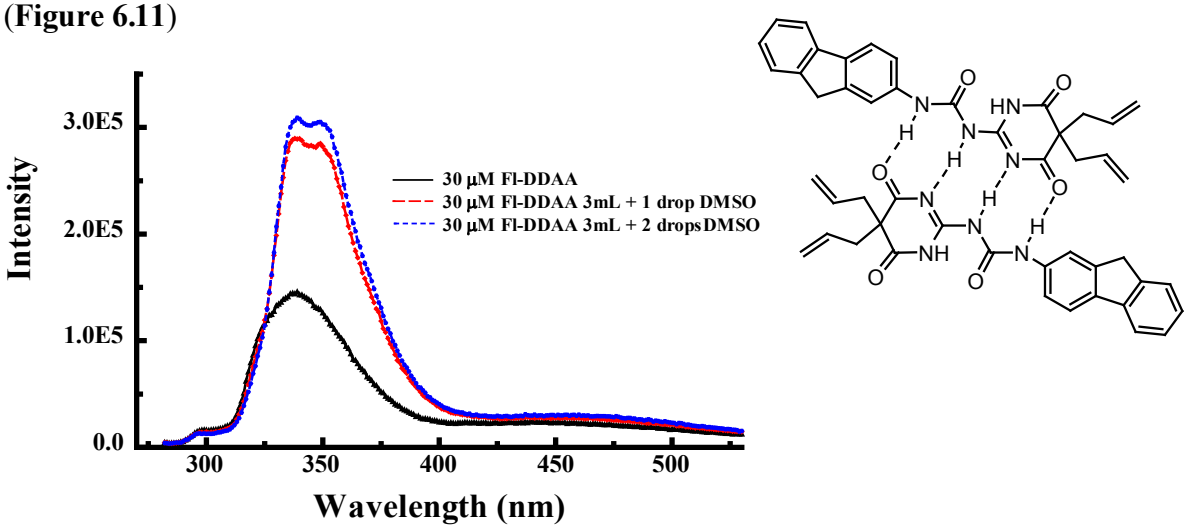

Figure 6.11 Fluorescence spectra of 30 μM compound **9** (Fl-DDAA) in (black) CH_2Cl_2, (red) CH_2Cl_2 with 1 drop DMSO and (blue) CH_2Cl_2 with 2 drops DMSO solutions. λ_{ex} 272 nm.

As shown in **Figure 6.11**, the black curve is the emission fluorescence spectrum of 30 μM **9** (Fl-DDAA). Upon addition of 1 to 2 drops of DMSO the fluorescence intensity in the emission spectrum of the same sample almost doubled (red dashed line and blue dotted line). Such intensity increase demonstrates that the compound **9** in the CH_2Cl_2 solution form $\mathbf{9}_2$ dimer molecules. In pure CH_2Cl_2 solution the self-quenching of dimerized molecule lowers the fluorescence intensity, but the self-dimerized hydrogen bondings are broken when DMSO is introduced in the solution (**Figure 6.11**). Since DMSO is an extremely polar solvent, the CH_2Cl_2 solution of compound **9** with 2 drops of DMSO only contains monomeric **9**.

To comfirm the self-quenching is not due to the fluorene residue itself, a control experiment was performed with a reference compound, acetamido fluorine, which contains a fluorene residue and an amide group. In the control experiment, a similar fluorescence emission spectrum of 30 μM acetamido fluorine was also recorded in fresh distilled CH_2Cl_2 in the absence and in the presence of several drops of DMSO. (**Figure 7.12**)

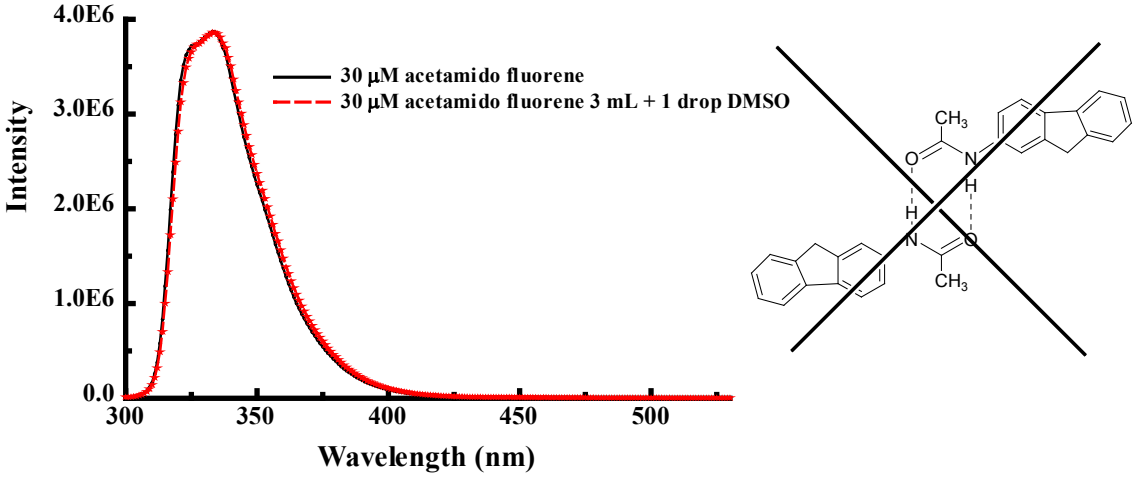

Figure 6.12 Fluorescence spectra of 30 μM acetamido fluorene in (black) CH_2Cl_2, and (red) CH_2Cl_2 with 1-2 drops DMSO solutions.

For the reference compound acetamido fluorene CH_2Cl_2 solution, the addition of DMSO does not give any rise of fluorescence intensity. The very little changes in fluorescence intensity and pattern illustrated that the acetamido fluorene does not form homodimers as compound **9** in the CH_2Cl_2 solution, since the hydrogen bonding would be interrupted upon addition of DMSO if the intermolecular dimerized hydrogen bonding exist. There is no complementary hydrogen bonding array present in acetamido fluorene although from the structure it may form dimer with two pairs of hydrogen bonding motif.

Fluorescence titration experiments were performed with compound **9** (Fl-DDAA) in CH_2Cl_2 solution at fixed concentration. The addition of compound **4** (Fc-DDAA) in this solution leads to a remarkable and quick decrease in the fluorescence intensity, which reveals that the homodimer (**9-9**) and monomer (**9**) equilibrium of compound **9** is interrupted by the addition of **4**. The added **4** solution also contains its homodimer and monomer molecules (**4-4** and **4**). The scheme for such process can be written as:

$$\mathbf{9} + \mathbf{9} \overset{K_{dim}}{\rightleftharpoons} \mathbf{9_2} \qquad K_{dim} = 1.92\times10^4 \text{ (K was obtained from NMR)}$$

$$\mathbf{4} + \mathbf{4} \overset{K_{dim}}{\rightleftharpoons} \mathbf{4_2} \qquad K_{dim} = 2.23\times10^4 \text{ (K was obtained from NMR)}$$

$$\mathbf{9} + \mathbf{4} \overset{K_{dim}}{\rightleftharpoons} \mathbf{9\text{-}4} \qquad K_{dim} = 8.0\times10^4 \text{ (K to be obtained from quenching plot by fitting)}$$

Scheme 6.5 Heterodimerization process of compound **9** and **4.**

If monomer **4** cannot interact with monomer **9**, we should observe the fluorescence intensity of solution **9** decrease linearly. The corresponding spectra and intensity plot are shown in **Figure 6.13**.

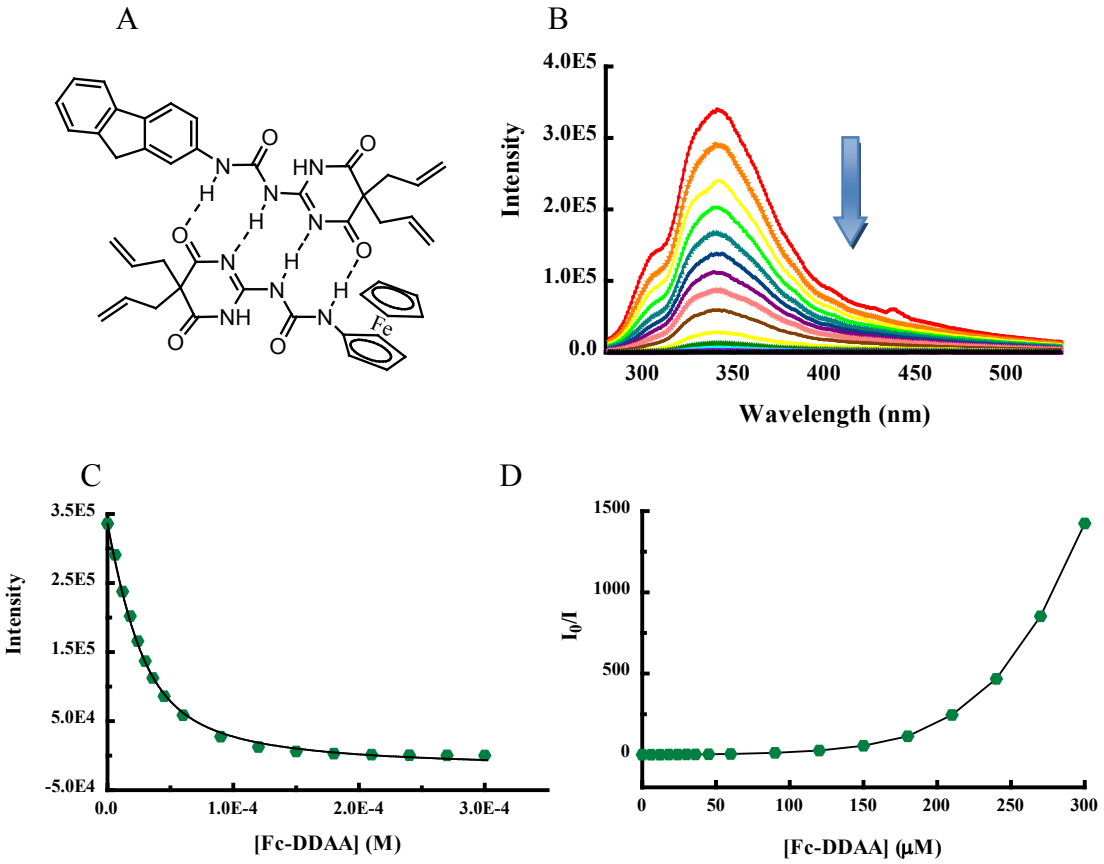

Figure 6.13 (A) Structure of heterodimer **9-4**, (B) fluorescence spectra, (C) intensity plot and (D) Stern-Volmer plot of 30 μM compound **9** (Fl-DDAA) at different concentrations of **4** (Fc-DDAA) in CH_2Cl_2 solution. λe_x 272 nm (I@340 nm)

The heterodimer's stability and binding affinity are comparable to those of the homodimers, otherwise the two homodimers will associate and react with each other very weakly in the mixing process. It is anticipated that a strong heterodimer **9-4** is formed through the quadruple hydrogen bonds. The binding constant calculated from data obtained from **Figure 6.13** C is 7.97×10^4 M^{-1}.

We also plotted the Stern-Volmer plot of fluorescence of compound **9** titrated with **4**. The Stern-Volmer plot has upward curvature, concave toward the y-axis (**Figure 6.13** D), which indicates combined dynamic and static quenching. These results suggest that the quenching can be assigned as the photoinduced electron transfer between the ferrocene residue and the excited state fluorene residue through a quadruple hydrogen-bonded pathway in the heterodimer **9-4** (FlDDAA-FcDDAA), which is consistent with our hypothesis.

In the control experiments, the addition of ferrocene to compound **9** (Fl-DDAA) solution also result in a decrease in intensity, but there is almost no binding between them. (**Figure 6.14**) The calculated binding constant K is only 2.8×10^3. These results illustrated that the strong binding behavior between **9-4** is due to the quadruple hydrogen moiety, not the ferrocene residue.

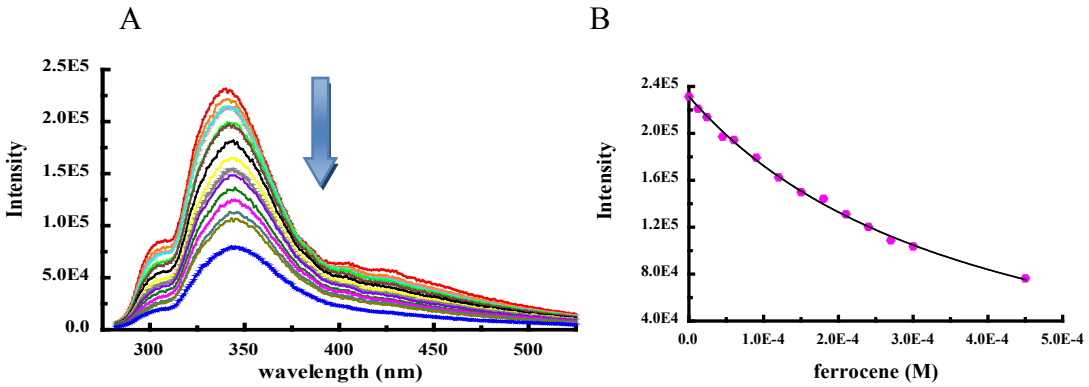

Figure 6.14 (A) Fluorescence spectra and (B) intensity plot of 30 μM compound **9** (Fl-DDAA) at different concentrations of ferrocene in CH_2Cl_2 solution. λ_{ex} 272 nm (I@340 nm)

To investigate heterodimer formation between **9** and other DDAA compounds, we also performed similar fluorescence experiments with compound **9** and compound **3** (isp-DDAA).

(**Figure 6.15**) The isopropyl residue is not redox active as ferrocene residue, so it could be used as a photochemical inert reference DDAA compound.

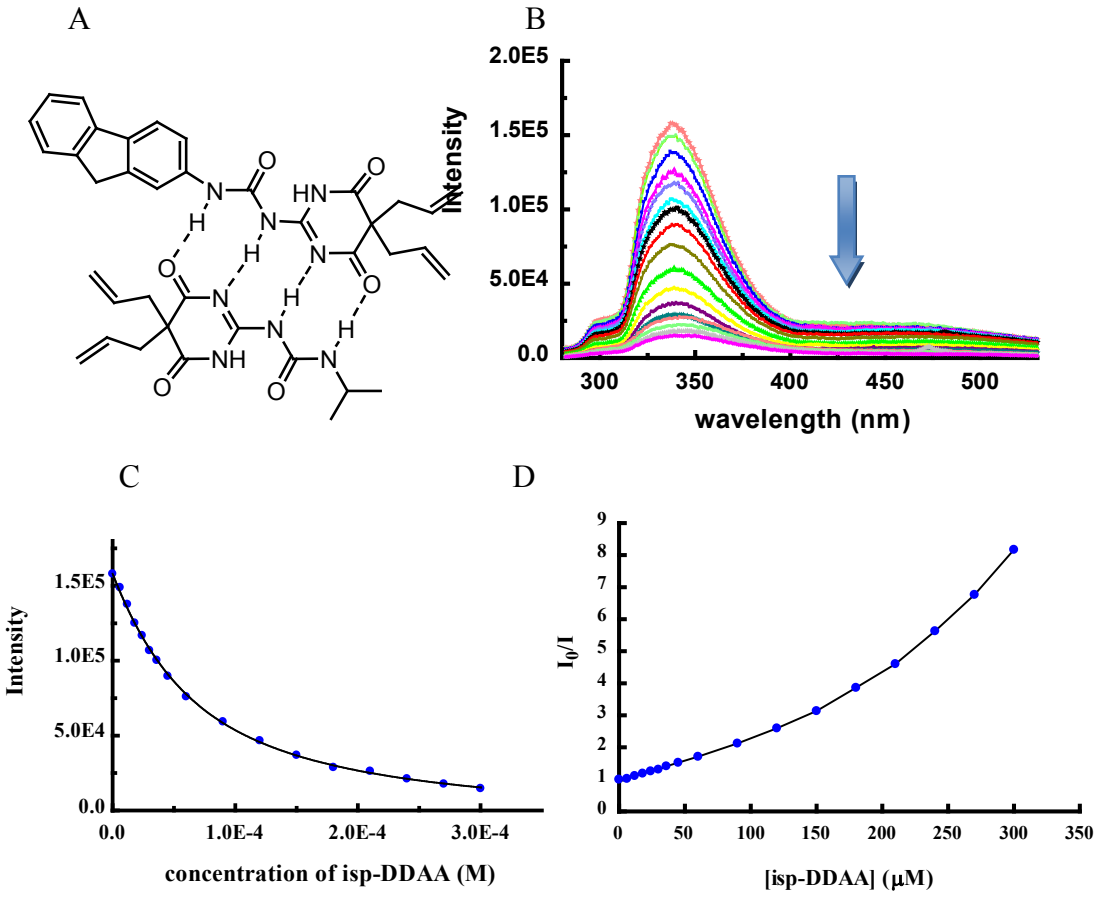

Figure 6.15 (A) Structure of heterodimer **9-3**, (B) fluorescence spectra, (C) intensity plot and (D) Stern-Volmer plot of 30 μM compound **9** (Fl-DDAA) at different concentrations of **3** (isp-DDAA) in CH_2Cl_2 solution. λ_{ex} 272 nm (I@340 nm)

Similarly, the addition of compound **3** (isp-DDAA) to compound **9** (Fl-DDAA) also results in fluorescence quenching and we observe the Stern-Volmer plot is also upward (**Figure 6.15** D) as the addition of **3** to **9**. We anticipate that Fc-DDAA is electron donor in heterodimers since it is electron rich, but isp-DDAA is not a good electron donor or acceptor. However,

increasing concentrations of isp-DDAA lead to the replacement of **9-9** dimer by **9-3** heterodimer, in which the fluorene is in a monomeric form. The calculated K is 1.99×10^4.

In CH_2Cl_2 solutions, the addition of Fc-DDAA or ispDDAA both result in fluorescence quenching of Fl-DDAA. The addition of a redox active or inactive residue both result in fluorescence quenching. However, a closer look at the titration data given in **Figure 6.16** shows that the overlap of the two Stern-Volmer plots, Fc-DDAA can quench the fluorescence much faster and stronger.

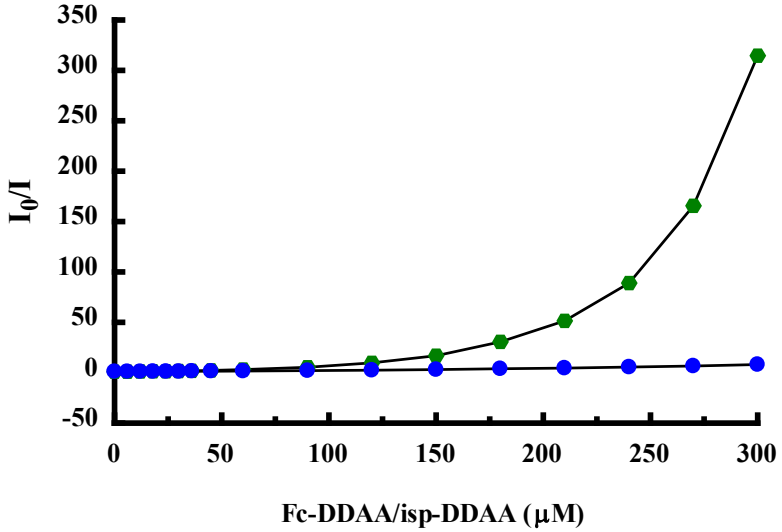

Figure 6.16 Stern-Volmer plots of 30 μM compound **9** (Fl-DDAA) quenched by compound **3** (isp-DDAA, blue) and compound **4** (Fc-DDAA, green).

In another set of control experiments, the addition of compound **3** to acetamido fluorene has the same effect but the binding constant obtained is about half of the value corresponding to **3** and **9** interactions, since acetamido fluorene and isp-DDAA can form two pairs of hydrogen bonding in the heterodimer. (**Figure 6.17** A and B) The calculated binding constant between them is 1.10×10^4.

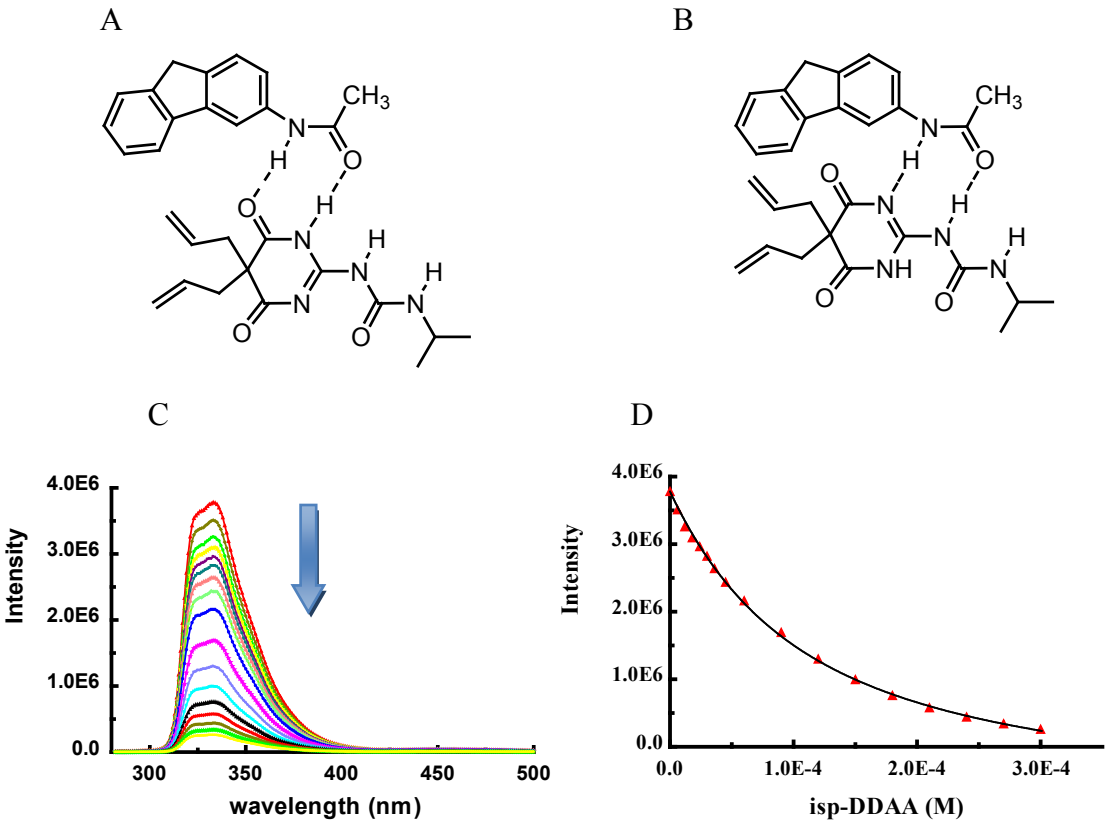

Figure 6.17 (A) and (B) Structures of heterodimer **9-3** may formed, (C) fluorescence spectra and (D) intensity plot of 30 μM acetamido fluorene at different concentrations of **3** (isp-DDAA) in CH_2Cl_2 solution. λ_{ex} 272 nm (I@338 nm)

In summary for the fluorescence titration experiments obtained for compound **9** (Fl-DDAA), the addition of compound **3** (isp-DDAA) and compound **4** (Fc-DDAA) can both lead to fluorescence intensity decrease of **9** while **4** can quench **9** much faster and stronger than **3**. Ferrocene interacts with **9** very weakly. The reference compound acetamido fluorene also binds to **3,** but the K value is lower.

Similar fluorescence experiments are performed with compound **6**, **7** and **8**. (**Figure 6.18 - Figure 6.20**)

A

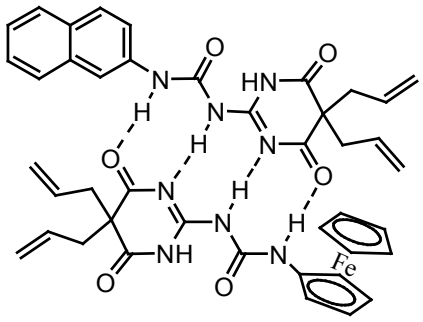
O
N
H
HN
O
N
H
N
O
O
N
H
N
H
O
NH
O
N
O
Fe

B

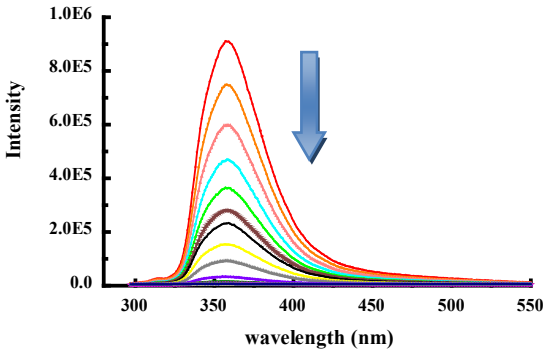
1.0E6
8.0E5
6.0E5
4.0E5
2.0E5
0.0
Intensity
300
350
400
450
500
550
wavelength (nm)

C

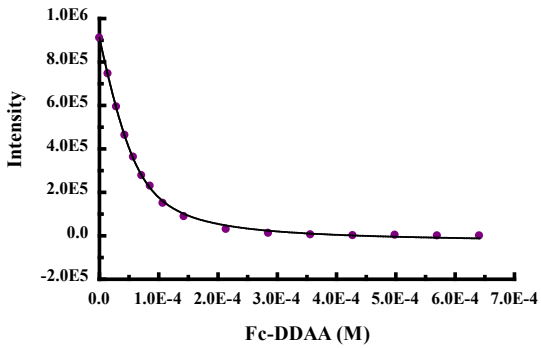
1.0E6
8.0E5
6.0E5
4.0E5
2.0E5
0.0
-2.0E5
Intensity
0.0
1.0E-4
2.0E-4
3.0E-4
4.0E-4
5.0E-4
6.0E-4
7.0E-4
Fc-DDAA (M)

D

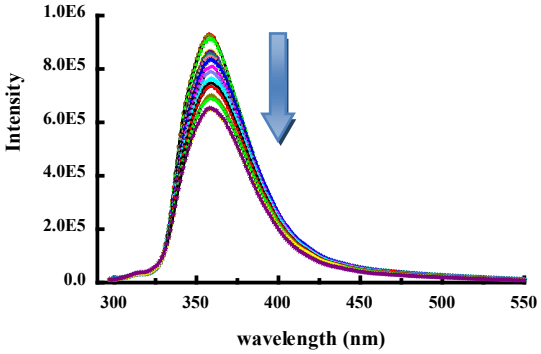
1.0E6
8.0E5
6.0E5
4.0E5
2.0E5
0.0
Intensity
300
350
400
450
500
550
wavelength (nm)

E

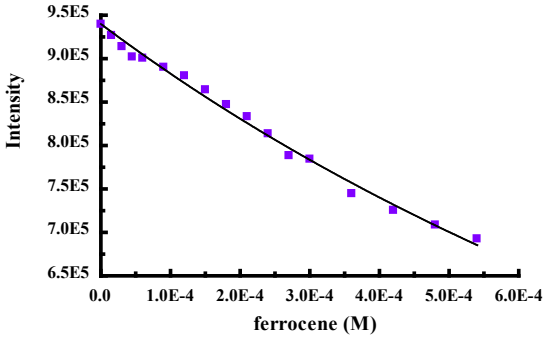
9.5E5
9.0E5
8.5E5
8.0E5
7.5E5
7.0E5
6.5E5
Intensity
0.0
1.0E-4
2.0E-4
3.0E-4
4.0E-4
5.0E-4
6.0E-4
ferrocene (M)

F

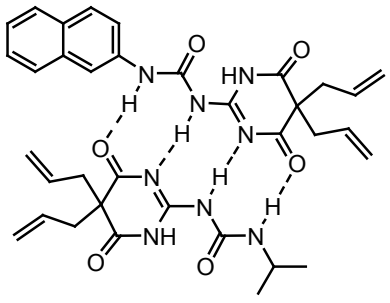
O
N
H
HN
O
N
H
N
O
O
N
H
N
H
O
NH
O
N

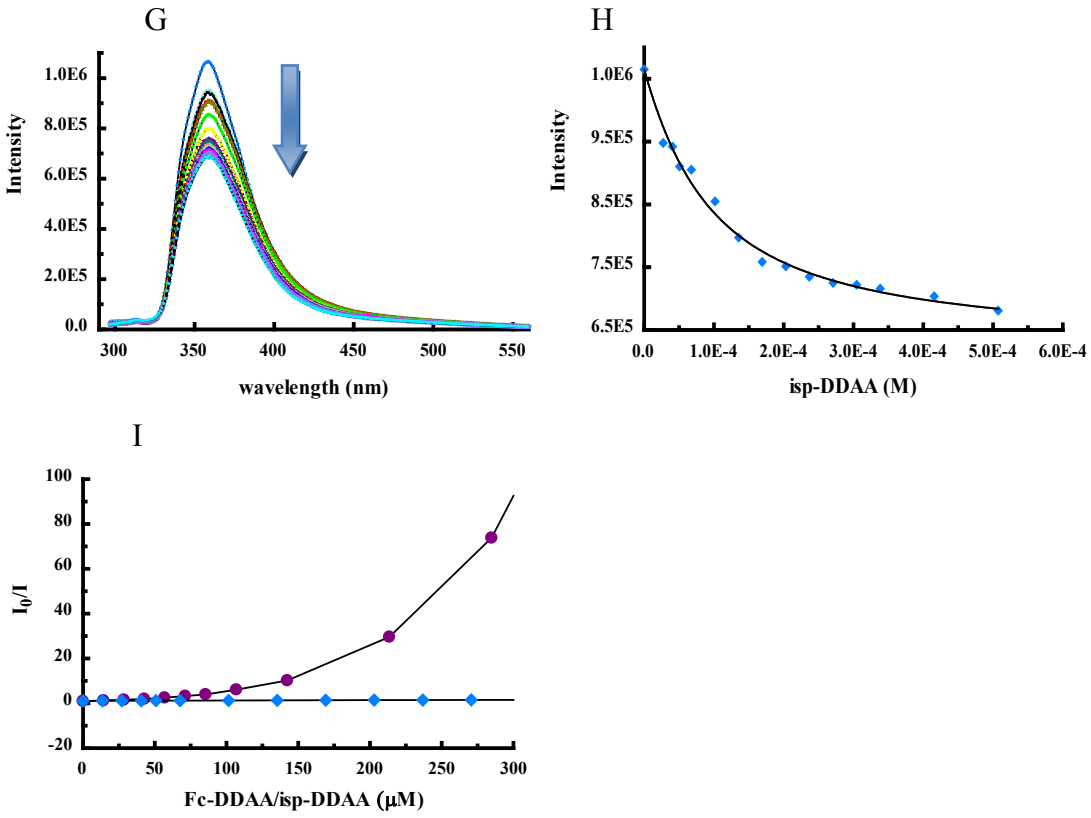

Figure 6.18

(A) Structure of heterodimer **6-4**, (B) fluorescence spectra, (C) intensity plot of 30 μM compound **6** (2-Naph-DDAA) at different concentrations of **4** (Fc-DDAA) in CH_2Cl_2 solution. λ_{ex} 286 nm (I@357 nm)

(D) Fluorescence spectra and (E) intensity plot of 30 μM compound **6** (2-Naph-DDAA) at different concentrations of ferrocene in CH_2Cl_2 solution. λ_{ex} 286 nm (I@358 nm)

(F) Structure of heterodimer **6-3**, (G) fluorescence spectra, (H) intensity plot and of 30 μM compound **6** (2-Naph-DDAA) at different concentrations of **3** (isp-DDAA) in CH_2Cl_2 solution. λ_{ex} 286 nm (I@359 nm)

(I) Stern-Volmer plots of compound **6** (2-Naph-DDAA) quenched by compound **3** (isp-DDAA, sky blue) and compound **4** (Fc-DDAA, purple).

The photochemistry behavior of compound **6** (2-Naph-DDAA) is very similar to that of **9** (Fl-DDAA). Upon addition of compound **3** (isp-DDAA) or compound **4** (Fc-DDAA), the fluorescence intensity of **6** decreases. The binding constant value obtained from the titration experiments between **6** and **4** are much higher than that from **6** and **3**. The Stern-Volmer plot

also indicated that the binding of **6** to **4** is stronger than to **3**. However, as compound **4** can quench the intensity of **6** to an extremely low value, while no significant intensity reduction is observed in the quenching by compound **3** (**Figure 6.18** B, C, G and H). In the titration experiments with ferrocene, we only observe very weak binding (**Figure 6.18** D and E).

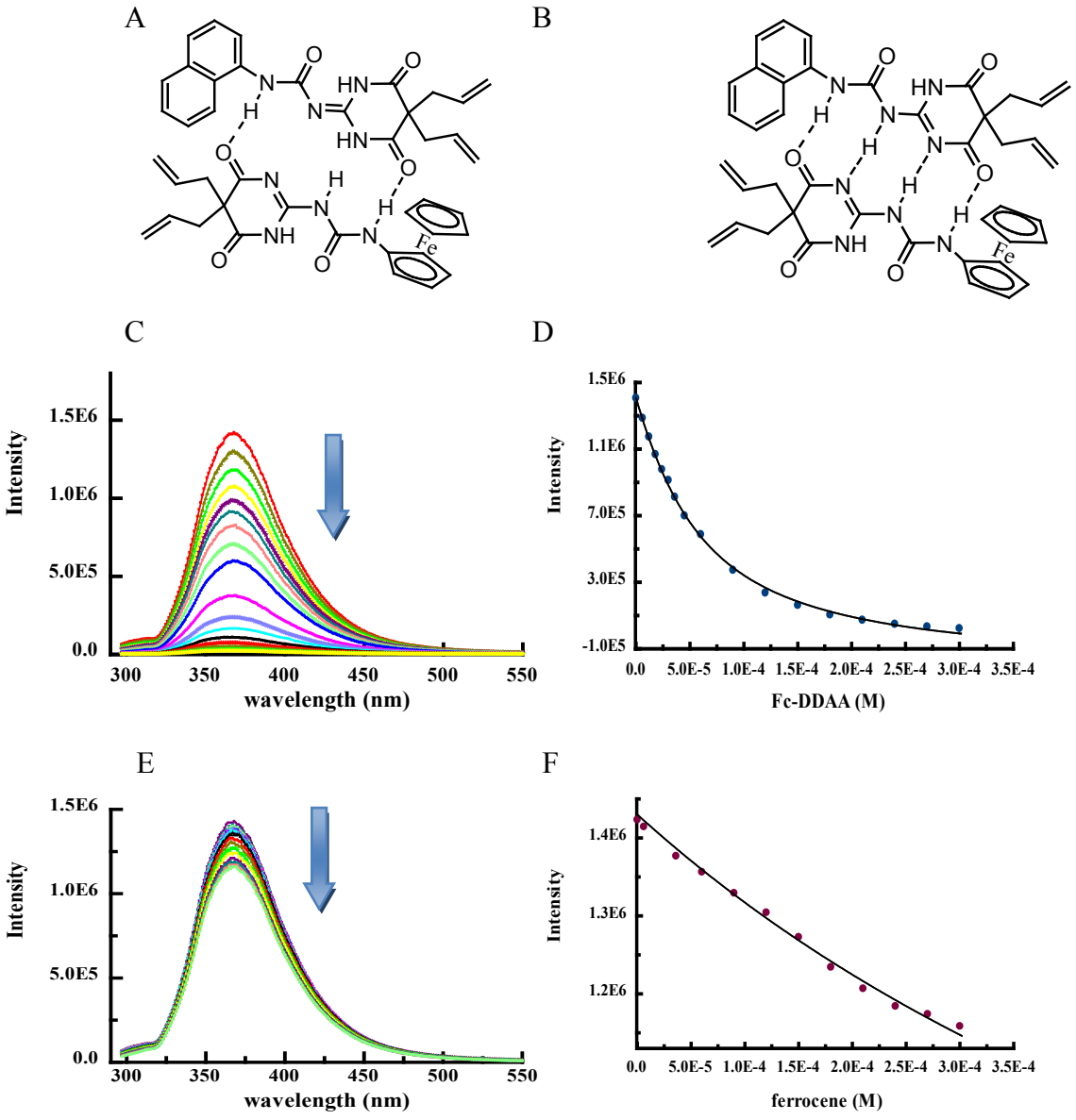

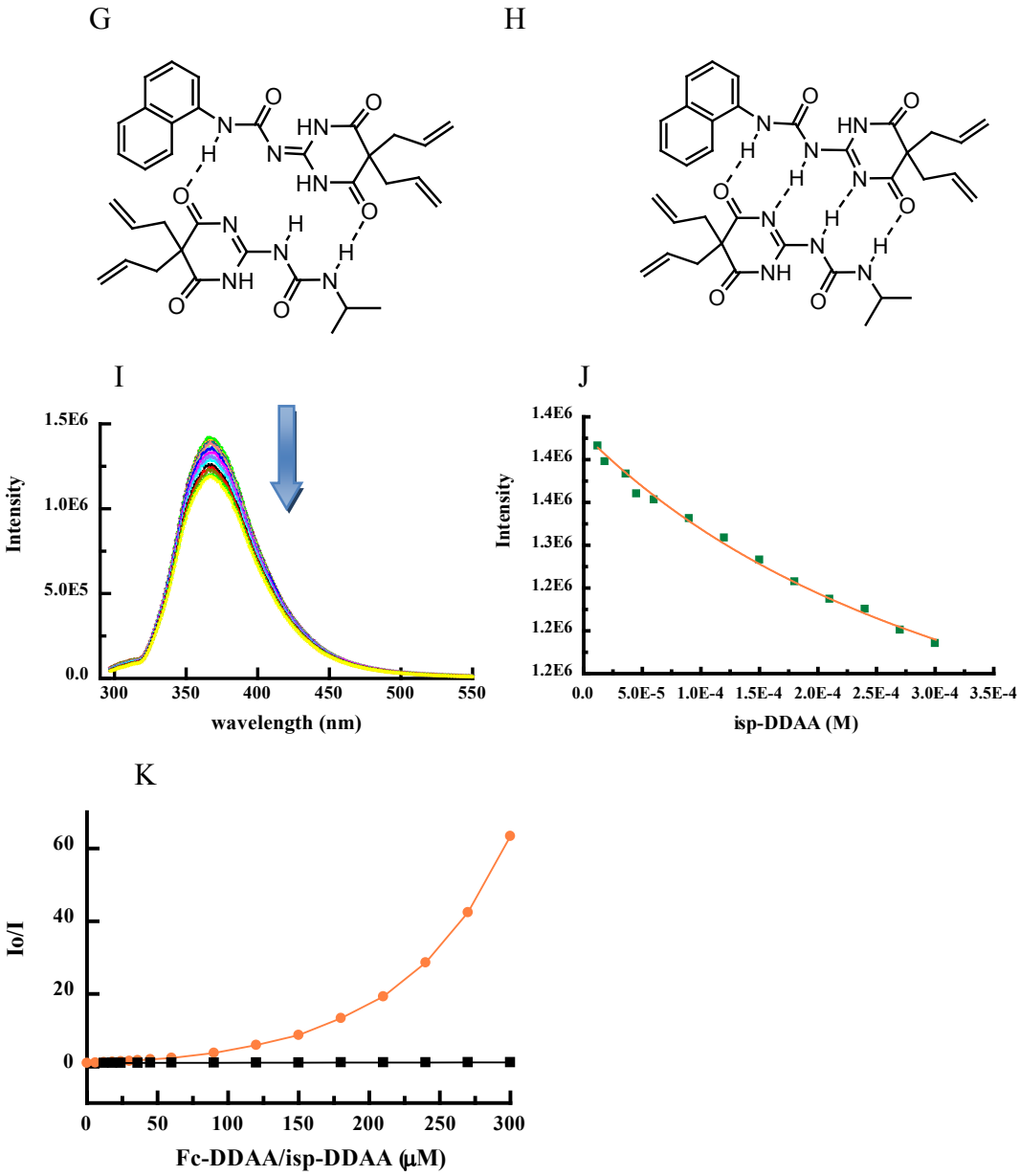

Figure 6.19

(A) Structure of heterodimer **7-4**, (B) fluorescence spectra, (C) intensity plot of 30 μM compound **7** (1-Naph-DADA) at different concentrations of **4** (Fc-DDAA) in CH_2Cl_2 solution. λ_{ex} 282 nm (I@365 nm)

(D) Fluorescence spectra and (E) intensity plot of 30 μM compound **7** (1-Naph-DADA) at different concentrations of ferrocene in CH_2Cl_2 solution. λ_{ex} 282 nm (I@365 nm)

(F) Structure of heterodimer **7-3**, (G) fluorescence spectra, (H) intensity plot and of 30 μM compound **7** (1-Naph-DADA) at different concentrations of **3** (isp-DDAA) in CH_2Cl_2 solution. λ_{ex} 282 nm (I@366 nm)

(I) Stern-Volmer plots of compound **7** (1-Naph-DADA) quenched by compound **3** (isp-DDAA, black) and compound **4** (Fc-DDAA, orange).

The data and results obtained from **Figure 6.19** are of much interest to analyze the binding behavior of compound **7**. From the crystal structure it is known that compound **7** forms a DADA dimer in the solid state. If compound **7** is also in its DADA tautomer form, the binding between **7** and **4** should be much weaker according to the Jorgenson's secondary interactions model (**Figure 6.19** A). However, the K value obtained from **Figure 6.19** C and D is 2.3×10^4, which indicates that the binding is still strong. We anticipate that the structure of compound **7** is induced to its DDAA form under the effect of compound **4** and form a DDAA-DDAA heterodimer as shown in **Figure 6.19** B. It is observed that ferrocene does not play an important role in the binding to compound **7** in control experiment (**Figure 6.19** E and F) since the calculated K value is as low as 1.2×10^3. We conclude that the strong binding behavior between **7** and **4** is due to compound **4** and its planar DDAA hydrogen bonding motif, not the ferrocene residue.

On the other hand, fluorescence titration experiments of compound **3** are also performed. It is interesting that not only compound **3** slightly quench the fluorescence intensity of **7**, but also the calculated K value corresponding to this experiment is extremely low (2.7×10^3, **Figure 6.19** I and J). As mentioned before, isopropyl is an inert group compared to ferrocenyl, so compound **3** may not be strong enough to induce compound **7** to its DDAA form. If compound **7** is a DADA structure and compound **3** is DDAA structure, the weak binding between them can be explained. We assume that the structure of heterdimer **7-3** is 1-Na-DDAA-DDAA-Fc (**Figure 6.19** B), while the structure of **7-4** is 1-Na-DADA-DDAA-isp (**Figure 6.19** G), respectively. Another reason for the weak binding

between **7** and **3** is that the isopropyl residue in compound **3** is neither a good electron donor nor acceptor. The electron transfer process is obvious in **7**-**4** but hardly takes place in **7**-**3**.

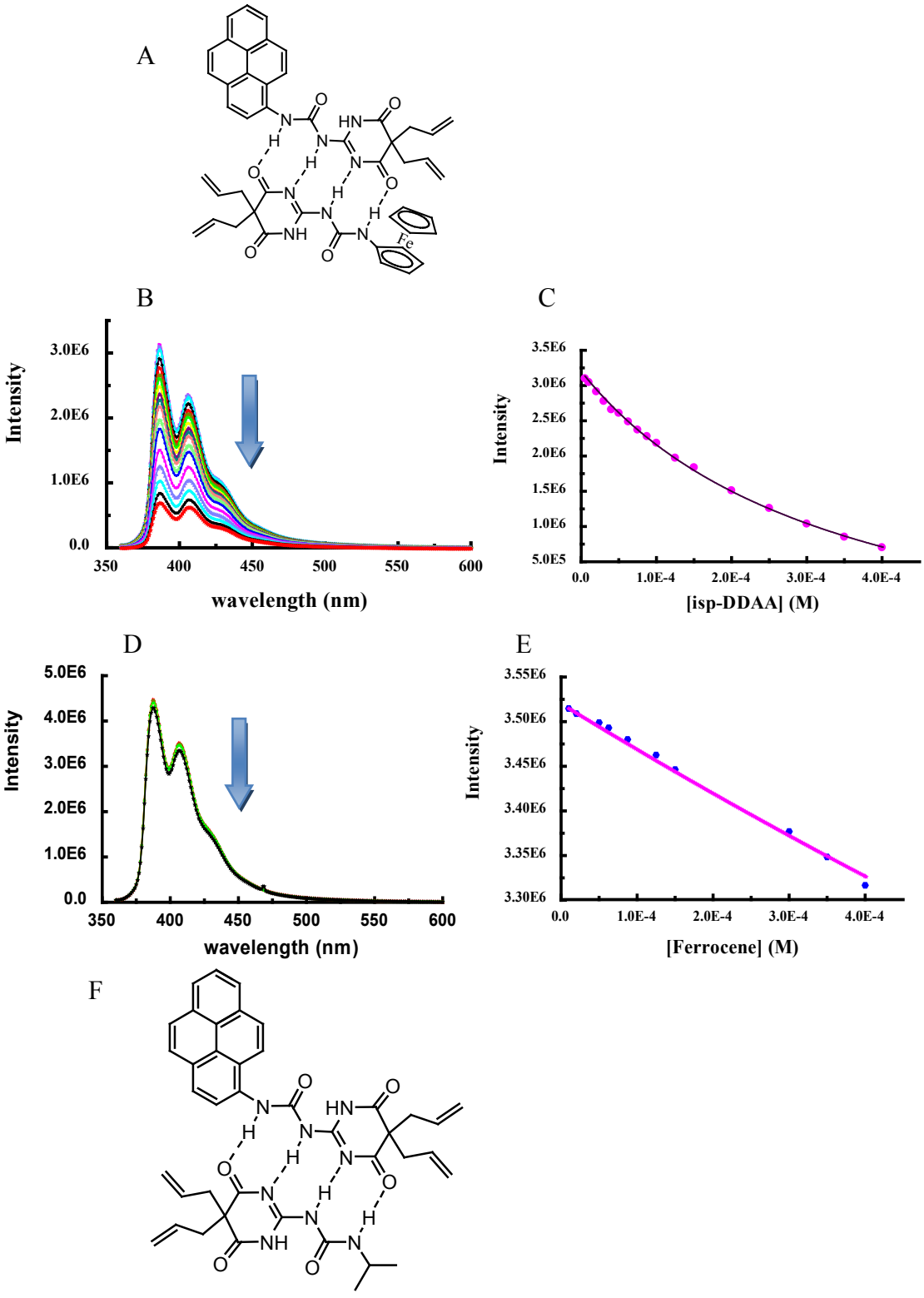

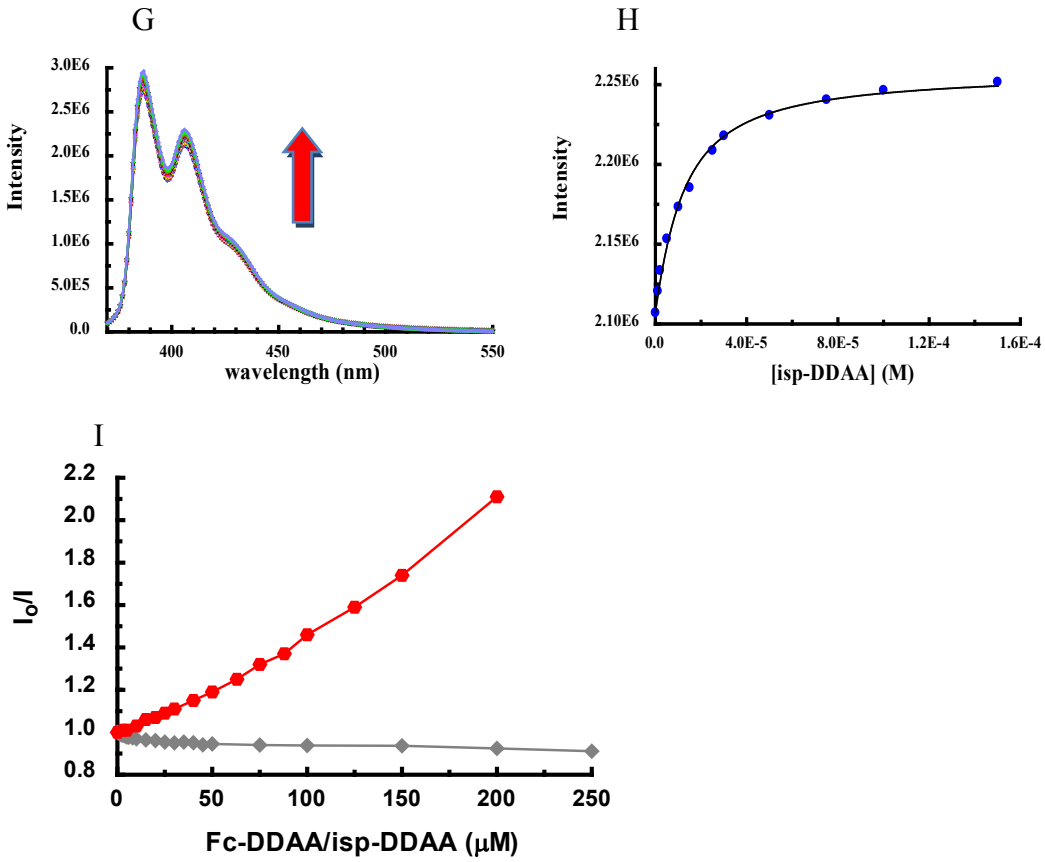

Figure 6.20
(A) Structure of heterodimer **8**-**4**, (B) fluorescence spectra, (C) intensity plot of 5 μM compound **8** (pyr-DDAA) at different concentrations of **4** (Fc-DDAA) in CH_2Cl_2 solution. λ_{ex} 350 nm (I@386 nm)
(D) Fluorescence spectra and (E) intensity plot of 5 μM compound **8** (pyr-DDAA) at different concentrations of ferrocene in CH_2Cl_2 solution. λ_{ex} 350 nm (I@386 nm)
(F) Structure of heterodimer **8**-**3**, (G) fluorescence spectra, (H) intensity plot and of 5 μM compound **8** (pyr-DDAA) at different concentrations of **3** (isp-DDAA) in CH_2Cl_2 solution. λ_{ex} 350 nm (I@406 nm)
(I) Stern-Volmer plots of compound **8** (pyr-DDAA) quenched by compound **3** (isp-DDAA, grey) and compound **4** (Fc-DDAA, red).

Different results are obtained with the fluoresence experiments of compound **8**. The binding between compound **8** and compound **4** is very weak, with a calculated binding constant K 2.9×10^3. The addition of compound **4** decreases the fluoresence intensity in **8**

(**Figure 6.20** B and C), but it does not decrease to almost zero as in the quenching of compound **6** and **7** (**Figure 6.18** B and C, **Figure 6.19** C and D), which indicates that compound **4** does not quench **9** strongly.

It is quite interesting to observe the growth of fluorescence as the addition of compound **3** in **9** (**Figure 6.20** G and H). As mentioned before, the isopropyl residue is not redox active, so it could be used as neither acceptor nor donor in the electron transfer process. Therefore, increasing concentrations of compound **3** lead to the replacement of **8-8** dimer by the **8-3** heterodimer, in which the pyrene is in a monomeric form. Thus, the addition of a redox inactive residue results in the release of quenched fluorescence which is caused by pyrene itself in the **8-8** dimer. In contrast to the results obtained from titration experiments of compound **6**, **7** and **9** by **3**, this strong binding behavior demonstrates that whether the isopropyl group is redox active is not the only reason to affect the binding in heterodimers. The calculated binding constant values are listed in **Table 6.4**.

Table 6.4 Calculated binding constant K from fluorescence emission experiments

Comp.	**3** (isp-DDAA)	**4** (Fc-DDAA)	ferrocene
6 (2Na-DDAA)	1.3×10^{4}	6.5×10^{4}	5.3×10^{2}
7 (1Na-DADA)	2.7×10^{3}	2.3×10^{4}	1.2×10^{3}
8 (pyr-DDAA)	1.02×10^{5}	2.9×10^{3}	2.1×10^{2}
9 (Fl-DDAA)	2.0×10^{4}	8.0×10^{4}	2.8×10^{3}

A Stern-Volmer plot of fluorescence titrations of compound **6-9** by compound **4** is shown in **Figure 6.21**. We observe the quenching by 4 is most significant in **9**, and decreases as the order **6**, **7** and **8**. This illustrated the binding strength between them, consistent with the results obtained for K values (**Table 6.4**).

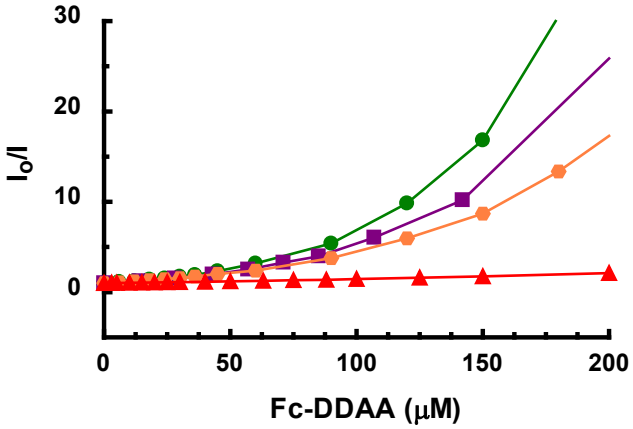

Figure 6.21 Stern-Volmer plot of fluorescence titrations of 30 μM **9** (Fl-DDAA, green), 30 μM **6** (2-Na-DDAA, purple), 30 μM **7** (1-Na-DDAA, orange) and 5 μM **8** (pyr-DDAA, red) in CH_2Cl_2.

In conclusion, we have shown that ureido pyrimidinedione derivatives **3**–**9** self-recognize, forming stable dimers, assisted by the formation of two intramolecular hydrogen bonds, which increase the structural rigidity of each monomer and facilitate the formation of four parallel intermolecular hydrogen bonds. Preorganization by intramolecular hydrogen bonding and cooperative intermolecular interactions results in high stability. The tendency toward tautomerization in compound **6** and **7** leads to our study in the energy of dimerization interactions by computing calculation. The photophychemical studies in this

work provide clear evidence that strong binding takes place in the heterocomplex, and the corresponding stability and binding behavior are also well studied.

The results presented here will provide new opportunities for development of well-defined structures in nanoscale assembly. These ureido pyrimidinedione compounds and their strong and selective complexation will make them broadly useful in supramolecular chemistry.

6.7 Experimental

Materials:

All synthetic procedures were performed in an inert atmosphere of dry nitrogen. All chemicals used were reagent grade (Aldrich, Acros, VWR, TCI) and were used as received. Column chromatography was performed with Scientific Adsorbents silica gel (63-200 μm). Samples for ^{1}H NMR NMR spectroscopy were prepared with $CDCl_3$ (99.99%D) purchased from Cambridge Isotope Laboratories. ^{1}H NMR and ^{13}C NMR spectra were recorded on a Bruker 400 MHz spectrometer. Chemical shifts are reported in ppm relative to tetramethylsilane (TMS). Methylene chloride was distilled to remove the trace amount of stabilizer, which can cause error in fluorescence experiments. Chloroform-*d* and methylene chloride-d_2 was deacidified by running through a column of activated basic aluminum oxide. Other solvents were used without further purification. The UV-visible spectra were recorded using Shimadzu UV-2101PC spectrophotometer. The emission spectra were recorded using a SpexFluoroMax spectrophotometer.

Preparation of R-DDAA:

5,5-diallyl-2-amino-1H-pyrimidine-4,6-dione (**2**) was prepared as reported by Sanjayan, G. J.[59]

1-(5,5-diallyl-4,6-dioxo-1,4,5,6-tetrahydro-pyrimidin-2-yl)-isopropyl-urea (**3**)

1-(5,5-diallyl-4,6-dioxo-1,4,5,6-tetrahydro-pyrimidin-2-yl)-ferrocenyl-urea (**4**)

Compounds **3** and **4** were prepared as reported previously by our group.[68]

1-(5,5-diallyl-4,6-dioxo-1,4,5,6-tetrahydro-pyrimidin-2-yl)-phenyl-urea (**5**)

NaH (80mg, 2mmol, 60%in mineral oil) was carefully dissolved in dry DMF (10mL). Mixture was allowed to go to room temperature, meanwhile 5,5-diallyl-2-amino-1H-pyrimidine-4,6-dione (414 mg, 2mmol) was slowly dissolved to the above solution, followed by heated to 70^{o}C for 2hours to form Na-salt. The mixture was cooled down and then dropwise added a solution of dry dichloromethane (10mL) containing phenyl isocyanate (0.36mL, 2mmol). The reaction was heated to 70^{o}C on an oil bath for 12 hours. After cooling the reaction was quenched with CH_3COOH (0.11mL, 2mmol)

Solvent was removed under vacuum and the residue was dissolved in $CHCl_3$, washed with water and brine. The organic layer was dried over Na_2SO_4 and concentrate to give crude product, which was further purified by column chromatography (SiO_2, 9:1 $CHCl_3$/Hexane) to give white solid product Phenyl-DDAA (~80mg, 12%). Product was re-crystallized in $CHCl_3$ and white crystals were obtained (48mg, 8%).

^{1}H NMR (400 MHz, $CDCl_3$) δ= 12.61 (s, 1H, NH), 11.27 (s, 1H, NH), 10.44 (s, 1H, NH), 7.61-7.59 (d, 2H, CH-benzene), 7.33-7.28 (t, 2H, CH-benzene), 7.19 (s, $CHCl_3$), 7.11-7.07 (t,

1H, CH-benzene), 5.66-5.57 (m, 2H, -CH_2CHCH_2), 5.56-5.05 (t, 4H, -CH_2CHCH_2), 2.73-2.67(d, 4H, -CH_2CHCH_2), *2.10(Acetone), *1.48(water) ppm. ^{13}C NMR ($CDCl_3$): δ=180.17, 170.94, 156.21, 155.68, 137.73, 130.74, 129.20, 124.80, 121.19, 120.33, 77.48/77.16/76.84 ($CHCl_3$), 58.70, 42.92, 29.85 (grease) ppm. MS (FAB):326 $(M+H)^+$

1-(5,5-diallyl-4,6-dioxo-1,4,5,6-tetrahydro-pyrimidin-2-yl)-2-naphtyl-urea (**6**)

6 is prepared using the procedure described for **5** by reacting 2-Naphthyl isocyanate (0.67 mL, 4mmol) instead of phenyl isocyanate with 5,5-diallyl-2-amino-1H-pyrimidine-4,6-dione (828mg, 4mmol) Na-salt. Pure 2-Naph-DADA was obtained (165mg, 11%).

^{1}H NMR (400 MHz, $CDCl_3$) δ= 12.81 (s, 1H, NH), 11. 76 (s, 1H, NH), 10.74 (s, 1H, NH), 7.98-7.94 (m, 2H, CH-naphthalene), 7.91-7.88 (m, 1H, CH-naphthalene), 7.84-7.82 (m, 1H, CH-naphthalene), 7.57-7.53 (m, 4H, CH-naphthalene), 7.19 (s, $CHCl_3$), 7.11-7.07 (t, 1H, CH-benzene), 5.66-5.57 (m, 2H, -CH_2CHCH_2), 5.56-5.05 (t, 4H, -CH_2CHCH_2), 2.73-2.67(d, 4H, -CH_2CHCH_2), *2.10(Acetone), *1.48(water) ppm. ^{13}C NMR ($CDCl_3$): δ=180.17, 170.94, 156.21, 155.68, 137.73, 130.74, 129.20, 124.80, 121.19, 120.33, 77.48/77.16/76.84 ($CHCl_3$), 58.70, 42.92, 29.85 (grease) ppm. MS (FAB):377 $(M+H)^+$

1-(5,5-diallyl-4,6-dioxo-1,4,5,6-tetrahydro-pyrimidin-2-yl)-1-naphtyl-urea (**7**)

7 is prepared using the procedure described for **5** by reacting 1-Naphthyl isocyanate (0.67 mL, 4.0 mmol) instead of phenyl isocyanate with 5,5-diallyl-2-amino-1H-pyrimidine-4,6-dione (828mg, 4mmol) Na-salt. Pure 1-Naph-DADA was obtained (125mg, 8.3%).

^{1}H NMR (400 MHz, $CDCl_3$) δ= 12.81 (s, 1H, NH), 11. 76 (s, 1H, NH), 10.74 (s, 1H, NH),

7.98-7.94 (m, 2H, CH-naphthalene), 7.91-7.88 (m, 1H, CH-naphthalene), 7.84-7.82 (m, 1H, CH-naphthalene), 7.57-7.53 (m, 4H, CH-naphthalene), 7.27 (s, $CHCl_3$), 7.57-7.53 (m, 4H, CH-naphthalene), 5.76-5.67 (m, 2H, -CH_2CHCH_2), 5.20-5.16 (t, 4H, -CH_2CHCH_2), 2.75-2.69(d, 4H, -CH_2CHCH_2) ppm; ^{13}C NMR ($CDCl_3$): δ=180.79, 171.35, 157.11, 154.74, 134.69, 132.01, 129.20, 128.91, 127.57, 125.88, 123.59, 121.33, 58.95, 43.11 ppm; MS (FAB):377 $(M+H)^+$

1-(5,5-diallyl-4,6-dioxo-1,4,5,6-tetrahydro-pyrimidin-2-yl)-1-pyrenyl-urea (**8**)

A solution of dry dichloromethane (10 mL) containing 1-aminopyrene (0.217g, 1mmol) was stirred at room temperature for 15 min, in the presence of N-ethyldiisopropylamine (0.11 mL, 1 mmol). Another dichloromethane (10 mL) solution contains triphosgene (198 mg, 0.33 mmol) at 0^{o}C is added in 1-aiminopyrene solution drop by drop carefully. Then the solution was mixed with a solution of dry pyridine (10 mL) solution which contained 5,5-diallyl-2-amino-1H-pyrimidine-4,6-dione (0.514g, 2 mmol). The reaction mixture was heated to 90 ^{o}C for 48 hours. After cooling, the solvents were removed under vacuum. The residue was taken in ethylacetate and was washed with water and brine. The organic layer was dried over Na_2SO_4 and concentrated to give crude product, which was further purified by column chromatography (SiO_2, 3:1 $CHCl_3$/EtOAc) and **8** was obtained (52mg, 11.5 %).

^{1}H NMR (400 MHz, $CDCl_3$) δ= 12.76 (s, 1H, NH), 11. 57 (s, 1H, NH), 10.88 (s, 1H, NH), 8.51-8.42 (m, 2H, CH-pyrene), 8.41-8.24 (m, 3H, CH-pyrene), 8.15-7.97 (m, 4H, CH-pyrene), 7.27 (s, $CHCl_3$), 5.38-5.30 (m, 2H, -CH_2CHCH_2), 5.03-4.92 (t, 4H, -CH_2CHCH_2),

2.65-2.60(d, 4H, -C*H*$_2$CHCH$_2$) ppm; ^{13}C NMR ($CDCl_3$): δ=179.24, 168.17, 155.84, 136.51, 135.11, 131.86, 129.20, 128.68, 127.61, 126.83, 125.96, 125.73, 125.29, 125.16, 125.08 123.16, 121.57, 58.64, 42.46 ppm; MS (FAB): 451 $(M+H)^+$

1-(5,5-diallyl-4,6-dioxo-1,4,5,6-tetrahydro-pyrimidin-2-yl)-9-H-2-fluorenyl-urea (**9**)

NaH (80mg, 2mmol, 60% in mineral oil) was carefully dissolved in dry DMF (10 mL). Mixture was allowed to go to room temperature, meanwhile 5,5-diallyl-2-amino-1H-pyrimidine-4,6-dione (414 mg, 2 mmol) was slowly dissolved to the above solution, followed by heated to 70^{o}C for 2hours to form Na-salt. Mixture was cooled down and then dropwise added a solution of dry dichloromethane (10 mL) containing 9-H fluorenyl isocyanate (514 mg, 2 mmol). The reaction was heated to 75^{o}C on an oil bath for 12 hours. After cooled the reaction was quenched with CH_3COOH (0.11mL, 2mmol). Solvent was removed under vacuum and the residue was dissolved in $CHCl_3$, washed with water and brine. The organic layer was dried over Na_2SO_4 and concentrate to give crude product, which was further purified by column chromatography (SiO_2, 9:1 $CHCl_3$/Hexane) to give white solid product Fl-DDAA (310mg, 37.4%). Product was re-crystallized in $CHCl_3$ and white crystals. ^{1}H NMR (400 MHz, CD_2Cl_2) δ= 12.56 (s, 1H, NH), 11.00 (s, 1H, NH), 10.22 (s, 1H, NH), 7.90 (s, 1H, CH-benzene), 7.74-7.49 (m, 4H, CH-benzene), 7.40-7.25 (m, 3H, CH-benzene), 5.69-5.55 (m, 2H, -CH_2CHCH_2), 5.26 (s, CH_2Cl_2), 5.26-5.08 (t, 4H, -CH_2CHCH_2), 2.78-2.74(d, 4H, -C*H*$_2$CHCH$_2$) ppm.

^{13}C NMR (*d*-DMF): δ=156.92, 153.02, 139.08, 134.35, 132.18, 130.67, 129.55, 129.01, 128.08, 127.43, 125.56, 124.39, 120.40, 116.09, 113.55, 57.03 ppm. MS (FAB): 414 $(M+H)^+$,

437 $(M+Na)^+$. The anticipated structures of all these compounds were confirmed by ^{1}H-NMR and MS (FAB)

References

[1] (a) Hollingsworth, M. D. *Science* **2002**, *295*, 2410. (b) Lehn, J. M., *Science* **2002**, *295*, 2400.

[2] Pedersen, C. J., *J. Am. Chem. Soc*. **1968**, *89*, 7017.

[3] Atwood, J. L.; Barbour, L.J.; Jerga, A., *PNAS* **2002**, *99*, 4837.

[4] Gibb, C. L. D.; Gibb, B. C., *J. Am. Chem. Soc.* **2004**, *126*, 11408.

[5] Liu, S.; Ruspic, C.; Mukhopadhyay, P.; Chakrabarti, S.; Zavalij, P. Y.; Isaacs, L., *J. Am. Chem. Soc.* **2005**, *127*, 15959.

[6] Wheate, N. J.; Kumar, P. G. A.; Torres, A. M.; Aladrich-Wright, J. R.; Price, W. S., *J. Phys. Chem. B* **2008**, *112*, 2311.

[7] Fang, X.; Ko#gerler, P.; Isaacs, L.; Uchida, S.; Mizuno N., *J. Am. Chem. Soc.* **2004**, *131*, 432.

[8] Kim, J.; Jung, I. S.; Kim, S. Y.; Lee, E.; Kang, J. K.; Sakamoto, S.; Yamguchi, K.; Kim, K., *J. Am. Chem. Soc*. **2000**, *122*, 540.

[9] Day, A. I.; Aronold, A. P.; Blanch, R. J.; Snushall, B., *J. Org. Chem.* **2001**, *66*, 8094.

[10] Jeon, W.S.; Moon, K.; Park, S.H.; Chun, H.; Ko, Y.H.; Lee, J.Y.; Lee, E.S.; Samal, S.; Selvapalam, N.; Rekharsky, M.V.; Sindelar, V.; Sobransingh, D.; Inoue, Y.; Kaifer, A.E.; and Kim, K., *J. Am. Chem. Soc.* **2005**, *127*, 12984.

[11] Whang, D.; Kim, K., *J. Am. Chem. Soc.* **1997**, *119*, 451.

[12] Roh, S. G.; Park, K. M.; Park, G. J.; Sakamoto, S.; Yamaguchi, K.; Kim, K., *Angew. Chem. Int. Ed.* **1999**, *38*, 638.

[13] Lee, J. W.; Kim, K.; Kim, K., *Chem. Commun.* **2001**, 1042.

[14] Lagona, J.; Mukhopadhyay, P.; Chakrabarti, S.; Isaacs, L., *Angew. Chem. Int. Ed.* **2005**, *44*, 4844.

[15] Ong, W; Kaifer, A. E., *Organometallics* **2003**, *21*, 4181.

[16] Rekharsky, M. V.; Mori, T.; Yang, C.; Ko, Y. H.; Selvapalam, N. Kim, H.; Sobrasingh, D.; Kaifer, A. E.; Liu, S.; Isaacs, L.; Chen, W.; Moghaddam, S.; Gilson, M. K.; Kim, K.; Inoue, Y., *PNAS* **2007**, *104,* 52, 20737.

[17] Lee, J. W.; Samal, S.; Selvapalam, N. Kim, H. J.; Kim, K., *Acc. Chem. Res.* **2003**, *36, 8*, 621.

[18] Jeon, W. S.; Kim, H.J.; Lee, C.; Kim, K., *Chem. Commun*. **2002**, 1828.

[19] Moon, K.; Grindstaff, J.; Sobransingh, D.; Kaifer, A. E., *Angew. Chem. Int. Ed.* **2004**, *43*, 5496.

[20] Ling, Y.; Mague, J. T.; Kaifer, A. E., *Chem. Eur. J.* **2007**, *13*, 7908.

[21] Sindelar, V.; Parker, S. E.; Kaifer, A. E., *New J. Chem*. **2007**, *31*, 725.

[22] Kim, H. J.; Jeon, W. S.; Ko, Y. H.; Kim, K., *Proc. Natl. Acad. Sci. USA* **2002**, *99*, 5007.

[23] Ong, W.; Gomez-Kaifer, M.; Kaifer, A. E., *Org. Lett.* **2002**, *4*, 1791.

[24] Ziganshina, A. Y.; Ko, Y. H.; Jeon, W. S.; Kim, K., *Chem. Commun*. **2004**, 806.

[25] Ling, Y.; Wang, W.; Kaifer, A. E., *Chem. Commun.* **2007**, 610.

[26] Wang, W.; Kaifer, A. E., *Angew. Chem. Int. Ed.* **2006**, *45*, 7042.

[27] Sindelar, V.; Moon, K.; Kaifer, A. E., *Org. Lett.* **2004**, *6,16*, 2665.

[28] Day, A. I.; Blanch, R. J.; Lorrenzo, S.; Lewis, G. R.; Dance, I., *Angew. Chem.* **2002**, *114*, 285; *Angew. Chem. Int. Ed.* **2002,** *41,* 275.

[29] Lehn, J. M. *Supramolecular Chemistry: Concepts and Perspecti*Ves; John Wiley & Sons: New York, 1995.

[30] Isnin, R; Salam, C.; Kaifer, A. E., *J. Org. Chem.* **1991**, *56*, 35.

[31] Moon, K.; Kaifer, A. E., *Org. Lett.* **2004**, *6*, 185.

[32] Sun, H.; Kaifer, A. E., *Organometallics* **2006**, *25*, 7, 1828.

[33] Denuault, G.; Mirkin, M. V.; Bard, A. J., *J. Electroanal. Chem.* **1991**, *308*, 27.

[34] Balzani, V.; Becher, J.; Credi, A.; Nielsen, M. B.; Raymo, F. M.; Stoddart, J.F.; Talarico, A. M.; Venturi, M., *J. Org. Chem.* **2000**, *65*, 1947.

[35] Zhang, D.; Zhang, Q.; Su, J.; Tian, H., *Chem. Commun*. **2009**, 1700.

[36] Norrild, J. C.; Sotofte, I, *J. Chem. Soc., Perkin Trans. 2*, **2002**, 303.

[37] Kim, H. J.; Heo, J.; Jeon, W. S.; Lee, E.; Kim, J.; Sakamoto, S. Yamaguchi, K.; Kim, K., *Angew. Chem. Int. Ed.* **2001**, *40*, 1526

[38] Jeon, W. S.; Kim, Ko, Y. H.; Hwang, I.; Lee, J. W.; Kim, S.-Y.; Kim, H.-J.; Kim, K., *Angew. Chem.* **2005**, *117*, 89; *Angew. Chem. Int. Ed.* **2005**, *44*, 87.

[39] Rauwald, U.; Scherman, O. A., *Angew. Chem. Int. Ed.* **2008**, *47*, 3950.

[40] Reczek, J.; Kennedy, A. A.; Halbert, B. T.; Urbach, A. R., *J. Am. Chem. Soc.* **2009**, *131*, 2408.

[41] Li, X. Q.; Feng, D. J.; Jiang, X. K.; Li, Z. T., *Tetrahedron* **2004**, *60*, 8275.

[42] Dong, H. D.; Hua, W.; Li, S., *J. Phys. Chem. A*. **2007**, *111*, 2941.

[43] Zou, S.; Schonherr, H.; Vancso, G. J., *Angew. Chem. Int. Ed.* **2005**, *44*, 956.

[44] W. Nernst, *Z. Phys, Chem*. **1892**, 8, 110.

[45] Merrick, J. P.; Moran, D.; Radom, L., *J. Phys. Chem. A.* **2007**, *111*, 11683.

[46] Yang, Y.; Yan, H. J.; Chen, C. F.; Wan, L., J. *Org. Lett.* **2007**, *9*, 4991.

[47] Park, T.; Zimmerman, S. C., *J. Am. Chem.Soc*. **2006**, *128*, 11582.

[48] Kyogoku, Y.; Lord, R. C.; Rich, A., *Proc. Natl. Acad. Sci. USA* **1967**, *57*, 250.

[49] Kyogoku, Y.; Lord, R. C.; Rich, A., *Biochim. Biophys. Acta* **1969**, *179*, 10.

[50] Hamilton, A. D.; Van Engen, D., *J. Am. Chem. Soc.* **1987**, *109*, 5035.

[51] Jorgensen, W. L.; Pranata, J., *J. Am. Chem. Soc.* **1990**, *112*, 2008.

[52] Pranata, J.; Wierschke, S. G.; Jorgenson, W. L., *J. Am. Chem. Soc.* **1991**, *113*, 2810.

[53] Beijer, F. H.; Kooijman, H.; Spek, A. L.; Sijbesma, R. P.; Meijer, E. W., *Angew. Chem,* **1998**, *110*, 79; *Angew. Chem. Int. Ed.* **1998**, *37*, 75.

[54] Beijer, F. H.; Sijbesma, R. P.; Kooijman, H.; Spek, A. L.; Meijer, E. W., *J. Am. Chem. Soc*. **1998**, *120*, 6761.

[55] Sun, H.; Kaifer, A. E., *Org. Lett.* **2005**, *7*, 3845.

[56] Wong, C. H.; Chow, H. F.; Hui, S. K.; Sze, K. H., *Org. Lett.* **2006**, *8*, 1811.

[57] Ong, H. C.; Zimmerman, S. C., *Org. Lett*. **2006**, *8*, 1589.

[58] Martin, A. M.; Butler, R. S.; Ghiviriga, I.; Giessert, R. E.; Abboud, K. A.; Castellano, R. K., *Chem. Commun.* **2006**, 4413.

[59] Baruah, P. K.; Gonnade, R.; Phalgune, U. D.; Sanjayan, G. J., *J. Org. Chem.* **2005**, *70*, 6461.

[60] Ciferri, A. Ed.; Taylor & Francis *Supramolecular Polymers*, 2nd ed., 2005.

[61] Reinhoudt, D. N.; Crego-Calama, M., *Science* **2002**, *295*, 2403.

[62] Sijbesma, R. P.; Beijer, F. H.; Brunsveld, L.; Folmer, B. J. B.; Hirschberg, J. H. K. K.; Lange, R. F. M.; Lowe, J. K. L.; Meijer, E. W., *Science* **1997**, *278*, 1601.

[63] Brunsveld, L.; Folmer, B. J. B.; Meijer, E. W.; Sijbesma, R. P., *Chem. Rev.* **2001**, *101,* 4071.

[64] Sijbesma, R. P.; Meijer, E. W., *Chem. Commun*. **2003**, 5.

[65] Zimmerman, S. C.; Corbin, P. S., *Struct. Bonding (Berlin)* **2000**, *96*, 63.

[66] Schmuck, C.; Wienand, W., *Angew. Chem., Int. Ed*. **2001**, *40*, 4363.

[67] Cui, L.; Gadde, S.; Shukla, A.; Sun, H.; Mague, J.; Kaifer, A. E., *Chem. Commun.* **2008**, 1446.

[68] Sun, H.; Steeb, J.; Kaifer, A. E., *J. Am. Chem. Soc*. **2006**, *128*, 2820.

[69] Fery-Forgues, S.; Delavaux-Nicot, B., *J. Photochem. Photobio A* **2000**, *132*, 137.